INTERFACIAL PROPERTIES AND PHASE EQUILIBRIA FOR MIXTURES RELEVANT IN THE OIL AND GAS INDUSTRY

Vorgelegt von
Oscar Gabriel Nino-Amezquita, M. Sc.
aus Bogotá (Kolumbien)

von der Fakultät III
Prozesswissenschaften
der Technischen Universitat Berlin
zur Erlangung des akademischen Grades

Doktor der Ingenieurwissenschaften
Dr.-Ing.

genehmigte Dissertation

Promotionsausschuss:

Vorsitzender: Prof. Dr.-Ing. habil. Günter Wozny
Gutachterin: Prof. Dr. rer. nat. habil. Sabine Enders
Gutachter: Prof. Dr.-Ing. Rudolf Eggers

Tag der wissenschaftlichen Aussprache: 24.02.2014

Berlin 2014

D83

ACKNOWLEDGMENTS

It would not have been possible to write this doctoral thesis without the help and support of the kind people around me, to only some of whom it is possible to give particular mention here. This work would have never been completed without the advising and support of Prof. Sabine Enders, who was always willing to help and worked together with me during all this time. During my time working with her it was possible for me to grow not only academically but also as a person. Furthermore I would like to thank all colleagues and co-workers at the Chair of Thermodynamics at the TU-Berlin. The permanent discussions and a nice working environment made my work of this Thesis a pleasant task. In particular I would like to thank all my former office companions, Tim Zeiner, Udo Dorn and Karin Daniel, with whom I shared a lot of time and many interesting academical and non-academical dialogues. My gratitude also goes to the Department of thermal separation processes, heat and mass transfer of the TU Hamburg-Harburg, led by Prof. Rudolf Eggers, for the support and the valuable experimental data that allowed validating various parts of this work. Also Prof. Günter Wozny is to be thanked for taking the time to take part of the proofing Comission. Twister B.V. is also to be thanked for the interesting discussions and financial support. Last but not least, I want to specially thank the DFG for the financial support (En291/6-1) during this work.

TABLE OF CONTENTS

LIST OF TABLES

LIST OF FIGURES

LIST OF SYMBOLS

Symbols

a	van der Waals attraction
a	dispersion coefficient, PC-SAFT
$a(T)$	temperature dependency of the binary interaction parameter, SAFT
b	van der Waals volume
b	dispersion coefficient, PC-SAFT
d	temperature - dependent segment diameter, SAFT
f	Helmholtz energy
g	Gibbs energy
k_{ij}	binary interaction parameter
m	number of segments, SAFT
N	number of carbon atoms in an n-alkane
N_{av}	Avogadro's number
P	pressure
Q_1^*	reduced quadrupole moment, PCP-SAFT
R	universal gas constant
T	temperature
X^{A_i}	non-bonded monomer fraction, SAFT
X_i	molar fraction of component i

Greek Symbols

β	mixing parameter, density gradient theory
Γ	adsorption isotherm

Δ	association strength, SAFT
$\Delta\omega$	grand thermodynamic potential
ε	dispersion energy, SAFT
ε^{AB}	association energy, SAFT
ζ_k	k-moment of the mean segment number
κ	influence parameter, density gradient theory
κ^{AB}	association volume, SAFT
μ	chemical Potential
ρ	density
ρ_A	Partial density of component A
σ	segment diameter, SAFT
σ	interfacial tension, density gradient theory

Subscripts

A, B	component A, component B
asso	association contribution (SAFT, PC(P)-SAFT)
c	critical
chain	chain contribution (SAFT, PC(P)-SAFT)
disp	dispersion contribution (SAFT, PC(P)-SAFT)
hs	hard sphere contribution (SAFT, PC(P)-SAFT)
ideal	ideal contribution (SAFT, PC(P)-SAFT)
i,ii	component i
ij, AB	mixture of i (or A) and j (or B)
j, jj	component j
k	k-moment (SAFT, PC(P)-SAFT)
mono	monomer contribution (SAFT, PC(P)-SAFT)
polar	polar contribution (SAFT, PC(P)-SAFT)

Superscripts

id	ideal
E	excess
A	component A
B	component B

1. INTRODUCTION

Nowadays, the role of oil in our lifes is extremely important. The oil industry produces a broad spectrum of substances which are vital for the everyday life, in the first level from regular energy sources as diesel or gasoline up to highly refined products separated from the crude oil. Additionally, the chemical industry relies on the delivery of raw materials derived from different steps in the oil industry for manufacture of a broad amount of products such as plastics, surfactants, specialty chemicals, coatings and many others. It is certainly not exaggerated to say the oil is the motor of society as we know it today.

Exactly due to this extreme importance of the supply of oil, and summed to the difficult reserves situation currently, new and old technologies are being rediscovered or further developed in order to increase the extraction efficiency of hydrocarbons worldwide. One example of this is the so called enhanced oil recovery. In this technique, a fluid can be pumped into the oil reservoir. It is expected that with help of this method, the oil and gas inside the reservoir will be taken out in a more efficient way. Options for a pumping fluid can be, for instance, the use of carbon dioxide or a mixture with water.

The main hindrance to a quick development of this procedure is the lack of knowledge of possible dependencies between pressure, temperature an concentration of the different present components for the extraction efficiency, which is directly linked to the revenue of the reservoir. Thermodynamics offers in this case a solution for the modelling of not only phase equilibria but also interfacial properties of these mixtures. Through the use of so called equations of state, it is possible to extrapolate the phase behaviour of single components to a whole mixture. Depending on the complexity of the mixtures, various models have been proposed, both empirical and theoretically based. The arising problem in the case of the oil industry is the high complexity of the mixtures present, since components of very different characteristics might be present, going from highly polar associating

molecules like water up to regular non-polar constituents. Therefore, the chosen model has to possess the capabilities to describe the behaviour not only of these highly differing substances but also of their mixtures.

In the recent years, molecular-based equations of state have been used to describe the vapour-liquid and liquid-liquid phase behaviour of various mixtures. Particularly the family of equations of states based on the statistical associating fluid theory (SAFT) have been widely used for this purpose. The advantage of a perturbation theory where the energetic state of alike or different molecules can be described through the sum of a reference state and all arising perturbations has led to extensions which take into account diverse possible interactions.

On the side of the description of the energetic properties of an interface, some works have been made, beginning with the original postulations from van der Waals about the inhomogeneities arising in the phase change region between two bulk phases. This approximation has been widely discussed through time and taken into account increasingly in the present, especially with the new advantages for calculations (computational and numerical) given in the computer age.

This work aims to establish a methodology that can be used for description of mixtures present in the oil industry. In order to achieve this, the modelling of the phase equilibria for pure components and several mixtures will be made with help of the perturbed-chain statistical associating fluid theory (PC-SAFT) equation of state. Moreover, the interfacial properties (density and concentration profiles across the interface, interfacial tensions and adsorption phenomena) of these mixtures will be calculated or predicted. In order to achieve this, different pure components will be taken into account, from purely non-polar hydrocarbons over sulphur containing substances, polar substances and, finally, water.

The work will begin with a review of the thermodynamic framework that allows the calculation of phase equilibria and interfacial properties of pure components and mixtures; the core models used for this will also be presented and described. In the latter sections, the results for a broad range of pure components will be presented, either with parameters fitted from the literature or found out during this work. In the

case of mixtures, an initial approach for binary mixtures of diverse substances will be presented, and correlations will be made when possible, in order to achieve as much predictability of the approach as possible. In both cases, the calculated or predicted values will be compared with values from the literature. Finally, a test for the viability of the extrapolation of the theoretical framework for multicomponent mixtures will be made through calculation of phase equilibrium and interfacial properties of a ternary system. This calculation assessment is of special importance, since it represents a pure prediction based on the knowledge acquired from the binary subsystems. The results will also be compared and validated with available experimental data. A short conclusion and outlook will summarize the results of this work and the recommended steps to follow if it is intended to go on with the work initiated during this PhD.

2. PHASE EQUILIBRIA OF LOW-MOLECULAR WEIGHT SYSTEMS

2.1. Thermodynamic Framework

Phase equilibrium is a phenomenon that can be observed for both pure components and mixtures of different substances. A phase can be defined as a region with alike physical and chemical properties. The number of possible phases available for a single component or a mixture is already dictated by Gibbs phase rule:

$$F = K - Ph + 2 \tag{1}$$

where F is the number of degrees of freedom, K the number of components in a mixture and Ph the number of phases. In the case of a pure substance (K=1), the maximum possible phases would be three (Ph=3), since this is the highest possible number to obtain non-negative values of degrees of freedom (F). In the case of a two-phase system (Ph=2), only one condition (e.g. pressure or temperature) are necessary to completely define the system. The extrapolation to binary mixtures (K=2) allows more degrees of freedom. In this case, a two-phase system needs to be defined with help of two conditions such as the mentioned above.

Regardless of the number of available phases in a system, the equilibrium principles are already fixed. These are the thermal, mechanical and chemical potential equality of all phases and all components:

$$\begin{aligned} &T^{\alpha} = T^{\beta} = ... = T^{\lambda} \\ &P^{\alpha} = P^{\beta} = ... = P^{\lambda} \\ &\mu_1^{\alpha} = \mu_1^{\beta} = ... = \mu_1^{\lambda} \\ &\mu_2^{\alpha} = \mu_2^{\beta} = ... = \mu_2^{\lambda} \\ &... \\ &\mu_n^{\alpha} = \mu_n^{\beta} = ... = \mu_n^{\lambda} \end{aligned} \tag{2}$$

All equalities are to be applied from a single up to multicomponent mixtures. In the special case of a pure component:

$$\begin{aligned} \mu^{\alpha} &= \mu^{\beta} \\ g^{\alpha} &= g^{\beta} \end{aligned} \tag{3}$$

Per definition:

$$g = h - Ts = u + Pv - Ts \tag{4}$$

Therefore in equilibrium ($dT = 0$ and $dP = 0$):

$$g^{\alpha} - g^{\beta} = u^{\alpha} - u^{\beta} + P\left(v^{\alpha} - v^{\beta}\right) - T\left(s^{\alpha} - s^{\beta}\right) \tag{5}$$

Integration between the two phases leads to:

$$\int_{\beta}^{\alpha} dg = u^{\alpha} - u^{\beta} + \int_{\beta}^{\alpha} P dv - T\left(s^{\alpha} - s^{\beta}\right) = g^{\alpha} - g^{\beta} \tag{6}$$

Equating the last two equations leads to:

$$\int_{\beta}^{\alpha} P dv = P\left(v^{\alpha} - v^{\beta}\right) \tag{7}$$

Equation 7 is also called Maxwell's criterion. This can be also explained graphically on the PV diagram for a pure fluid. Figure 1 shows a graphic description of this phenomenon. The area delimited by the isotherm below and the vapour pressure on the upper side must be equal to the area delimited above from the same isotherm and below from the vapour pressure.

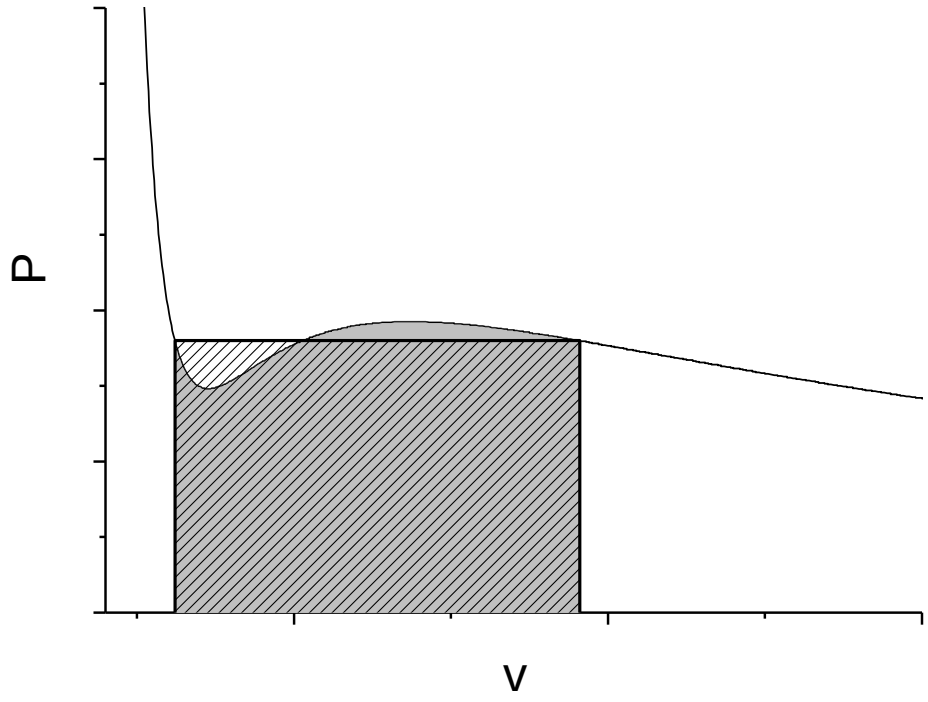

Figure 1: Graphic description of Maxwell's criterion.

In the case of a multicomponent system, the equality of chemical potentials in equation 2 can also be replaced by the isofugacity criterion:

$$\begin{aligned} f_1^{\alpha} &= f_1^{\beta} = \ldots = f_1^{\lambda} \\ f_2^{\alpha} &= f_2^{\beta} = \ldots = f_2^{\lambda} \\ &\ldots \\ f_n^{\alpha} &= f_n^{\beta} = \ldots = f_n^{\lambda} \end{aligned} \tag{8}$$

In principle, equation 2 contains all the necessary requirements for calculation of phase equilibria of pure substances and mixtures. Several options arise based on these conditions, and will be discussed in the following section.

2.2. Calculations of Phase Equilibria

Phase equilibria of pure and multicomponent systems can be calculated through several paths. This section intends to mention the most used ones, and will go deeper in the methodologies relevant for this work. Mainly, two paths are commonly used for description of vapour-liquid (VLE) and liquid-liquid (LLE) equilibria: Excess

Gibbs' energy models and equations of state. Though both methods intend to describe the same phenomenon, they show different approaches.

In general, the partial molar Gibbs' energy (chemical potential) of a component i can be split into an ideal term $\overline{g}_i^{id}$, describing the ideal Gibbs' energy of mixing and an excess term $\overline{g}_i^{E}$, describing all non-idealities of a mixture, which are dependent on the molar fraction x_i, the standard fugacity f_i^0 and the fugacity f_i. In such a case:

$$\overline{g}_i = \overline{g}_i^{id} + \overline{g}_i^{E}$$
$$\overline{g}_i = g_i^{pure} + RT \ln x_i + RT \ln\left(\frac{f_i}{x_i f_i^0}\right) \qquad (9)$$

The excess energy models try therefore to find a suitable expression for the excess Gibbs' energy of mixing, in order to find an analytical solution that will allow the calculation of activity coefficients. This alone would be enough for calculation of LLE of several mixtures; however, in the case of VLE, the vapour pressure of the pure components involved must be known. These models are usually based on binary interactions. In the case of multicomponent mixtures, the final excess energy will be equal to the sum of all binary subsystems' interactions. Several models can be applied to describe the excess partial energy, as to mention the ones from Porter [1], the Redlich-Kister expansion [2], the Wilson [3] model, the NRTL model [4], UNIQUAC [5] and its group contribution development UNIFAC [6, 7, 8].

Another way to calculate phase equilibria is through the so called equations of state (EOS). This methodology rests on calculations of the properties of the pure fluid as a base for calculations on mixtures. Several types of EOS have been developed throughout the years since the 19th century. Cubic EOS were the first type of equations that tried to describe the behaviour of a fluid beyond the ideal gas. The first equation of state able to describe properties of both a liquid and a gas was developed by van der Waals during his PhD thesis in 1873 [9]. The EOS uses the critical properties (temperature T_c and pressure P_c) for the calculation of pressure and volume of a fluid:

$$P = \frac{RT}{v-b} - \frac{a}{v^2}$$
$$a = \frac{27R^2T_c^2}{64P_c}, b = \frac{RT_c}{8P_c} \quad (10)$$

With P being the pressure, R being the universal gas constant, T the temperature and v the molar volume of the fluid. The parameters of the van der Waals EOS (vdW-EOS) have a physical meaning. While the parameter a accounts for interaction between molecules, the parameter b describes the real volume of a molecule. In general, the first term of the right side of the equation concerns the repulsion of “hard sphere molecules” and the attraction due to dispersion forces can be related to the second term. The vdW-EOS was and is a milestone in the understanding of the phenomena that cause phase separations and describing them; however, due to its simplicity, its application has become very limited. For a mixture:

$$a = \sum_i \sum_j x_i x_j a_{ij}$$
$$b = \sum_i \sum_j x_i x_j b_{ij} \quad (11)$$

with

$$a_{ij} = \sqrt{a_{ii} a_{jj}}$$
$$b_{ij} = \frac{b_{ii} + b_{jj}}{2} \quad (12)$$

The vdW EOS has been extended over the years, mainly with modification to the attractive part. It is in this case worth to mention the works that have led to Redlich-Kwong EOS [10], Soave-Redlich-Kwong EOS [11] and Peng-Robinson EOS (PR-EOS) [12].

A special case in the cubic EOS is the addition of a foreign term, which accounts association of molecules in a fluid. This equation, called cubic plus association [13] (CPA-EOS) is a hybrid that takes into account association through inclusion of an association term present in so called SAFT-type equations. This term will be

extensively discussed on a further section. CPA intends to better describe associating molecules, such as water, under a numerically lighter environment.

Several other versions of cubic equations have been developed over the years, mainly modifying the one or other term of the ones presented in this section. Examples of this are the Patel-Teja EOS [14], or the Volume Translated Peng-Robinson (VTPR) EOS [15]. The last EOS has also been used in combination with group contribution methods in order to define the parameters of the mixture.

The first changes in the repulsion part of the vdW-EOS were the proposed by Guggenheim [16] and Carnahan and Starling [17]; however, the development of this first replacement of the repulsion term opened the way to another type of EOS: The molecular based ones. This new group of EOS will be briefly discussed in the next section.

Molecular Based EOS

As mentioned, Guggenheim [16] proposed a model for the repulsion forces of a fluid:

$$P = \frac{RT}{v(1-y)^4} - \frac{a}{v^2} \tag{13}$$

with

$$y = \frac{b}{4v}$$
$$a = \frac{0.4963 R^2 T_c^2}{P_c}, b = \frac{0.18727 R T_c}{P_c} \tag{14}$$

It is to note here that the new EOS was not cubic anymore. The proposed model by Guggenheim [16] proved to be more accurate than the vdW-EOS for describing properties of argon.

Carnahan and Starling [17] followed the work made by Guggenheim and proposed another model to describe the repulsion of a fluid consistent of hard spheres:

$$P = \frac{RT\left(1 + y + y^2 - y^3\right)}{v\left(1-y\right)^3} - \frac{a}{v^2} \tag{15}$$

The Carnahan-Starling hard-sphere term has been extensively used in other theories. Boublik [18] extended this term to non-spherical systems:

$$P = \frac{RT\left(1 + \left(3\alpha - 2\right)y + \left(3\alpha^2 - 3\alpha + 1\right)y^2 - \alpha^2 y^3\right)}{v\left(1-y\right)^3} - \frac{a}{v^2} \tag{16}$$

In the limiting case, the hard sphere ($\alpha = 1$), the expression reduces to the one from Carnahan and Starling [17].

Beret and Prausnitz [19] developed the Perturbed hard-chain theory (PHCT) based on Prigogine's work [20] of the dependency of behaviour of molecules (motion and rotation) due to density. The PHCT-EOS defines the compressibility factor Z as:

$$Z = Z^{hc} - \frac{a}{RTv} \tag{17}$$

where

$$Z^{hc} = 1 + c\frac{4\left(\tau / \tilde{v}\right) - 2\left(\tau / \tilde{v}\right)^2}{\left(1 - \tau / \tilde{v}\right)^3} \tag{18}$$

$$\tilde{v} = \frac{v}{N_{av} r v^0} \tag{19}$$

$$a = -R\left(\frac{\varepsilon q}{k}\right)\left(r v^0\right)\sum_{n=1}^{4}\sum_{m=1}^{M}\left[\frac{mA_{nm}}{\tilde{v}^{m-1}}\right]\left[\frac{1}{T^{n-1}}\right] \tag{20}$$

N_{av} is the Avogadro number, v the reduced volume and τ a numerical constant. The term a is a Taylor series expansion on the reciprocal of the reduced volume v with

its coefficients A_{nm} .Three parameters are necessary to describe a fluid under the PHCT-EOS: rv^0 , the close-pack volume per mole times the segments per molecule, the characteristic energy per molecule $\varepsilon q/k$ and the degrees of freedom c . All parameters can be fitted to vapour pressures and molar volumes of the pure components. The work has been successful for modelling of different components present in the oil industry. Kim et al. [21] modified the expression of the PHCT by using a different attraction term. This new EOS was called the simplified perturbed hard-chain theory (SPHCT) EOS, which proved to be as accurate as the PHCT-EOS but with a much simpler mathematical handling. In the same year, Wertheim [22, 23] postulated his thermodynamic perturbation theory (TPT), which opened the way to a new family of EOS, also molecular based, but that will be discussed on the next section.

The SAFT EOS and its modifications

Wertheim's thermodynamic perturbation theory [22, 23] has been a milestone in the description of attraction forces of non-polar fluids. During this work, Wertheim defined the contribution of attraction forces due to association of molecules. Chapman et al. [24, 25, 26] integrated these concepts and applied it to a system of hard spheres forming a chain and developed the statistical associating fluid theory (SAFT). In the SAFT framework, the Helmholtz energy of a pure or mixed fluid can be described as the sum of the energy of a reference system and all its perturbations. The definition of this system is of importance. Chapman et al [24, 25, 26] defined the reference system as a hard-sphere-fluid which subsequently forms different chains and can have further interconnection steps such as association. Mathematically this means:

$$f = f_{ideal} + f_{mono} + f_{chain} + f_{asso} \tag{21}$$

The most applied SAFT- version is the given by Huang and Radosz [27] where the chain formation term is:

$$f_{mono} = (m-1)\ln y_{mono}(\sigma) \tag{22}$$

and the association based on Wertheim [22, 23]:

$$f_{assoc} = RT\sum_i X_i \left[\sum_{A_i} \left[\ln\left(X^{A_i} \right) - \frac{X^{A_i}}{2} \right] + \frac{1}{2} M_i \right] \tag{23}$$

$$\Delta^{A_i B_j} = d_{ij}^3 g_{ij}(d_{ij}) \kappa^{A_i B_j} \left[\exp\left(\frac{\varepsilon^{A_i B_j}}{kT} \right) - 1 \right] \tag{24}$$

The radial distribution function is in this case the expression described from Carnahan and Starling [17]. In this case, it is necessary to define a so called association scheme. Huang and Radosz have given an extensive explanation of this in their paper [27]. The resulting free monomer fractions X^{A_i} can be seen in Table 1.

The segment contribution is a sum of the hard-sphere reference fluid, given by Carnahan and Starling [17] and a power series developed by Alder et al. [28] and refitted by Chen and Kreglewski [29]:

$$f_{ideal} = f_{hs} + f_{disp} \tag{25}$$

$$f_{hs} = \frac{4\eta - 3\eta^2}{(1-\eta)^2} \tag{26}$$

$$f_{disp} = \sum_i \sum_j D_{ij} \left[\frac{u}{kT} \right]^i \left[\frac{\eta}{\tau} \right]^j \tag{27}$$

Table 1: Free monomer fractions defined for each association scheme [27].

Association Scheme	X^{A_i}
1	$\frac{-1+\left(1+4\rho\Delta^{A_iB_j}\right)^{1/2}}{2\rho\Delta^{A_iB_j}}$
2A	$\frac{-1+\left(1+8\rho\Delta^{A_iB_j}\right)^{1/2}}{4\rho\Delta^{A_iB_j}}$
2B	$\frac{-1+\left(1+4\rho\Delta^{A_iB_j}\right)^{1/2}}{2\rho\Delta^{A_iB_j}}$
3A	$\frac{-1+\left(1+12\rho\Delta^{A_iB_j}\right)^{1/2}}{6\rho\Delta^{A_iB_j}}$
3B	$\frac{-\left(1-\rho\Delta^{A_iB_j}\right)+\left(\left(1+\rho\Delta^{A_iB_j}\right)^2+4\rho\Delta^{A_iB_j}\right)^{1/2}}{4\rho\Delta^{A_iB_j}}$
4A	$\frac{-1+\left(1+16\rho\Delta^{A_iB_j}\right)^{1/2}}{8\rho\Delta^{A_iB_j}}$
4B	$\frac{-\left(1-2\rho\Delta^{A_iB_j}\right)+\left(\left(1+2\rho\Delta^{A_iB_j}\right)^2+4\rho\Delta^{A_iB_j}\right)^{1/2}}{6\rho\Delta^{A_iB_j}}$
4C	$\frac{-1+\left(1+8\rho\Delta^{A_iB_j}\right)^{1/2}}{4\rho\Delta^{A_iB_j}}$

The term of Chen and Kreglewski was fitted to simulation data for a square-well fluid:

$$u(r)=\begin{cases}\infty & r<\sigma\\ -u & \sigma\le r<\lambda\sigma\\ 0 & r\ge\lambda\sigma\end{cases} \tag{28}$$

The type of potential that is used for the model, and certain other assumptions, have given birth to several versions of SAFT-EOS. Just to mention, the SAFT-VR (variable range) developed by Jackson and coworkers [30] version takes the range of influence for the square-well fluid as an additional parameter. Furthermore, other potentials different from the square-well one can be used inside the SAFT-

Framework. Examples of this are the use of a Lennard-Jones potential in the soft-SAFT EOS [31] and the use of Mie-Potentials in the SAFT-VR-Mie work of Lafitte et al. [32]. Another possibility is the deeper change of the reference system. This is the case of the PC-SAFT, which will be discussed more extensively, due to its relevance for this work, in a separate section.

The PC(P)-SAFT EOS

The PC-SAFT EOS (PC= Perturbed Chain) was developed by Gross and Sadowski [33, 34] based on the SAFT EOS. In this model the chain-length dependence of the attractive (dispersive) interactions is also taken into account. A hard-chain fluid serves as a reference for the perturbation theory, differing from spherical molecules, as in the original SAFT version. Molecules are conceived as chains composed of tangent spherical segments. The pair potential for the segment of a chain is given by a modified square-well potential of the form:

$$u(r) = \begin{cases} \infty & r < \sigma - s_1 \\ 3\varepsilon & \sigma - s_1 \le r < \sigma \\ -\varepsilon & \sigma \le r < \lambda\sigma \\ 0 & r \ge \lambda\sigma \end{cases} \tag{29}$$

The equation of state is given has then an ideal gas contribution (id), a hard-chain contribution (hc), and perturbation contributions, which accounts for the attractive interactions of dispersion forces (disp) or association (asso):

$$f = f_{id} + f_{hc} + f_{disp} + f_{asso} \tag{30}$$

For a non- associating substance this EOS contains three pure-component parameters: the segment diameter (σ), the interaction energy related to the dispersion interaction (ε), and the number of segments (m). In the case of associating molecules it is necessary to add the bonding energy related to association (ε^{AB}) as well as the association volume of the molecule (κ^{AB}).

Due to its importance for this work, all the terms will be discussed in this section. The ideal part of the Helmholtz energy can be described as:

$$f_{ideal} = RT\ln(\rho RT) + RT\sum_i X_i \ln(X_i) \tag{31}$$

with ρ being the molar density and X_i the molar fraction. The hard-chain contribution to the reference system is described as follows:

$$\frac{f_{chain}}{RT} = \bar{m} f_{hs} - \sum_i X_i (m_i - 1)\ln(g_{ii}^{hs}) \tag{32}$$

$\bar{m}$ is the average length of the chain, f_{hs} is the hard-sphere free energy and g_{ii}^{hs} is the radial distribution function of the hard sphere. Mathematically:

$$\bar{m} = \sum_j X_j m_j \tag{33}$$

$$g_{ii}^{hs} = \frac{1}{(1-\zeta_3)} + \frac{d_i}{2}\frac{3\zeta_2}{(1-\zeta_3)} + \frac{d_i^2}{4}\frac{2\zeta_2^2}{(1-\zeta_3)^3} \tag{34}$$

$$d_i(T) = \sigma_i\left[1 - 0.12\exp\left(-\frac{3\varepsilon_i}{kT}\right)\right] \tag{35}$$

d_i is the temperature dependent diameter of the sphere, which is dependent of the temperature-independent diameter σ_i and the depth of the potential ε_i. Furthermore:

$$\zeta_k = \frac{\pi}{6} N_{AV}\rho\sum_i X_i m_i d_i^k \tag{36}$$

The different moments ζ_k are also used in the Helmholtz energy of the hard spheres:

$$f_{hs} = \frac{1}{\zeta_0}\left[\frac{3\zeta_1\zeta_2}{1-\zeta_3} + \frac{\zeta_2^3}{\zeta_3(1-\zeta_3)^2} + \left(\frac{\zeta_2^3}{\zeta_3^2} - \zeta_0\right)\ln(1-\zeta_3)\right] \tag{37}$$

The dispersion part is based on the theory of Barker and Henderson [35]:

$$\frac{f_{disp}}{RT} = -2\pi N_{AV}\rho I_1(\eta,\bar{m})\overline{m^2\varepsilon\sigma^3} - \pi N_{AV}\rho\bar{m}C_1 I_2(\eta,\bar{m})\overline{m^2\varepsilon^2\sigma^3} \tag{38}$$

where $I_1(\eta,\bar{m})$ and $I_2(\eta,\bar{m})$ are the integral of the pair potential and its derivative with respect to the density:

$$I_1(\eta,\bar{m}) = \int_1^\infty u(x)g^{hc}(m,x\frac{\sigma}{d})x^2dx \tag{39}$$

$$I_2(\eta,\bar{m}) = \frac{\partial}{\partial\rho}\left[\rho\int_1^\infty u(x)^2 g^{hc}(m,x\frac{\sigma}{d})x^2dx\right] \tag{40}$$

Gross and Sadowski [33] developed these integrals as power series of the reduced density ($\eta = \zeta_3$) of the form

$$I_1(\eta,\bar{m}) = \sum_{i=0}^{6} a_i(m)\eta^i \tag{41}$$

$$I_2(\eta,\bar{m}) = \sum_{i=0}^{6} b_i(m)\eta^i \tag{42}$$

where the coefficients are defined as

$$a_i(m) = a_{0i} + \frac{m-1}{m}a_{1i} + \frac{m-1}{m}\frac{m-2}{m}a_{2i} \tag{43}$$

$$b_i(m) = b_{0i} + \frac{m-1}{m}b_{1i} + \frac{m-1}{m}\frac{m-2}{m}b_{2i} \tag{44}$$

These so called universal constants were fitted to molecular simulations in the work of Gross and Sadowski [33]. The values can be seen in Table 2.

Table 2: Universal constants for the PC-SAFT EOS [33].

i	a_{0i}	a_{1i}	a_{2i}	b_{0i}	b_{1i}	b_{2i}
0	0.9105631	-0.308402	-0.090615	0.7240947	-0.57555	0.0976883
1	0.6361281	0.1860531	0.4527843	2.2382792	0.6995096	-0.255757
2	2.6861348	-2.503005	0.5962701	-4.002585	3.8925673	-9.155856
3	-26.54736	21.419794	-1.724183	-21.00358	-17.21547	20.642076
4	97.759209	-65.25589	-4.130211	26.855641	192.67226	-38.80443
5	-159.5915	83.31868	13.776632	206.55134	-161.8265	93.626774
6	91.297774	-33.74692	-8.672847	-355.6024	-165.2077	-29.66691

Other terms in the dispersion contribution (Eq. 38) are:

$$\overline{m^2\varepsilon\sigma^3} = \sum_i \sum_j X_i X_j m_i m_j \left(\frac{\varepsilon_{ij}}{kT}\right) \sigma_{ij}^3 \tag{45}$$

$$\overline{m^2\varepsilon^2\sigma^3} = \sum_i \sum_j X_i X_j m_i m_j \left(\frac{\varepsilon_{ij}}{kT}\right)^2 \sigma_{ij}^3 \tag{46}$$

For the application of the equations of state to mixtures made from the component i and j mixing rules must be specified. The perturbation theory of Barker and Henderson [35] makes use of an average radial distribution function and thus treats the segments of a chain as indistinguishable. Within this concept, a rigorous application of the perturbation theory to a mixture is in principle possible. However, the mathematical expressions are not available in analytical form. Therefore, two mixing rules were used for the application of the PC-SAFT to mixtures, namely:

$$\sigma_{ij} = \frac{1}{2}(\sigma_i + \sigma_j) \tag{47}$$

$$\varepsilon_{ij} = \sqrt{\varepsilon_i \varepsilon_j}(1 - k_{ij}) \tag{48}$$

where k_{ij} is the so called binary interaction parameter. The binary interaction parameter will be fitted to phase equilibrium data. Additionally for the dispersion contribution (equation 38):

$$C_1 = \left(1 + Z^{hc} + \rho \frac{\partial Z^{hc}}{\partial \rho}\right)^{-1} \tag{49}$$

$$C_1 = \left[1 + \bar{m}\frac{8\eta - 2\eta^2}{(1-\eta)^4} + (1-\bar{m})\frac{20\eta - 27\eta^2 + 12\eta^3 - 2\eta^4}{[(1-\eta)(2-\eta)]^2}\right]^{-1} \tag{50}$$

The association contribution is taken from the SAFT [22, 23, 24] framework:

$$f_{assoc} = RT\sum_i X_i \left[\sum_{A_i}\left[\ln\left(X^{A_i}\right) - \frac{X^{A_i}}{2}\right] + \frac{1}{2}M_i\right] \tag{51}$$

$$\Delta^{A_iB_j} = d_{ij}^3 g_{ij}(d_{ij})\kappa^{A_iB_j}\left[\exp\left(\frac{\varepsilon^{A_iB_j}}{kT}\right) - 1\right] \tag{52}$$

The value for X^A can be taken, depending on the association model, from Table 1. The intermolecular interaction diameter is defined as

$$d_{ij} = \frac{1}{2}\left(d_i + d_j\right) \tag{53}$$

and the intermolecular distribution function:

$$g_{ij}\left(d_{ij}\right) = \frac{1}{1-\zeta_3} + \frac{3d_{ii}d_{jj}}{d_{ii}+d_{jj}}\left(\frac{\zeta_2}{(1-\zeta_3)^2}\right) + 2\left(\frac{d_{ii}d_{jj}}{d_{ii}+d_{jj}}\right)^2\left(\frac{\zeta_2^2}{(1-\zeta_3)^3}\right) \tag{54}$$

Two parameters are important in the association contribution, the association volume $\kappa^{A_iB_j}$ and the association energy $\varepsilon^{A_iB_j}$.

In order to better describe the behaviour of polar components, Gross and Vrabec developed the PCP-SAFT-EOS [36, 37], a further development of the PC-SAFT-EOS [33, 34]. Additional to the original PC-SAFT, a contribution taking polar interactions (polar) into account is described [36, 37]:

$$f = f_{id} + f_{hc} + f_{disp} + f_{assoc} + f_{polar} \tag{55}$$

The heart of the PCP-SAFT-EOS is the new additional term f_{polar} in Eq. 92. In order to derive an expression for this quantity the starting point is the Padé- approximation in terms of the Helmholtz energy. This can be done for substances exhibiting either a dipole (e.g. acetone, chloromethane) or a quadrupole term (e.g. carbon dioxide). In the case of a quadrupolar contribution, the polar term is defined as:

$$\frac{f_{polar}}{RT} = \frac{f_{quadrupole}}{RT} = \frac{A_2 / RT}{1 - A_3 / A_2} \tag{56}$$

with A_2 and A_3 as the second-order and third-order perturbation terms, respectively. Gross [36] suggested for these terms the following expressions:

$$\begin{aligned} &\frac{A_2}{RT} = -K_{A2}\eta J_{2,11}^{QQ} \qquad \frac{A_3}{RT} = K_{A3}\eta^2 J_{3,111}^{QQ} \\ &K_{A2} = \frac{27}{8}\frac{\varepsilon_1^2\sigma_1^3 Q_1^{*4}}{m_1 d_1^3 (kT)^2} \quad K_{A3} = \frac{81}{4}\frac{\varepsilon_1^3\sigma_1^6 Q_1^{*6}}{(kT)^3 m_1^2 d_1^6} \end{aligned} \tag{57}$$

where Q_1^* is the reduced quadrupole moment and reads:

$$Q_1^{*2} = \frac{10^{-19} Q_1^2}{k m_1 \varepsilon_1 \sigma_1^5} \tag{58}$$

where the quadrupole moment Q_1^2 is measured in 10^{-26}erg$^{1/2}$*cm$^{5/2}$ and k is the Boltzmann-constant. The expression for the calculation of the quantities $J_{2,11}^{QQ}$ and $J_{3,111}^{QQ}$ are also fitted to molecular simulations, as in the case of the dispersion term:

$$I_1(\eta, \bar{m}) = \sum_{i=0}^{6} a_i(m)\eta^i \tag{59}$$

$$I_2(\eta,\bar{m}) = \sum_{i=0}^{6} b_i(m)\eta^i \tag{60}$$

with [36]

$$a_i(m) = a_{0i} + \frac{m-1}{m} a_{1i} + \frac{m-1}{m}\frac{m-2}{m} a_{2i} \tag{61}$$

$$b_i(m) = b_{0i} + \frac{m-1}{m} b_{1i} + \frac{m-1}{m}\frac{m-2}{m} b_{2i} \tag{62}$$

The values for these coefficients can be found in the literature [36]. Gross and Vrabec [37] developed an analogous, very similar term for dipolar molecules. The slight changes of the new term can be seen in the literature [37].

3. THE INTERFACIAL TENSION

3.1. Generalities

The characteristics of interfaces between two phases differ greatly from those of the bulk phases. Cohesion forces compel molecules in the interface to exert a certain tension that keeps the interfacial area to an energetic minimum. This can be seen in the differential of the Gibbs Energy of a system:

$$dG = -SdT + VdP + \sigma dA + \sum_i \mu_i dn_i \tag{63}$$

At thermodynamic equilibrium, the first, second and fourth terms vanish. Also at equilibrium, the total Gibbs Energy of the system has to be minimized, meaning:

$$\sigma = \left(\frac{dG}{dA} \right)_{T,P,n=const.} \tag{64}$$

This means, the interfacial tension is the required amount of energy to increase the interfacial area of a two-phase system.

Interfacial tensions are of great importance for industrial applications. Therefore, it is of interest to know about methods to measure them and also to model interfacial tension of several systems. This chapter will show some available methods for measurements of interfacial tensions. Additionally, the density gradient theory, part of the core of this work, will be explained.

3.2. Measurement of the interfacial tension

Several kinds of measurements can be made for the definition of the interfacial tension of a pure substance or a mixture. The first methods can be defined as the microbalance methods. To directly measure interfacial tensions using a

microbalance, a plate, ring, or other probe with a given shape is brought into contact with the interface. Once wetted by one the liquids, this liquid will adhere to the probe and climb as the result of capillary force, increasing the interfacial area and leading to a force tending to pull the probe toward the plane of the interface. The force is directly related to the interfacial tension and can be measured by a microbalance. The force acting along the contact line is then equal to the weight of the liquid meniscus standing above the plane of the fluid-fluid interface. This force, measured by the microbalance, is used to calculate the interfacial tension:

$$\sigma = \frac{F}{p\cos\theta} \tag{65}$$

where p is the perimeter of the three-phase contact line and θ is the contact angle measured for the liquid meniscus in contact with the object surface.

Two main techniques for measurements of the surface tension with a help of a microbalance can be mentioned: the Wilhelmy plate [38] and du Nouy [39] ring methods. The Wilhelmy plate technique is used both static and in detachment trials, whereas the du Nouy ring is strictly a detachment method. In the static case, the plate remains in contact with liquid during the entire measurement. If the instrument operates in the detachment mode, the interfacial tension is measured by measuring the force required to separate the ring or plate from contact with the interface. One of the most important inconvenients of the microbalance methods is the strong effect impurities, e.g. remaining surfactants on the surface, can exert on a surface tension measurement [40].

A second group of measurements is based on capillary forces. One of the most known methods within this group is the capillary rise method. The basis for the capillary rise method is to measure the height of the meniscus in a round glass tube having the known inner radius. For small-diameter tubes (i.e., radius much smaller than height) the shape of the meniscus is spherical, and the surface tension can be calculated by using the following equation:

$$\sigma = \frac{\Delta\rho g h r}{2\cos\theta} \tag{66}$$

where $\Delta\rho$ is the density difference between both phases, g is gravity, h is the height of the tube, r its radius and $\cos\theta$ the cosine of the wetting angle, which can be taken in several cases to unity, if wetting is uniform. The method is very accurate, but has some difficulties as well. Building of a capillary that is uniform enough is one of the main difficulties. Additionally, the exact definition of the inner radius of the capillary tube is not always a task easy to solve [40]. The method cannot be used to measure accurately the interfacial tension between two liquids.

Techniques that calculate the interfacial tension based in the shape of a drop are widely used. The techniques of curved interface shape analysis are particularly attractive in research due to its relative simplicity in instrumentation. The experimental setup requires a camera with a low-magnification lens to record the shape of the drop. The interfacial tension can be easily calculated from the dimensions of a drop taken from the photographic picture and by using numerical solutions to surface descriptive equations, i.e. Young-Laplace. Modern instruments generally use image analysis software whose role is to match the entire drop profile to the best fit of the theoretical curve describing the shape of the drop. One good example of this group of methods is the pendant-drop method. In this method, a fluid is injected through a needle in a chamber with an environment in equilibrium with the liquid to be measured. The shape of the drop formed is directly related to the interfacial tension of the fluid. A camera then takes an image of the drop and a computer uses this data to solve the Young-Laplace equation, allowing describing the surface tension. Additionally, the densities of the fluids in equilibrium have to be known.

The pendant drop method requires also very good cleanliness of the equipment, since impurities can strongly affect the measured value of the interfacial tension. Furthermore, the ratio between the radius of the needle and the radius of the forming drop is of great importance, since this is directly related to the precision of the measurement [40].

3.3. The Density Gradient Theory

The density gradient theory (DGT) was first proposed by van der Waals [41] and further developed from Cahn and Hilliard [42] for pure components and extended by Poser and Sanchez [43] to binary mixtures. The core of the theory lies on calculation of the interfacial properties based on bulk-properties of the binary mixture and the surface tension of the pure component. This model can be applied both for VLE and LLE.

The DGT [41, 42, 43] density gradient theory of inhomogeneous systems provides a means for relating an equation of state to surface properties. The density gradient theory leads to a general expression for the Helmholtz free energy density of an inhomogeneous system. With help of the use of this expression in combination with an equation of state a method was developed for calculating the surface tension and density profiles of a pure liquid and mixtures in equilibrium with its vapour.

Using this approach the surface tension of mixtures consisting of non-polar component can be predicted within the experimental error. However, the calculation of surface tension as well as phase equilibria of mixture, where polar or associating components are involved, is more challenging. The applied equation of state has to be chosen with great care.

The DGT for pure substances

The original postulation of the DGT was made by van der Waals [41], but more recently rediscovered by Cahn and Hilliard [42]. In their work, they defined the Helmholtz energy of a non-uniform system. In their paper, they defined the characteristic of a certain property (e.g. concentration c) in a non-uniform system as dependent on both the value of this property on a certain point and the characteristics of this property in the immediate environment. Therefore, the free energy of the system can be described as a function of the property and its derivatives. They also assumed property and derivatives to be able to be treated as

independent variables [42]. In example of the concentration, the Helmholtz energy can then be described in general as a Taylor series around a solution of uniform concentration:

$$f\left(c,\nabla c,\nabla^2 c,...\right)=f_0\left(c\right)+\kappa_1\nabla^2 c+\kappa_2\left(\nabla c\right)^2+... \tag{67}$$

An integration over the total volume of the solution leads to:

$$F=N_V\int_V f dV \tag{68}$$

$$F=N_V\int_V\left[f_0\left(c\right)+\kappa_1\nabla^2 c+\kappa_2\left(\nabla c\right)^2+...\right]dV \tag{69}$$

Further mathematical treatment allows simplifying the equation. The divergence theorem

$$\int_V\left[\kappa_1\nabla^2 c\right]dV=\int_V\left(d\kappa_1/dc\right)\left(\nabla c\right)^2 dV+\int_S\left(\kappa_1\nabla c.n\right)dS \tag{70}$$

Conditions can be defined in such a way that the second term of this integral vanishes. The result for the overall Helmholtz energy is then:

$$F=N_V\int_V\left[f_0\left(c\right)+\kappa\left(\nabla c\right)^2+...\right]dV \tag{71}$$

where

$$\begin{aligned}\kappa&=-d\kappa_1/dc+\kappa_2\\ \kappa&=-\left[\frac{\partial^2 f}{\partial c\partial\nabla^2 c}\right]_0+\left[\frac{\partial^2 f}{\left(\partial\left|\nabla c\right|\right)^2}\right]_0\end{aligned} \tag{72}$$

This equation can be also applied to a flat interface, a non-homogeneous system. In such a case, the properties of the non-homogeneous system only vary perpendicularly to the planar interface. Cutting the Taylor series to the second term results in

$$F = AN_V \int_{-\infty}^{\infty} \left[f_0(c) + \kappa \left(dc/dz \right)^2 \right] dz \tag{73}$$

The interfacial tension is within the Cahn-Hilliard [42] framework as the difference of energy between the actual Helmholtz energy of the system and the one in the case of a homogeneous system (e.g. in equilibrium):

$$\sigma = N_V \int_{-\infty}^{\infty} \left[f_0(c) + \kappa \left(dc/dz \right)^2 - c\mu_B(e) - (1-c)\mu_A(e) \right] dz \tag{74}$$

Or

$$\sigma = N_V \int_{-\infty}^{\infty} \left[\Delta f(c) + \kappa \left(dc/dz \right)^2 \right] dz \tag{75}$$

$$\begin{aligned} \Delta f(c) &= f_0(c) - \left[c\mu_B(e) + (1-c)\mu_A(e) \right] \\ \Delta f(c) &= c\left[\mu_B(c) - \mu_B(e) \right] + (1-c)\left[\mu_A(c) - \mu_A(e) \right] \end{aligned} \tag{76}$$

Eq. 76 shows the condition for a mixture where only one property c (initially concentration) changes across the interface. This expression, which depicts the present inhomogeneities in the interface, is also often called the grand thermodynamic potential, often noted also as $\Delta\omega$. In this case, μ depicts the chemical potential of components A and B in dependence of the property c or at the equilibrium condition e.

Since the original analysis has been made for any property changing along a non-uniform system, an analogy will firstly be made for a pure component. In the case of a pure component, the property changing across the interface is the density. Therefore

$$\sigma = N_V \int_{-\infty}^{\infty} \left[\Delta f(\rho) + \kappa \left(d\rho/dz \right)^2 \right] dz \tag{77}$$

$$\Delta f(\rho) = f_0(\rho) - f(e) \tag{78}$$

The definition of the surface tension (Eqs. 75 and 77) is an integral that has to be minimized [42]. This can be done by applying the Euler Equation to the integrand, resulting in:

$$\Delta f(\rho) - \kappa(d\rho/dz)^2 = const \tag{79}$$

The value of the constant can be defined by analysing the boundary conditions. At $z = \infty$ and $z = -\infty$, the sum of both terms have to be zero, since at these values the system should be in the bulk phases, where changes in Helmholtz Energy are non-existent. This leads to the condition:

$$\Delta f(\rho) = \kappa(d\rho/dz)^2 \tag{80}$$

Replacing in Eq. 77:

$$\sigma = 2N_V \int_{-\infty}^{\infty} \left[\Delta f(\rho)\right] dz \tag{81}$$

Eq. 80 can also be used to change the undefined values of the coordinates ($z = \infty$ and $z = -\infty$) for the well-defined densities of the bulk phases in equilibrium:

$$\sigma = 2N_V \int_{\rho_\alpha}^{\rho_\beta} \left[\kappa \Delta f(\rho)\right]^{1/2} d\rho \tag{82}$$

Also with help of Eq. 80 it is possible to calculate the variation of the density of the fluid across the interface:

$$z = z_0 + \int_{\rho_0}^{\rho} \left(\frac{\kappa}{\Delta f(\rho)}\right)^{1/2} d\rho \tag{83}$$

where z_0 is an arbitrary point given for the coordinates at the density ρ_0.

The so called influence parameter κ , as already noticed, has a theoretical background and can be defined as the second moment of the Ornstein-Zernike correlation function; however, analytical functions are not available. Due to this hindrance, the influence parameter can also be treated as a semiempirical parameter that can be fitted to one surface tension at one single temperature. Once this is done, the DGT framework is supposed to be able to describe the surface tension dependency over a wide range of temperature, assuming a correct mathematical description of the energetic inhomogeneities arising in the interface.

The DGT for mixtures

The original work of Cahn and Hilliard [42] takes into account the change of one variable (concentration, density) across the interface. This is not the case for mixtures on a vapour-liquid equilibrium. For this systems, not only the density, but also concentration of the components change continuously through the interface. Poser and Sanchez [43] postulated an analogous Equation that allows describing both changes across the interface and also calculating the surface tension of a given mixture:

$$\sigma = \int_{-\infty}^{\infty} \left(\Delta f + 0.5 \sum_i \sum_j \kappa_{ij} \frac{d\rho_i}{dz} \frac{d\rho_j}{dz} \right) dz \tag{84}$$

where Δf follows the description given in Eq. 76, and in this case, the so called grand thermodynamic potential not only varies in the density but also in the composition of each present substance. In order to reduce the amount of variables, so called partial densities have been defined:

$$\rho_i = \rho X_i \tag{85}$$

These variables are able to describe the simultaneous changes within the interface of a multicomponent system. Eq. 84 is also subject to some conditions, a group of differential equations equal to the number of components in the system. These equations have the form

$$\frac{\partial \Delta f}{\partial \rho_i} - \sum_j \kappa_{ij} \frac{d^2 \rho_j}{dz^2} = 0 \tag{86}$$

Once the system of equations is solved, and therefore the partial density profiles across the interface, it is possible to integrate Eq. 84 and thus calculate the interfacial tension of a given mixture.

One of the problems for this is the definition of the influence parameters of the mixtures, κ_{ij}. A modified geometric mixing rule can be used to give a value to these parameters in the form of:

$$\kappa_{ij} = \beta \sqrt{\kappa_j \kappa_j} \tag{87}$$

The value of β dictates the path to follow in order to calculate the system of differential equations explained in Eq. 86. As an example, the development for a binary system can be seen. Mixtures with more components will follow the same methodology. In the case of a binary system, the interfacial tension can be written as

$$\sigma = \int_{-\infty}^{\infty} \left(\Delta f + 0.5 \kappa_A \left(\frac{d\rho_A}{dz} \right)^2 + \kappa_{AB} \frac{d\rho_A}{dz} \frac{d\rho_B}{dz} + 0.5 \kappa_B \left(\frac{d\rho_B}{dz} \right)^2 \right) dz \tag{88}$$

Subject to

$$\frac{\partial \Delta f}{\partial \rho_A} - \kappa_A \frac{d^2 \rho_A}{dz^2} - \kappa_{AB} \frac{d^2 \rho_B}{dz^2} = 0 \tag{89}$$

$$\frac{\partial \Delta f}{\partial \rho_B} - \kappa_{AB} \frac{d^2 \rho_A}{dz^2} - \kappa_B \frac{d^2 \rho_B}{dz^2} = 0 \tag{90}$$

Depending on the value of κ_{AB} two cases are possible. In the case of a mixed influence parameter exactly equal to a geometric mixing rule ($\beta = 1$), the system of equations 89 and 90 reduce to an algebraic equation of the type:

$$\kappa_B^{0.5}\frac{\partial \Delta f}{\partial \rho_A}-\kappa_A^{0.5}\frac{\partial \Delta f}{\partial \rho_B}=0 \tag{91}$$

This means, for a given partial density ρ_A there is at least one density ρ_B that can fulfil the condition given before. This can be of use in order to calculate the density profiles necessary for calculation of the interfacial tension. A continuous variation of the partial density ρ_A will result in the same amount of corresponding points of ρ_B, which allow to calculate Eq. 88 numerically. In order to get full information about the density profiles, the following equation can be used in order to calculate the coordinates perpendicular to the interface:

$$z = z_0 + \int_{\rho_B(z_o)}^{\rho_B(z)} \sqrt{\frac{\kappa'}{\Delta\omega(\rho_A,\rho_B)}}\, d\rho_B \tag{92}$$

where

$$\kappa' = \kappa_B + 2\kappa_{AB}\left(\frac{d\rho_A}{d\rho_B}\right) + \kappa_A\left(\frac{d\rho_A}{d\rho_B}\right)^2 \tag{93}$$

In the case of a mixing rule differing from the geometric one ($\beta \neq 1$), a different treatment has to be made. Solution of the differential equation system (Eqs. 89 and 90) can be done with means of a change of variables in order to make a simplification of the system [44]:

$$\begin{aligned} \nu_1 &= \kappa_A\rho_A + \kappa_{AB}\rho_B \\ \nu_2 &= \kappa_{AB}\rho_A + \kappa_B\rho_B \end{aligned} \tag{94}$$

Reducing the system to:

$$\left(\frac{\partial\, \Delta\omega(\rho_A,\rho_B)}{\partial\, \rho_A}\right) = \left(\frac{\partial^2 \nu_1}{\partial\, z^2}\right) \tag{95}$$

$$\left(\frac{\partial \Delta\omega(\rho_A,\rho_B)}{\partial \rho_B}\right)=\left(\frac{\partial^2 \nu_2}{\partial z^2}\right) \tag{96}$$

A discretization scheme results in a system of equations that can be casted on one single non-linear operator $L\langle\ \rangle$. The system to be solved is then

$$L\langle u\rangle = 0 \tag{97}$$

where u contains all variables resulting from the discretization process. An implicit solver may then be used. This methodology has been successfully applied to elliptic problems. With help of one experimental point and the mentioned methodology it is then possible to recalculate the interfacial tension. In this case, density profiles have already been determined fully in the framework of the numerical method.

Some other information about the interfacial phenomena of a mixture can also be calculated with help of the data gotten with help of the DGT, for example the calculation of adsorption isotherms. Telo da Gama and Evans [45], as well as Wadewitz and Winkelmann [46] describe the symmetrized interface segregation $\Delta C(z)$:

$$\Delta C(z)=\frac{\rho_A(z)-\rho_A^L}{a_A}-\frac{\rho_B(z)-\rho_B^L}{a_B} \tag{98}$$

where

$$a_i=\frac{\rho_i^L-\rho_i^V}{\rho_A^L-\rho_A^V+\rho_B^L-\rho_B^V} \tag{99}$$

Once the symmetrized interface segregation is calculated the relative adsorption can also be defined as:

$$\Gamma_{AB}=-a_A\int_{-\infty}^{+\infty}\Delta C(z)dz \tag{100}$$

4. APPLICATION OF THE DENSITY GRADIENT THEORY FOR PURE COMPONENTS

4.1. Non-polar Substances

The first step in the application of the DGT was the calculation of the phase equilibrium of the pure substances, with help of the given PC-SAFT parameters from the literature [33]. Later, the surface tension at one temperature was taken from the literature [47,48,49,50]. The fitted influence parameters are listed in Table 3. Figure 2 shows also the results of the calculation for n-alkanes at a wide temperature range. It is to note that the combination of the DGT + PC-SAFT is able to describe all given components with the fitted influence parameter. Figure 3 shows further results that prove the ability of the DGT to describe the interfacial tension of hydrocarbons, in this case a cyclic one (cyclohexane) and an aromatic one (toluene).

Table 3: Influence parameter κ for non-polar components using PC-SAFT.

Pure component	10^{-20} κ [Jm^5/mol^2]
Methane	1.973
Propane	10.00
Butane	17.81
Pentane	25.91
Hexane	36.298
Heptane	50.92
Toluene	31.89
Cyclohexane	34.07
Nitrogen	1.048

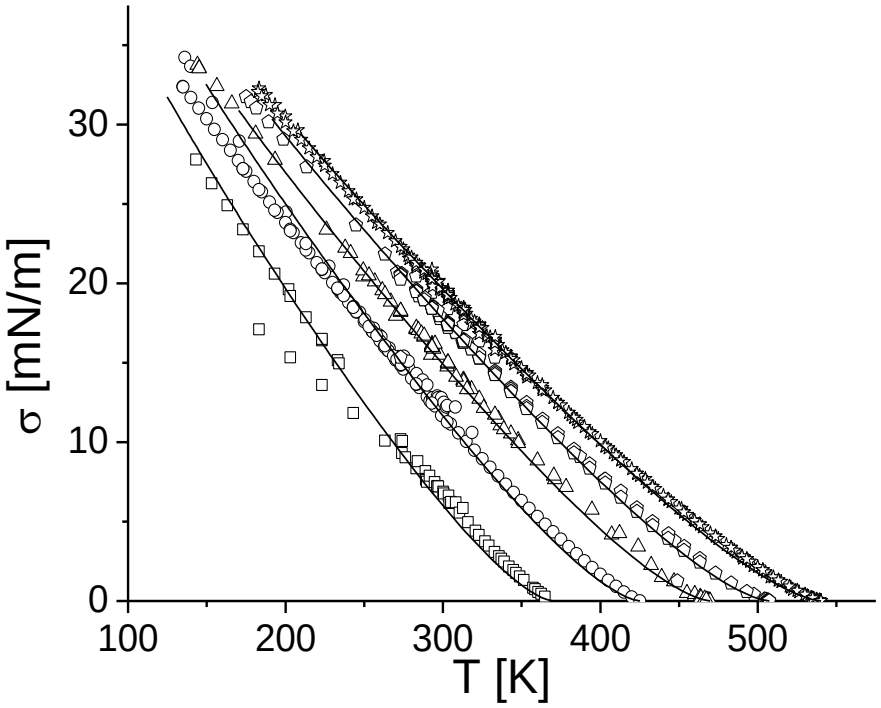

Figure 2: Comparison between experimental [47,48,49,50] and calculated (lines) interfacial tensions for n-alkanes: squares: n-propane, circles: n-butane, triangles: n-pentane, pentagons :n-hexane, stars: n-heptane.

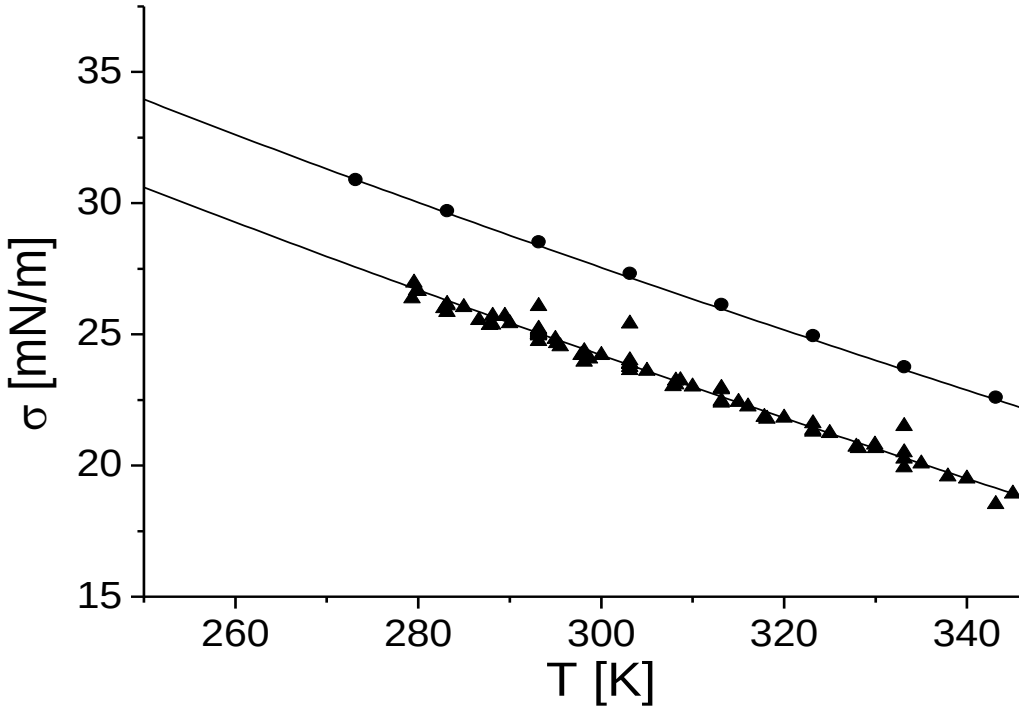

Figure 3: Comparison between experimental [47] and calculated (lines) surfaces tensions for cyclohexane (triangles) and toluene (circles).

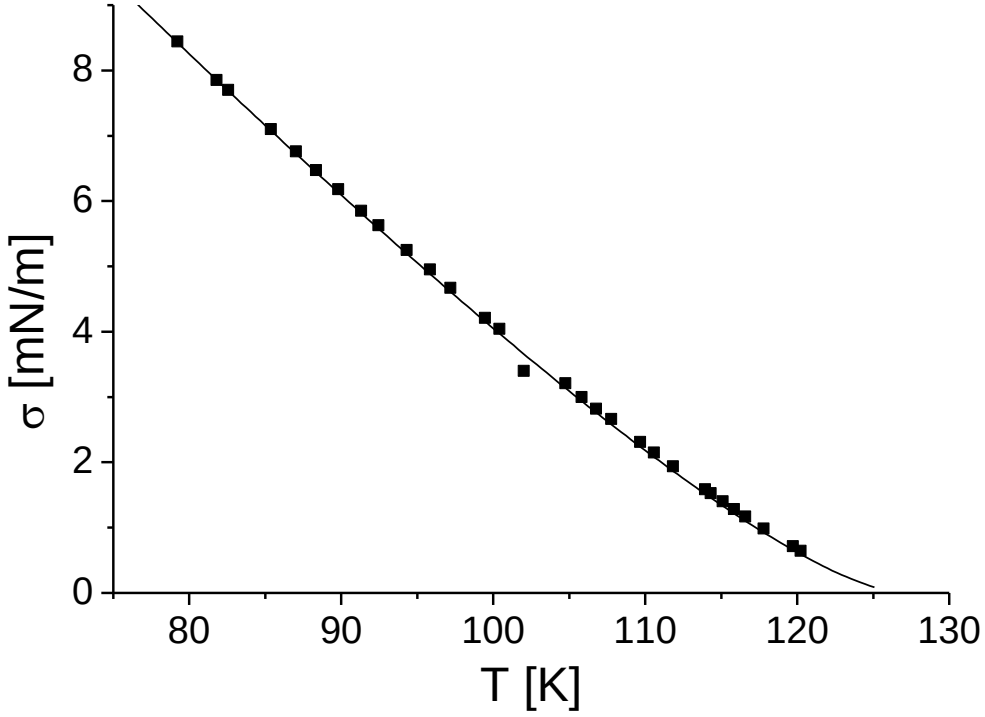

Figure 4: Comparison between experimental surface tensions [47] and calculated ones (line) for nitrogen.

The influence parameters for n-alkanes given in Table 3 can be also expressed as function of the carbon number N:

$$\kappa_{alkanes}^{PC-SAFT} = \left(1.17164 - 0.09767N + 1.0178N^2\right)10^{-20}\,\frac{Jm^5}{mol^2} \qquad (101)$$

Ethane was not included in the parameter estimation. Using Eq. 101 the κ-value for ethane can be calculated and the surface tension of ethane as function of temperature can be predicted. Using Eq. 101 with N=2 the k-value should be $\kappa_{ethane} = 5.0475\times10^{-20}\,Jm^5/mol^2$. The predicted surface tensions together with experimental values taken from the literature [47] are depicted in Figure 5. The theoretical framework does an excellent job in surface tension calculation of ethane.

Decane was also not included in the parameter fitting procedure (see Table 3). Using the relation (Eq. 101) with N=10 results for $\kappa_{decane} = 101.98\times10^{-20}\,Jm^5/mol^2$. Applying this value allows the prediction of the surface tension for decane. The comparison between the predicted and experimental surface tensions is shown in Figure 6.

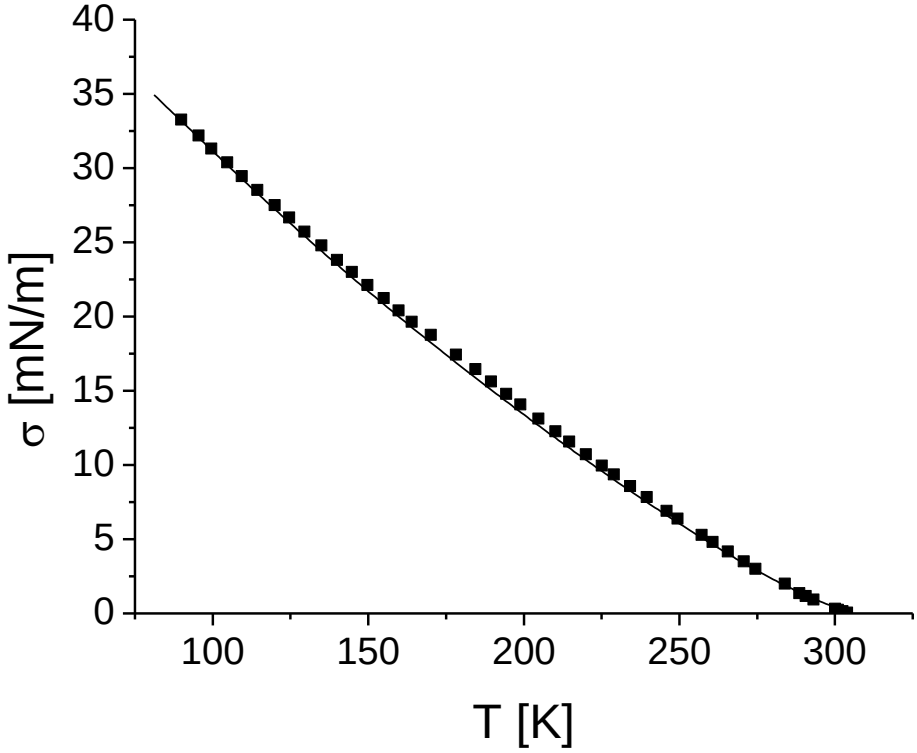

Figure 5: Experimental (squares [47]) and predicted surface tension (solid line) for ethane using PC-SAFT-EOS with Eq. 101.

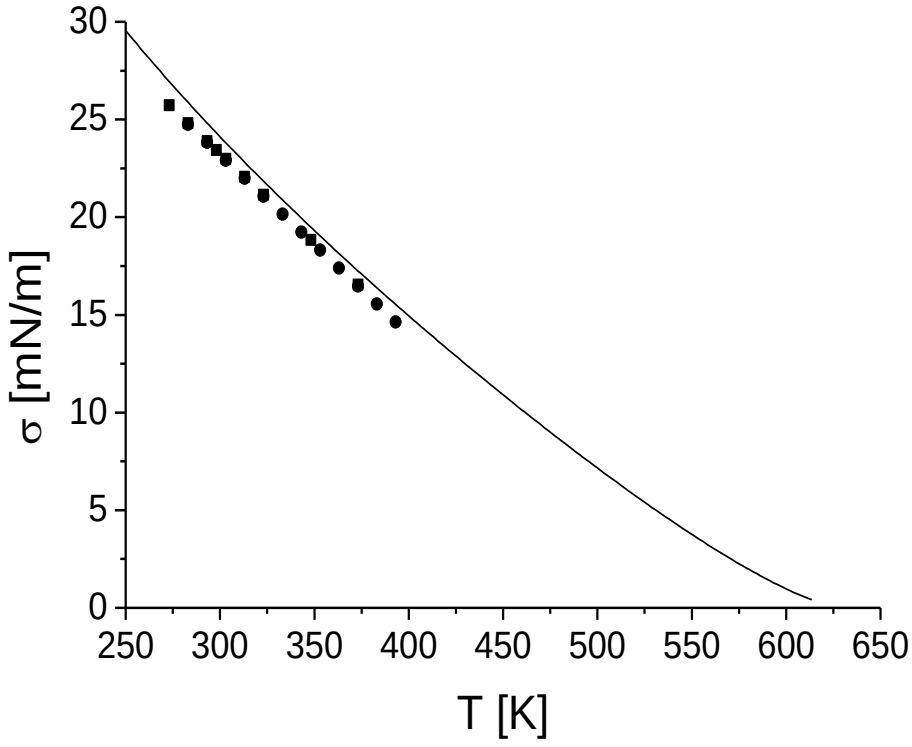

Figure 6: Experimental (squares [51] and circles [49]) and predicted surface tension for n-decane using PC-SAFT-EOS with Eq. 101.

Although Eq. 101 was used for extrapolation from N=7 to N=10 the predicted surface tension of decane is very close to experimental data (Figure 6).

4.2. Polar Substances

Simple Polar Components

Molecules with dipolar moments, namely acetone and chloromethane, were selected in order to preliminary study the performance of the PCP-SAFT-EOS for dipolar molecules for the calculation of surface tensions. Figure 7 demonstrates the performance of the PCP-SAFT-EOS in comparison with the performance of the PC-SAFT-EOS for acetone. Both equations of state are able to describe the experimental values with a high accuracy. The influence of temperature on the surface tension is slightly different. At low temperatures the PC-SAFT-EOS shows slightly better results. However at high temperatures, close to the critical temperature, the PCP-SAFT-EOS leads to slightly better results.

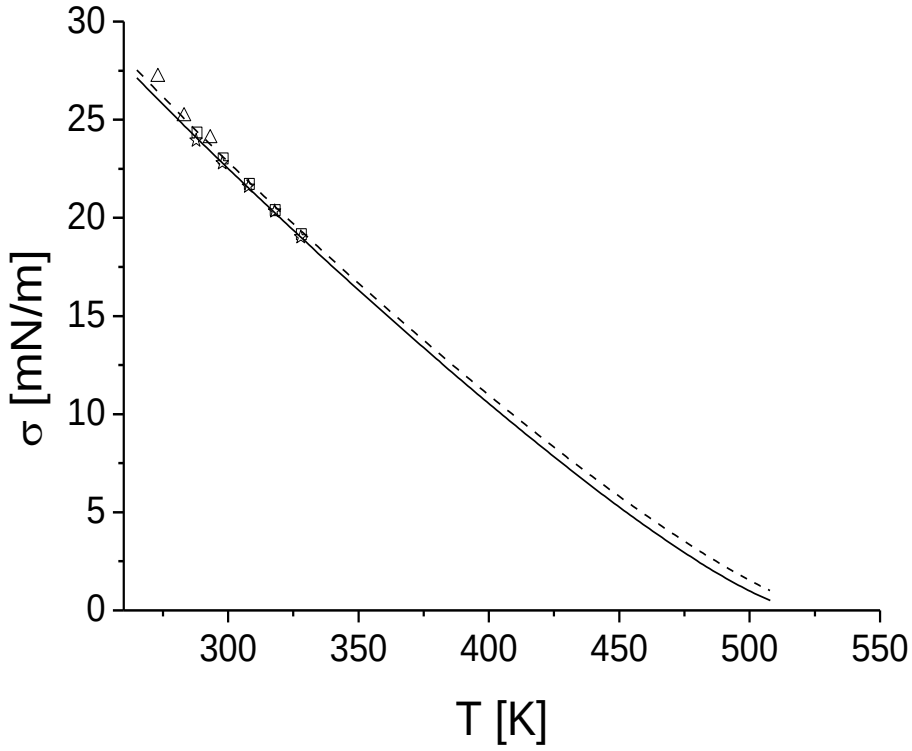

Figure 7: Comparison of experimental (squares [52], triangles [53] and stars [54]) and calculated surface tensions of acetone (PCP-SAFT-EOS: solid line, $\kappa = 11.49 \times 10^{-20}\, Jm^5 / mol^2$; PC-SAFT-EOS: broken line, $\kappa = 11.57 \times 10^{-20}\, Jm^5 / mol^2$).

For chloromethane the experimental surface tension taken from the literature [55, 56, 57] can also be modelled using DGT in combination with PCP-SAFT-EOS (Figure 8).

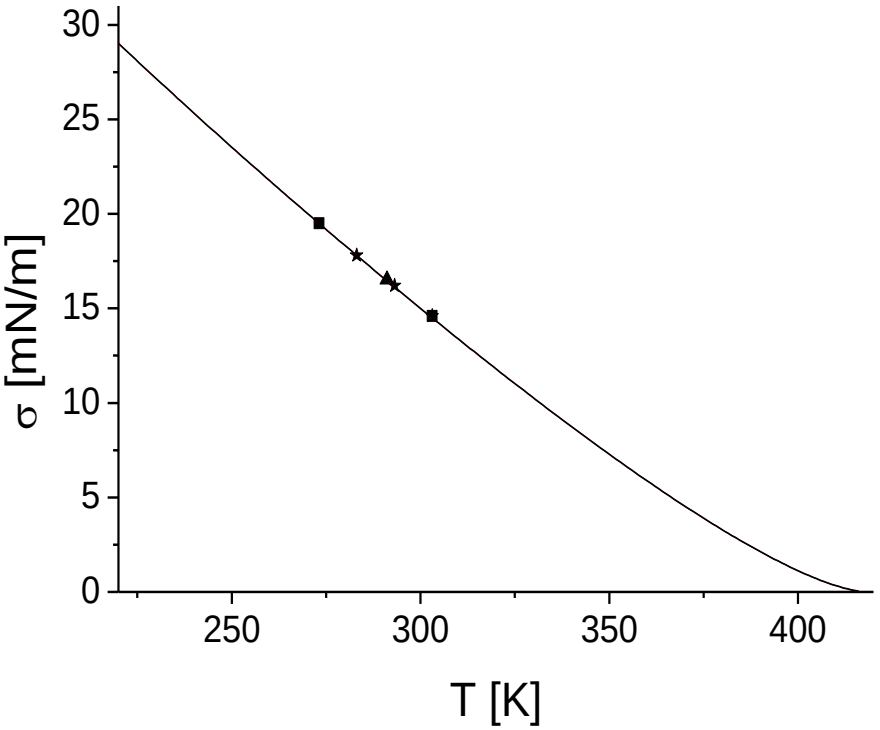

Figure 8: Comparison of experimental (squares [55], triangles [56] and stars [57]) and calculated surface tension of chloromethane using PCP-SAFT-EOS (solid line, $\kappa = 5.67 \times 10^{-20}\, Jm^5 / mol^2$).

One important molecule having a quadrupole moment is CO_2. In Figure 9 the calculated liquid volumes of CO_2 using PC-SAFT and PCP-SAFT are compared with experimental data taken from the literature. The pure component parameters were taken from Gross [36]. It can be clearly recognized the improvement of the calculation results, if the quadrupole of CO_2 is included in the theoretical framework, especially in the critical region. The improvement of the calculated liquid volumes leads to an improvement in the calculated surface tension (Figure 10).

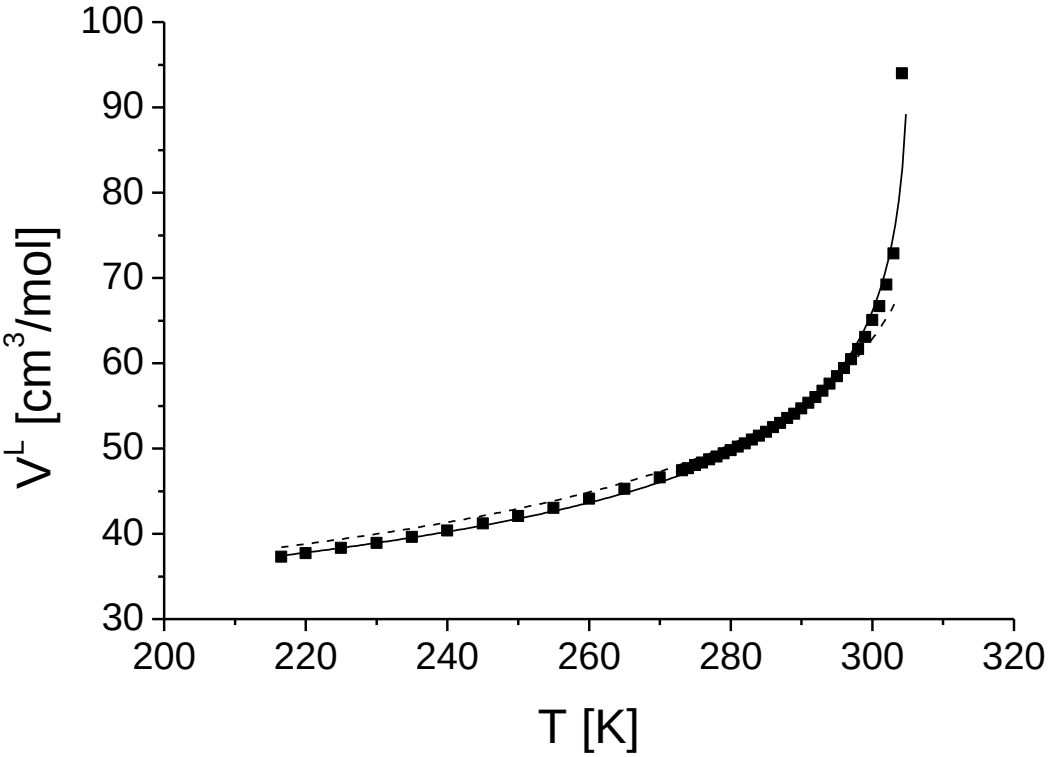

Figure 9: Comparison between calculated liquid volumes of CO_2 using PCP-SAFT (solid line) and PC-SAFT (broken line) with experimental data [57] (symbols).

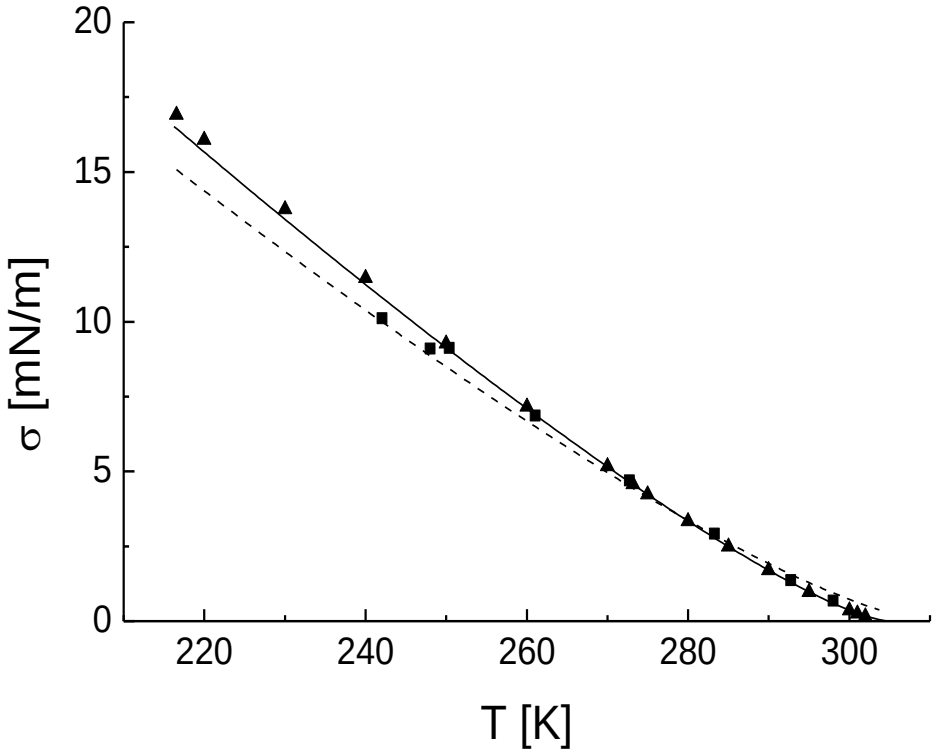

Figure 10: Experimental (squares [48] and triangles [49]) and calculated surface tension of CO_2 using PC-SAFT-EOS (dashed line) with $\kappa = 2.312 \times 10^{-20} Jm^5 / mol^2$ and PCP-SAFT-EOS (solid line) with $\kappa = 2.327 \times 10^{-20} Jm^5 / mol^2$.

Analyzing the data given in Figure 10, it can be concluded the density gradient theory in combination with the PCP-SAFT EOS is able to calculate the temperature dependency of the surface tension of CO_2 in an excellent agreement with experimental data.

Polar Components Exhibiting Self-Association

Water molecules show a strong tendency to form associates through hydrogen bonding. The original association model in the PCP-SAFT-EOS was the so-called 2B association model [34]; however, there has been some discussion about this. Several authors have made SAFT-type parameterization assuming the so called 4C association model [e.g. 58]. Within the 4C model four association sites are assumed for the molecule. The parameters must therefore be fit for the new model. For the parameter fitting procedure liquid volumes and vapour pressure data [48] were applied. A comparison of the parameters related to both association models can be seen in Table 4. The liquid density plays a crucial role for the calculation of the surface properties. For these reason, the experimental [48] and calculated liquid volumes are compared in Figure 11. This shows the improvement that the incorporation of the association model 4C instead of model 2B brings to the liquid volume, especially at lower temperatures.

Table 4: Comparison of parameters for water with the models 2B and 4C.

Model	m	σ [Å]	ε / k_B [K]	ε^{AB} / k_B [K]	κ^{AB}	Source
2B	1.0656	3.0007	366.51	2500.7	0.034868	[34]
4C	1.0656	3.0007	366.51	1800	0.01	This work

For the calculation of the association term in the PCP-SAFT framework the monomer mole fraction X_A plays an important role. This quantity is available by IR spectroscopy [59]. In Figure 12 the experimental data can be compared with the calculated results using PC-SAFT-EOS in combination with the 4C association model. The calculated values are very close to the experimental findings in the data published by Luck [59].

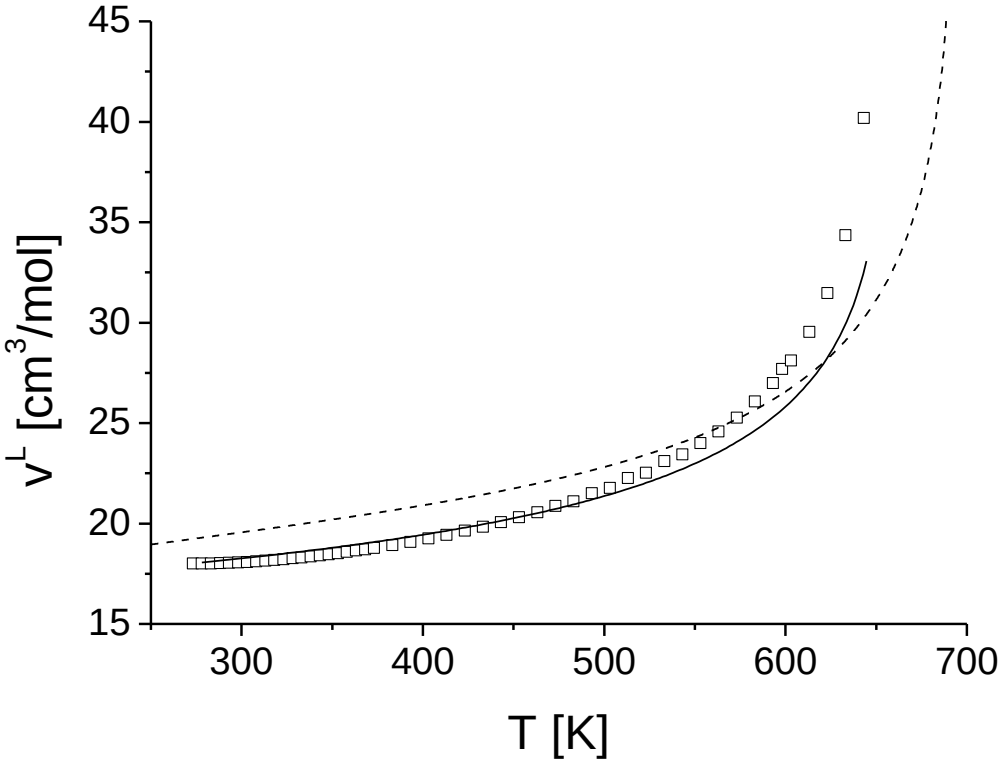

Figure 11: Experimental (open squares [48]) and calculated (solid line: PCP-SAFT-EOS-4C; broke line: PCP-SAFT-EOS-2B) liquid volumes of water.

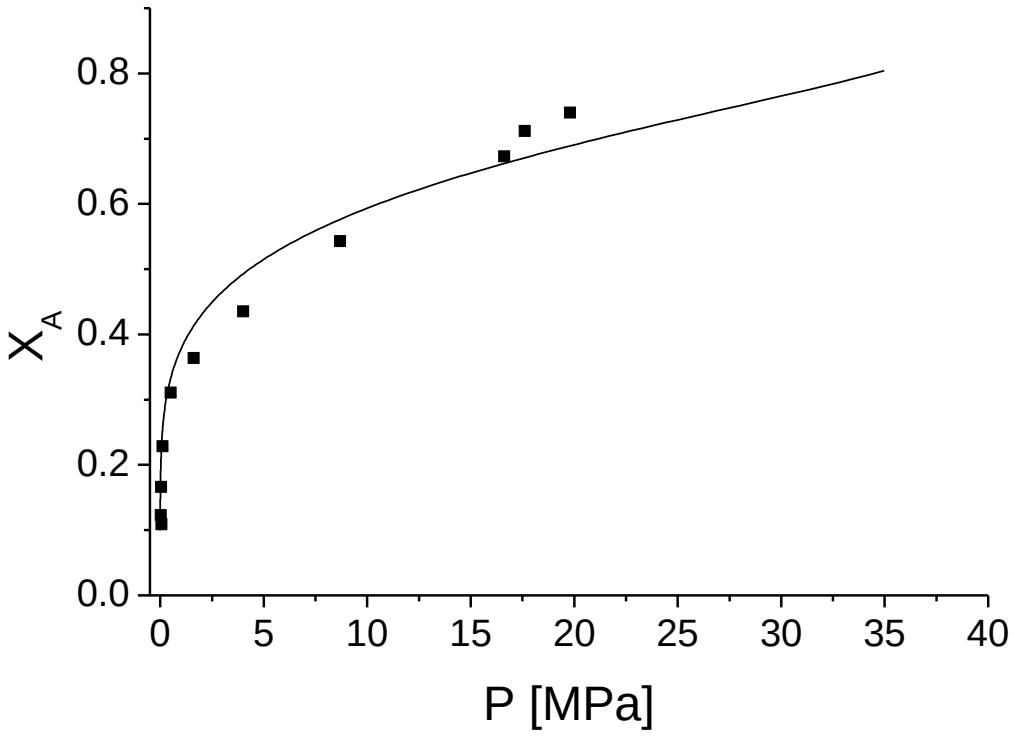

Figure 12: Experimental (squares [59]) and calculated (line PC-SAFT-EOS with 4C) free monomer mole fraction of water.

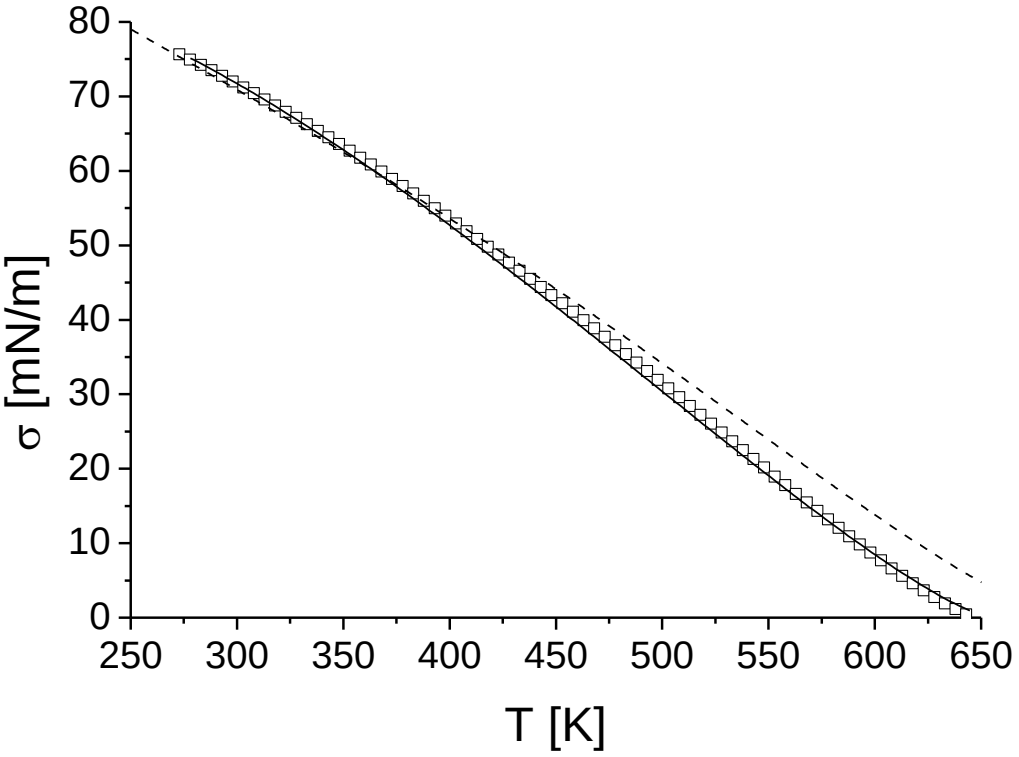

Figure 13: Experimental (open squares [47]) and calculated surface tension (broken line PC-SAFT-EOS with 2B [$\kappa = 1.3785 \cdot 10^{-20} Jm^5 / mol^2$] and solid line PC-SAFT-EOS with 4C [$\kappa = 0.84 \cdot 10^{-20} Jm^5 / mol^2$]) of water.

The modelled surface tension of water as function of temperature is compared with experimental data taken from the literature [47] and plotted in Figure 13. The calculated surface is improved if 4 association sites are taken into account instead of two. Using PCP-SAFT-EOS with four association sites leads to an excellent agreement between the calculated and the experimental data, even in the critical region, where problems could arise. Gloor et al. [60] performed also calculations of the surface tension of water using SAFT-VR DFT. In this work [60] the pure-component parameters were fitted to the VLE. The corresponding values of the surface tension obtained with this set of parameters using the SAFT-VR-DFT shows the correct sigmoidal shape as function of temperature, but they are not in quantitative agreement with the experimental data. This problem was solved by the application of surface tension data to the parameter fitting procedure [60]. Figure 14 shows the behaviour of the density profiles for water across the interface at different temperatures. This behaviour supports the idea of very fundamental principles: At the

critical point the two phases, vapour and liquid, become one. Therefore, at higher temperatures the length of the interface must increase into infinity.

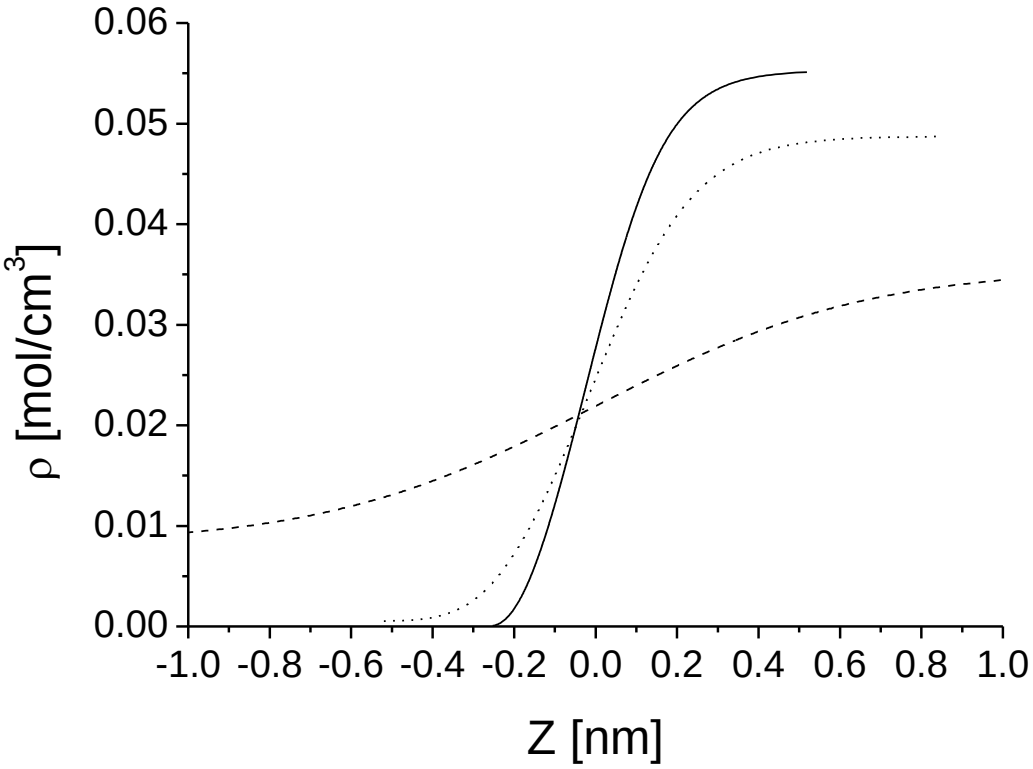

Figure 14: Density profiles for pure water at different temperatures (solid line: $T = 278.15K$; dotted line: $T = 460.48K$; broken line: $T = 626.24K$).

4.3. Substances containing Sulphur

Substances containing sulphur are of great importance in the oil industry, since many reservoirs also contains substances of this type. Therefore, it is necessary to gain knowledge about the liquid-vapour equilibrium of such pure substances. Three substances will be analysed: sulphur trioxide, sulphur dioxide and hydrogen sulphide.

Sulphur trioxide is a well-known pollutant. Due to its structure, the molecule lacks of polarity, which means that the VLE for this substance can be described with help of the original version of PC-SAFT proposed by Gross and Sadowski [33]; however, no parameters are available in the literature. Furthermore, experimental data is also very scarce. The available data [61] has been therefore used to make a parameter set under the PC-SAFT framework. The values of the PC-SAFT parameters can be seen in Table 5. A comparison between the experimental and the calculated values can be

seen in Figure 15, where only low deviations in comparison with the experimental data [61] can be observed. Additionally, the DGT has been applied with use of the fitted parameters and the influence parameter has been calculated, with a good agreement with the results from the literature, as seen in Figure 16.

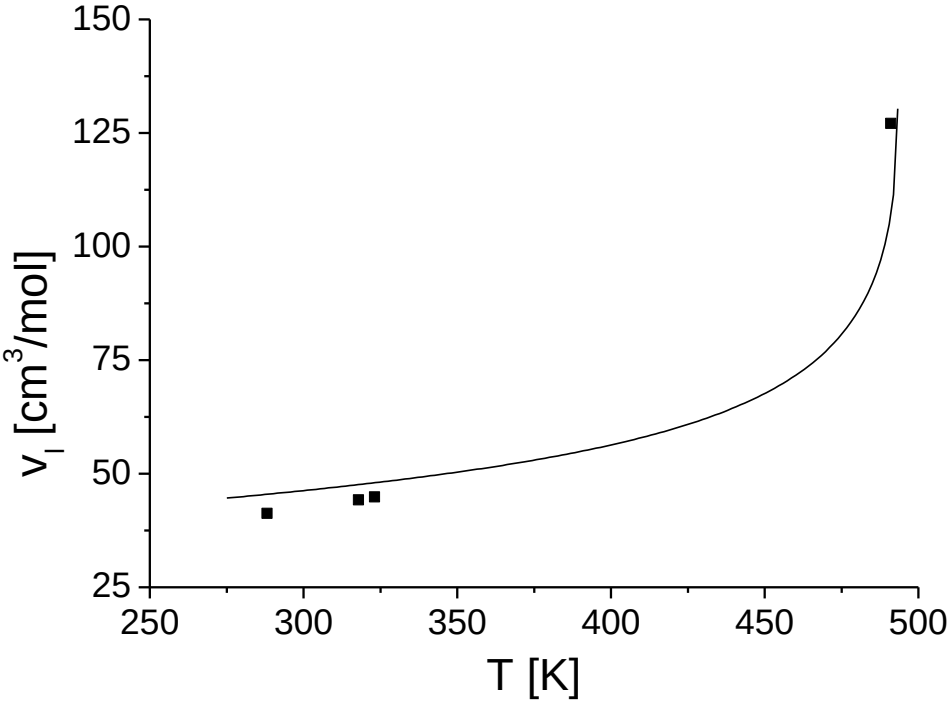

Figure 15: Comparison between literature molar volumes (squares [61]) and calculated values (solid line) for sulphur trioxide with the parameters from Table 5.

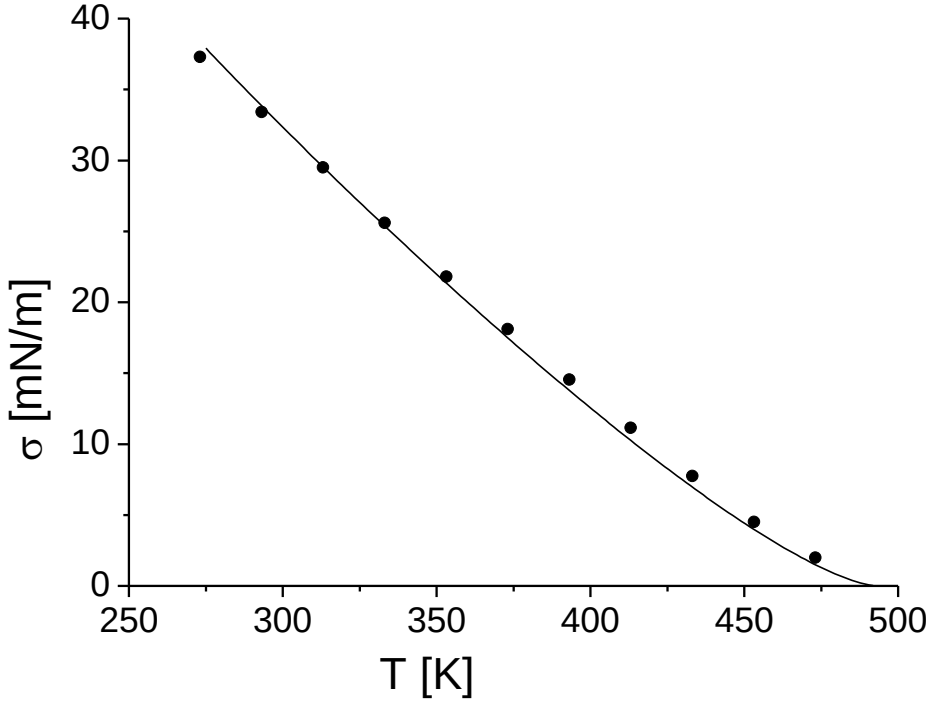

Figure 16: Experimental (circles [62]) and calculated surface tension (solid line with $\kappa = 5.675 \cdot 10^{-20}\, Jm^5 / mol^2$) of sulphur trioxide.

Table 5: Parameter set for the description of the properties of SO_3

Model	m	σ [Å]	ε / k_B [K]	Source
PC-SAFT	3.6315	3.4991	209.4	This work

A further sulphur-containing component of interest is sulphur dioxide. This molecule exhibits a dipolar moment of $\mu^{SO_2} = 1.62D$. Hence, the VLE of SO_2 has to be modelled in the PCP-SAFT framework. The available parameters from the literature [33] had described the substance without the polar contribution. Again, a new set of parameters was fitted to literature data [61, 63]. The inclusion of the dipolar contribution to the Helmholtz energy and the refitting of the parameters lead to an improvement in comparison with the experimental data [61, 63] in terms of the liquid molar volume, as seen in Figure 17. Additionally, a comparison with both approaches for calculation of the interfacial tension can be seen in Figure 18. The PCP-SAFT approach with the new parameters is able to capture the behaviour with dependency of temperature, even when reaching the critical point.

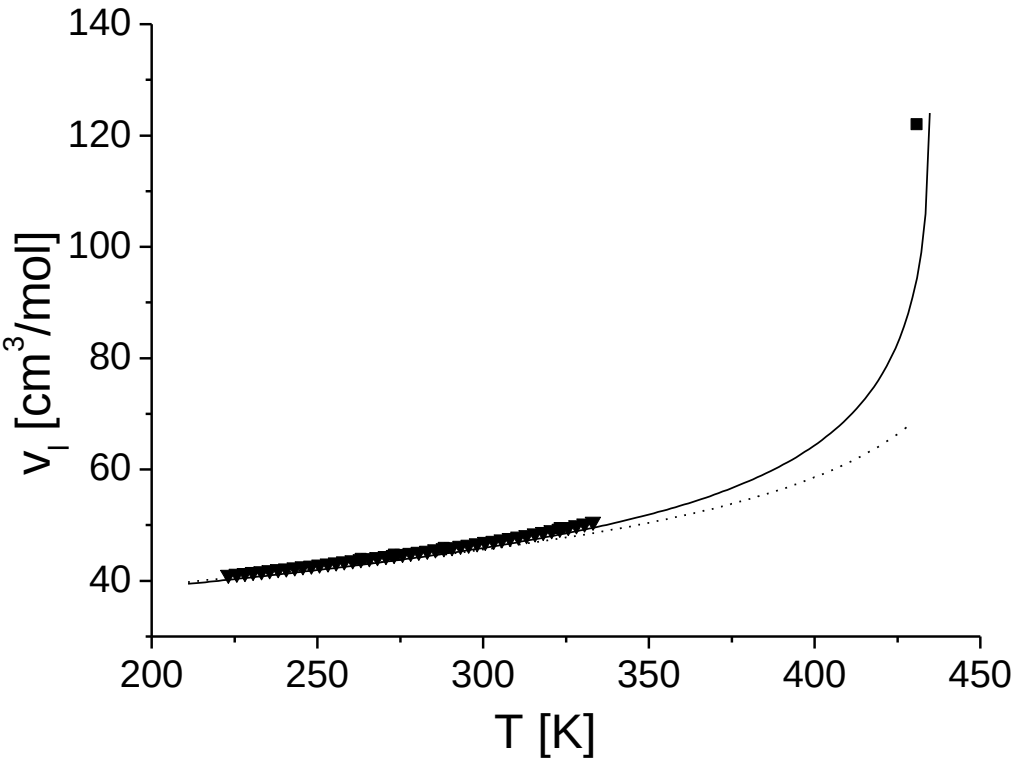

Figure 17: Comparison between literature molar volumes (squares [61] and triangles [63]) and calculated values with PC-SAFT (dotted line) and PCP-SAFT (solid line) for sulphur dioxide with the parameters from Table 6.

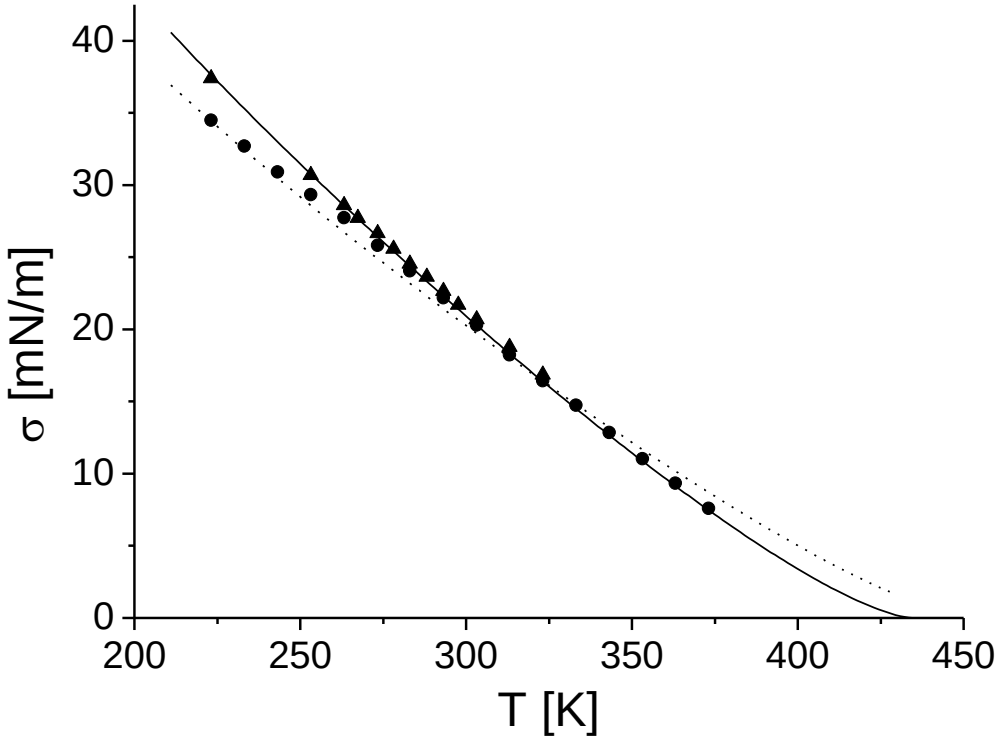

Figure 18: Experimental (circles [64] and triangles [65]) and calculated surface tension (dotted line PC-SAFT with $\kappa = 3.472 \cdot 10^{-20} Jm^5 / mol^2$ and solid line PCP-SAFT with $\kappa = 4.3725 \cdot 10^{-20} Jm^5 / mol^2$) of sulphur dioxide.

Table 6: Comparison of parameter sets for the description of the properties of SO_2

Model	m	σ [Å]	ε / k_B [K]	Source
PC-SAFT	2.8611	2.6826	205.35	[33]
PCP-SAFT	2.9101	2.6361	195.5	This work

In the case of some molecules, the understanding of the interaction phenomena between molecules is not complete, and a lot of different theories arise. Such is the case of H_2S, a highly relevant component of several oil and gas reservoirs. Apart from a set of parameters that describe the substance under the classical PC-SAFT framework [66], some authors have made an analysis of different self-association schemes for the molecules [67], and Tang and Gross [68] compared the effects of introducing both the association and the polar terms for the description of the phase equilibrium of H_2S. Fact is that the molecule shows an experimental dipolar moment of $\mu^{H_2S} = 0.97D$. On the other side, the validity of a self-association-scheme for this substance is not yet completely proven. In the case of water, the high electronegativity of oxygen induces the formation of hydrogen bonds with other molecules; such is also the case of nitrogen is several compounds. In the case of

sulphur, the electronegativity difference with hydrogen does not seem to be enough to induce the formation of such bridges between molecules of the same kind. Therefore, the proposed scheme for H_2S is the use of the dipolar term of PCP-SAFT, and to assume no self-association of the molecule. In the case of a mixture with self-associating compounds, it is very likely that, due to the presence of this partially charged hydrogen ends, the molecule will exhibit cross-association. Unfortunately, no parameter set was found with these characteristics, which led to a fitting of a new parameter set for H_2S. Table 7 shows a comparison between the parameters available in the literature and the new fitted parameter set.

Figure **19** shows the comparison of the calculated densities for H_2S compared with literature data [69]. Figure 20 shows a comparison between literature data [70, 71] and the application of the DGT combined with PCP-SAFT and the new parameter set, with $\kappa = 3.428 \cdot 10^{-20} Jm^5 / mol^2$ [72]. A more detailed analysis and comparison of the different models for H_2S can be seen in the work of Danzer [72]. Both phase equilibrium and interfacial tension of H_2S can be accurately described within the PCP-SAFT framework, ignoring self-association interactions. Furthermore, the model is also able to give good descriptions of under- and supercritical densities.

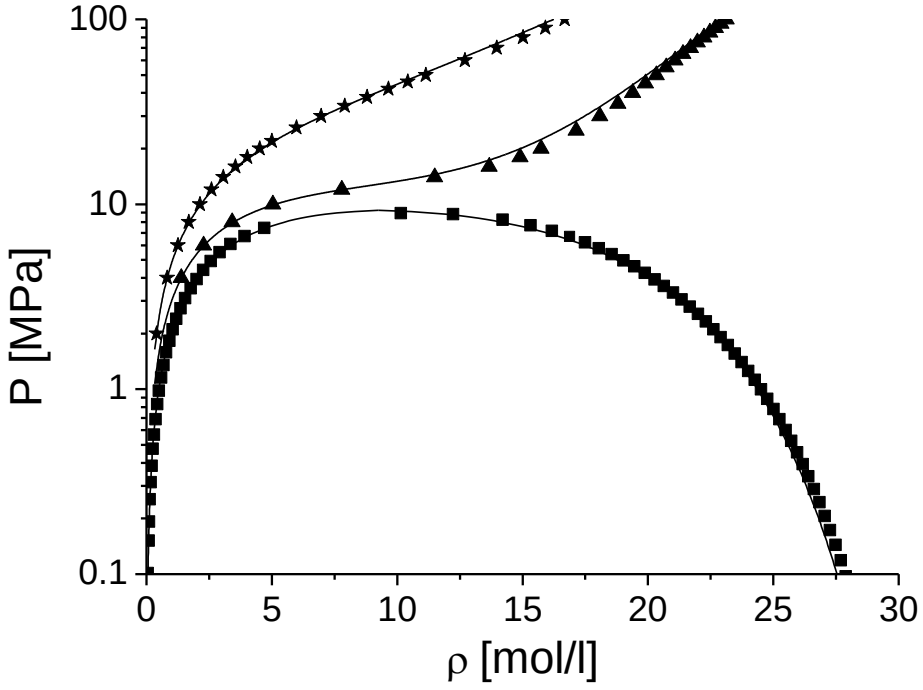

Figure 19: Comparison between literature densities [69] and calculated values (solid lines) from PCP-SAFT for H_2S. Squares: VLE densities; triangles: Isothermal densities at 400 K; stars: Isothermal densities at 600 K. The parameter from this work have been used for calculations.

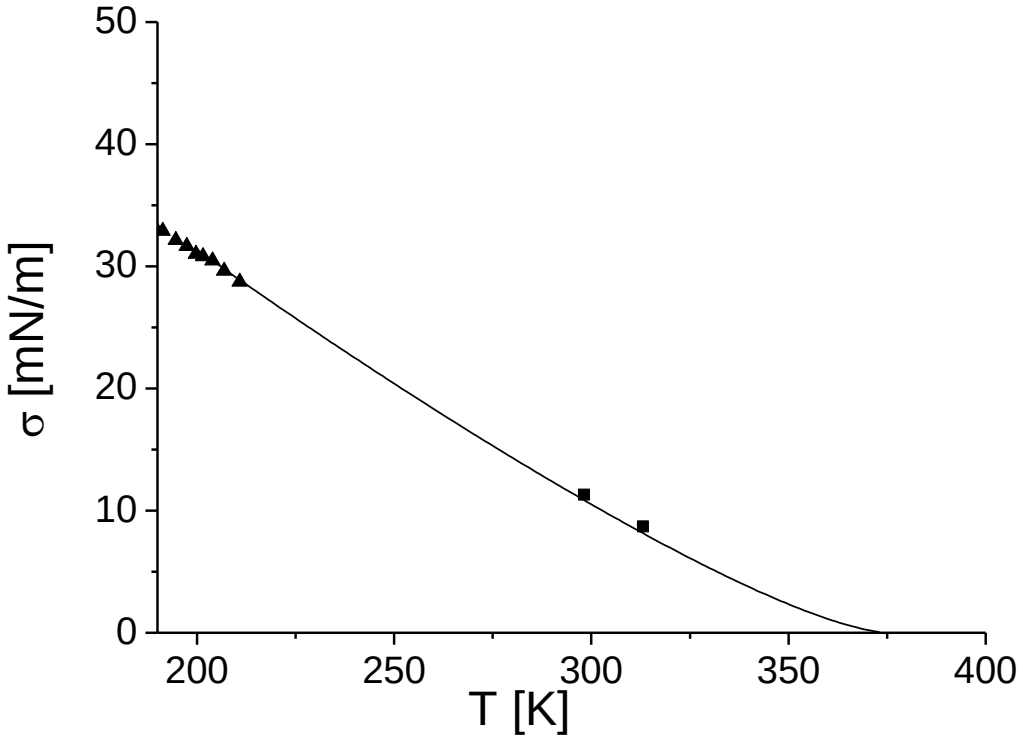

Figure 20: Comparison between experimental surface tensions (triangles [70] and squares [71]) and calculated values [72] from PCP-SAFT for H_2S with $\kappa = 3.428 \cdot 10^{-20}\, Jm^5 / mol^2$.

Table 7: Comparison of parameter sets for the description of the properties of H_2S

Model	M	σ [Å]	ε / k_B [K]	κ^{AB}	ε^{AB} / k_B [K]	Source
PC-SAFT	1.6686	3.0349	229	-	-	[66]
PC-SAFT (2B)	1.6517	3.0737	227.34	0.009952	426.03	[67]
PC-SAFT (3B)	1.5725	3.1373	231.46	0.009910	425.22	[67]
PC-SAFT (4C)	1.3935	3.3015	241.57	0.009915	424.7	[67]
PC-SAFT (2B)	1.649	3.055	229.84	0.001	536.6	[68]
PCP-SAFT (2B)	1.355	3.309	234.25	0.001	780.8	[68]
PCP-SAFT	1.6615	3.055	224.5	-	-	This work

5. APPLICATION OF THE DENSITY GRADIENT THEORY FOR MIXTURES

5.1. Binary Mixtures

Non-polar Mixtures

The simplest mixtures that can be regarded in the theoretical framework DGT + PC-SAFT are hydrocarbon mixtures. Since the purpose of this work is the description of mixtures that can represent multicomponent systems present in the oil industry, a mixture of a light hydrocarbon and a heavier one was first analysed. In this case, the system of methane + n-alkanes was calculated. In order to do predictions about the interfacial properties of the mixture, the equilibrium has to be described. Figure 21 shows the results of calculations for the system methane + n-heptane. A value for the binary interaction parameter $k_{ij} = 0.03$ was found to describe the VLE accurately at different temperatures. Furthermore, it is possible to predict the interfacial tension of mixtures of methane + n-heptane at 298K, as can be seen in Figure 22. It is actually expected that for hydrocarbon mixtures the value of the binary interaction parameter k_{ij} has to tend to zero. Figure 22 shows therefore calculations for the system methane + n-hexane at two different temperatures with the binary interaction parameter for the system set to zero. Furthermore, the pure geometrical mixing rule for the influence parameters should be sufficient for a prediction of the interfacial tension of the mixture. In both cases, the combination of the DGT with PC-SAFT EOS is able to describe the values of the interfacial tensions with accuracy inside the experimental error.

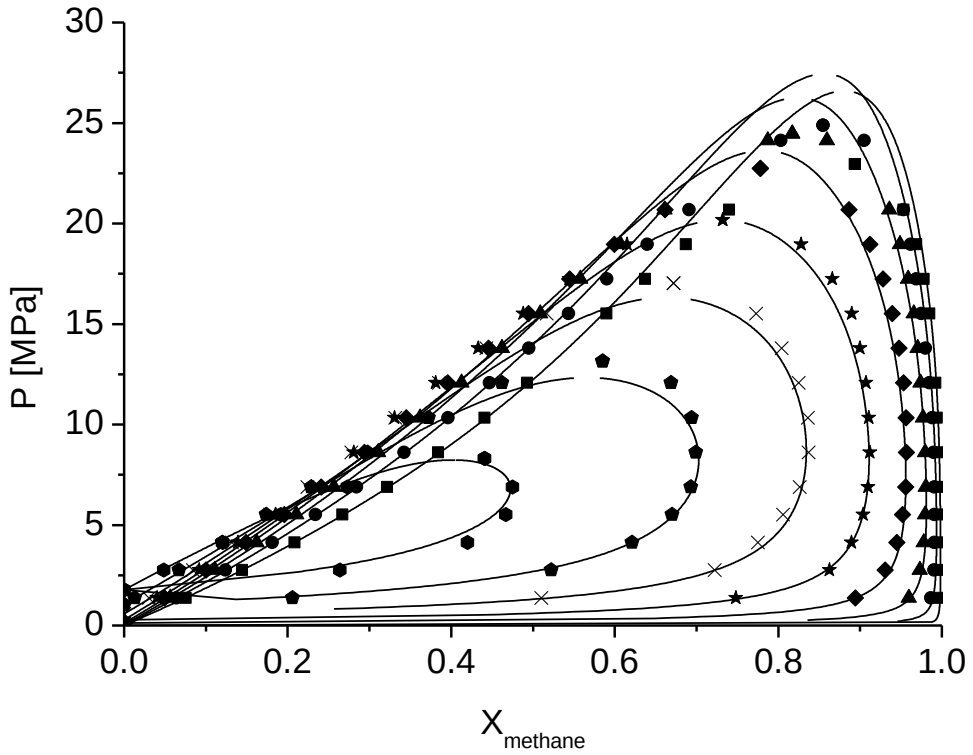

Figure 21: VLE of the system methane + n-heptane. Experimental Data [57] for 277.59 K (squares), 310.93 K (circles), 344.26 K (triangles), 377.59 K (diamonds), 410.93 K (stars), 444.26 K (crosses), 477.59 K (pentagons) and 510.93 K (hexagons). Solid lines represent the calculation with PC-SAFT with a $k_{ij} = 0.03$.

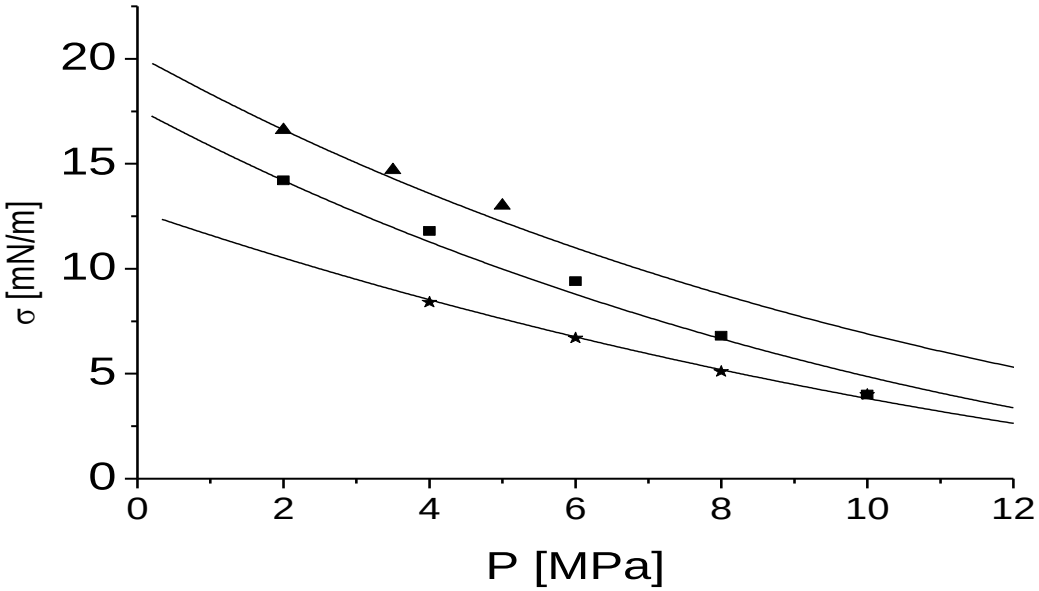

Figure 22: Comparison between experimental [73] and calculated (solid lines) surface tensions for different methane+ n-alkane mixtures : methane + hexane T=300K (squares), methane + hexane T=350K (stars), methane + heptane T=298K and $k_{ij} = 0.03$ (triangles).

Haslam et al. [74] suggested the integration of potentials all over the space in order to expand the methodology made by Hudson and McCoubrey [75] for a theoretical framework in order to define the binary interaction parameter k_{ij}. The work of Hudson and McCoubrey [75] defined a way to extrapolate London's Theory [76] to other r^6 dependant potentials. The extrapolation of Haslam et al. [74] extends the theory to any other non r^6 potential by an integration over the whole space in the form:

$$\psi_{ij} = \int_{\theta=0}^{\pi} \int_{\phi=0}^{2\pi} \int_{r_{ij}=\sigma_{ij}}^{\infty} \phi_{ij}(r_{ij}) r_{ij}^2 dr_{ij} \sin\theta d\phi d\theta \tag{102}$$

The potential function in this case for the London [76] dispersion and PC-SAFT [33] can be expressed as follows:

$$\begin{aligned} \phi_{ij}^{London} &= -\frac{3}{2} \frac{\alpha_{0,i}\alpha_{0,j}}{(4\pi\varepsilon_0)^2 r_{ij}^6} \frac{I_i I_j}{(I_i + I_j)} \\ \phi_{ij}^{PC-SAFT} &= \begin{cases} \infty & r < (\sigma - s_1) \\ 3\varepsilon & (\sigma - s_1) \le r < \sigma \\ -\varepsilon & \sigma \le r < \lambda\sigma \\ 0 & r \ge \lambda\sigma \end{cases} \end{aligned} \tag{103}$$

Through integration, the overall potential can be described for both London's potential and the potential within the PC-SAFT framework:

$$\begin{aligned} \frac{\psi_{ij}^{London}}{4\pi} &= -\frac{1}{3(4\pi\varepsilon_0)^2 \sigma_{ij}^3} \left(\frac{3}{2} \frac{I_i I_j}{(I_i + I_j)} \alpha_{0,i}\alpha_{0,j} \right) \\ \frac{\psi_{ij}^{PC-SAFT}}{4\pi} &= -\frac{\varepsilon_{ij}^{PC} \sigma_{ij}^3 \left(\lambda_{ij}^3 - 1 \right)}{3} \end{aligned} \tag{104}$$

It is to notice that in the case of PC-SAFT only the attractive (dispersive) interactions have been taken into account. Hence, both integrated potentials can be equated as follows:

$$\frac{1}{3(4\pi\varepsilon_0)^2 \sigma_{ij}^3} \left(\frac{3}{2} \frac{I_i I_j}{(I_i + I_j)} \alpha_{0,i}\alpha_{0,j} \right) = \frac{\varepsilon_{ij}^{PC} \sigma_{ij}^3 \left(\lambda_{ij}^3 - 1 \right)}{3} \tag{105}$$

Gross and Sadowski [33] already defined λ and set it to a fixed quantity of 1,5, and s_i to a value of 0,12σ. In the case of a pure substance it can be seen that

$$\frac{I_i}{4(4\pi\varepsilon_0)^2\sigma_{ii}^3}\left(\alpha_{0,i}^2\right)=\frac{\varepsilon_{ii}^{PC}\sigma_{ii}^3\left((1.5)^3-1\right)}{3}$$
$$\alpha_{0,i}=\sqrt{\frac{4*2.375\varepsilon_{ii}^{PC}\sigma_{ii}^6(4\pi\varepsilon_0)^2}{3I_i}} \qquad (106)$$
$$\alpha_{0,i}=2\sigma_{ii}^3(4\pi\varepsilon_0)\sqrt{\frac{2.375\varepsilon_{ii}^{PC}}{3I_i}}$$

$$\alpha_{0,j}=2\sigma_{jj}^3(4\pi\varepsilon_0)\sqrt{\frac{2.375\varepsilon_{jj}^{PC}}{3I_j}} \qquad (107)$$

The polarizabilities of components i and j may be replaced in equation 105:

$$\frac{1}{3\left(4\pi\varepsilon_0\right)^2\sigma_{ij}^3}\left(\frac{3}{2}\frac{I_iI_j}{(I_i+I_j)}4\sigma_{jj}^3\sigma_{ii}^3\left(4\pi\varepsilon_0\right)^2\sqrt{\frac{2.375\varepsilon_{jj}^{PC}}{3I_j}}\sqrt{\frac{2.375\varepsilon_{ii}^{PC}}{3I_i}}\right)=\frac{2.375\varepsilon_{ij}^{PC}\sigma_{ij}^3}{3} \qquad (108)$$
$$\frac{2\sigma_{jj}^3\sigma_{ii}^3}{\sigma_{ij}^6}\frac{\sqrt{I_iI_j}}{(I_i+I_j)}\sqrt{\varepsilon_{jj}^{PC}\varepsilon_{ii}^{PC}}=\varepsilon_{ij}^{PC}$$

At this point it is necessary to define the characteristics of the mixed parameters, σ_{ij} and ε_{ij}. This will help us find out an analytical expression for the binary interaction parameter k_{ij}:

$$\varepsilon_{ij}^{PC}=\left(1-k_{ij}\right)\sqrt{\varepsilon_{jj}^{PC}\varepsilon_{ii}^{PC}}$$
$$\sigma_{ij}=\frac{\sigma_{ii}+\sigma_{jj}}{2}$$
$$\frac{2^7\sigma_{jj}^3\sigma_{ii}^3}{\left(\sigma_{ii}+\sigma_{jj}\right)^6}\frac{\sqrt{I_iI_j}}{(I_i+I_j)}\sqrt{\varepsilon_{jj}^{PC}\varepsilon_{ii}^{PC}}=\left(1-k_{ij}\right)\sqrt{\varepsilon_{jj}^{PC}\varepsilon_{ii}^{PC}} \qquad (109)$$
$$k_{ij}=\left(1-\frac{2^7\sigma_{jj}^3\sigma_{ii}^3}{\left(\sigma_{ii}+\sigma_{jj}\right)^6}\frac{\sqrt{I_iI_j}}{(I_i+I_j)}\right)$$

As an example the binary interaction parameter using the ionisation potential given by Haslam et al [74] and the potential parameters given by Gross and Sadowski [33] for the binary system methane-pentane results in:

$$k_{C_1-C_5} = \left(1 - \frac{2^7 * 3.7729^3 * 3.7039^3}{(3.7729+3.7039)^6} \frac{\sqrt{12.61*10.28}}{(12.61+10.28)}\right)$$
$$k_{C_1-C_5} = \left(1 - \frac{128*53.7064*50.8133}{(7.4768)^6} \frac{11.3855}{(22.89)}\right) = 5.45*10^{-3} \quad (110)$$

It is possible to do such a calculation analogously for every single pair of the hydrocarbon group from C=1 to C=8 using the already available data.

Table 8: Calculated binary interaction parameters for PC-SAFT [33].

k_{ij}	CH_4	C_2H_5	C_3H_8	C_4H_{10}	C_5H_{12}	C_6H_{14}	C_7H_{16}
C_2H_5	2.87E-03	-	-	-	-	-	-
C_3H_8	2.89E-03	9.30E-04	-	-	-	-	-
C_4H_{10}	4.05E-03	3.11E-03	6.46E-04	-	-	-	-
C_5H_{12}	5.45E-03	5.30E-03	1.81E-03	2.94E-04	-	-	-
C_6H_{14}	6.44E-03	6.48E-03	2.52E-03	6.16E-04	6.08E-05	-	-
C_7H_{16}	7.63E-03	7.38E-03	3.08E-03	9.23E-04	2.03E-04	5.20E-05	-
C_8H_{18}	8.82E-03	8.93E-03	4.12E-03	1.52E-03	5.01E-04	2.15E-04	7.56E-05

The results from Haslam et al [74] for a similar SAFT model are comparatively higher for almost every single analyzed pair, as seen in Table 9.

Table 9: Calculated binary interaction parameters for SAFT-VR [74].

k_{ij}	CH_4	C_2H_5	C_3H_8	C_4H_{10}	C_5H_{12}	C_6H_{14}	C_7H_{16}
C_2H_5	1.57E-03	-	-	-	-	-	-
C_3H_8	4.88E-03	1.80E-03	-	-	-	-	-
C_4H_{10}	1.05E-02	6.47E-03	1.48E-03	-	-	-	-
C_5H_{12}	1.33E-02	8.87E-03	2.74E-03	2.00E-04	-	-	-
C_6H_{14}	1.95E-02	1.49E-02	6.60E-03	1.87E-03	9.10E-04	-	-
C_7H_{16}	2.26E-02	1.75E-02	8.29E-03	2.80E-03	1.54E-03	1.20E-04	-
C_8H_{18}	2.55E-02	2.03E-02	1.04E-02	4.09E-03	2.53E-03	4.50E-04	1.30E-04

The theory gives a hint about the behaviour of the binary interaction parameter for different mixtures. In this particular case of non-polar molecules (n-alkanes) it is possible to find out a value for the parameter which is very low; leading to the assumption than in this case the geometric mixing rule can be applied with the

expectation of minimal deviations. The work of Haslam et al. [74] also comprised an extrapolation to system of not only non-polar systems, but also mixtures containing polar or associating components. Some of the postulations made in this paper will be used in further sections of this work. The results of the work have proven to be useful in describing dispersion forces; however, other forces inside the SAFT framework were also discussed, but the results did not achieve the wished accuracy to describe equilibria. Therefore, this analysis will be left during this work up to this point.

Further mixtures of non-polar components can be used to prove the efficacy of the theoretical framework. Let us discuss now mixtures of hydrocarbons with nitrogen. The VLE of nitrogen + n-alkane systems at different temperatures is depicted from Figure 23 to Figure 25. It is possible to describe all the systems with the given binary interaction parameters. Additionally, it is possible to find a correlation between the number of carbons in the n-alkane chain and the value of the binary interaction parameter of the mixture with nitrogen, as seen in Figure 26. This dependency can be used to predict the VLE for other systems, such as the system nitrogen + n-nonane, as seen in Figure 27. The calculated values can describe the behaviour of this mixture in good manner over a wide range of temperatures.

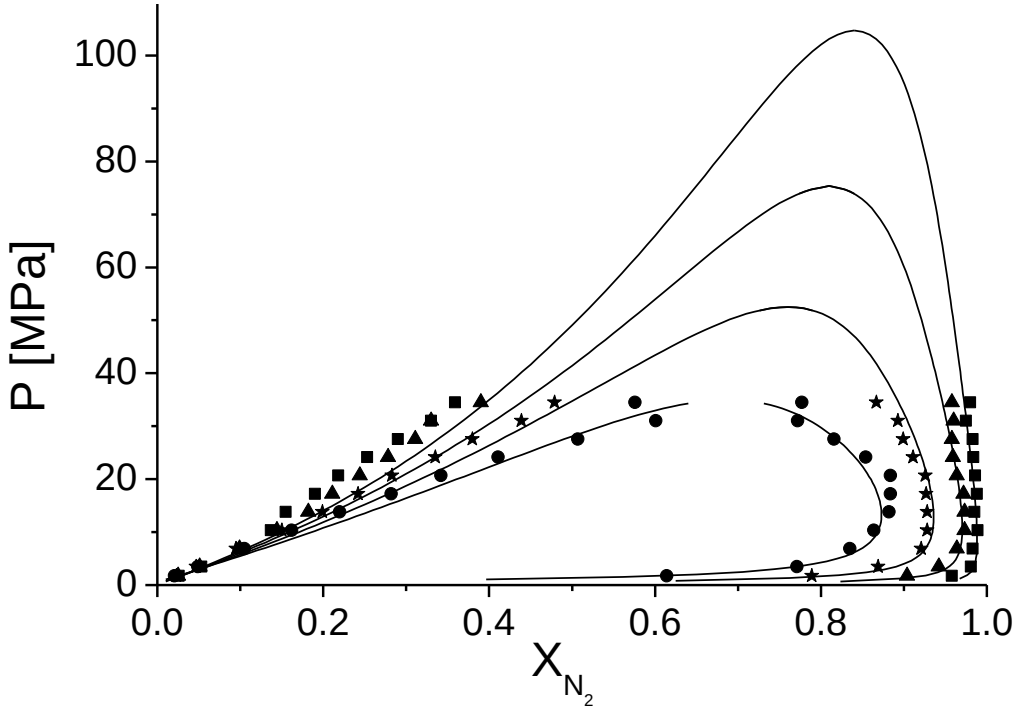

Figure 23: VLE for the system nitrogen + n-hexane. Data from the literature [77] at 310.93 K (squares), 344.23K (triangles), 377.59K (stars) and 410.93K (circles). Solid lines show the calculations with PC-SAFT with a $k_{ij} = 0.089$.

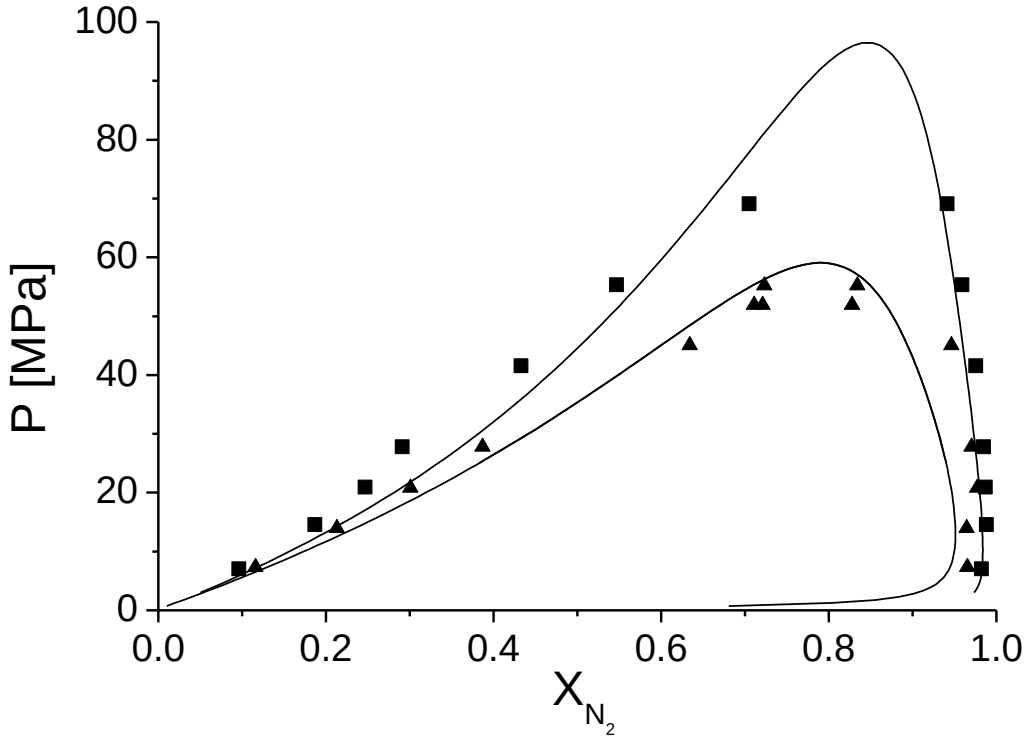

Figure 24: VLE for the system nitrogen + n-heptane. Data from the literature [57] at 352K (squares) and 399K (triangles). Solid lines show the calculations with PC-SAFT with a $k_{ij} = 0.09$.

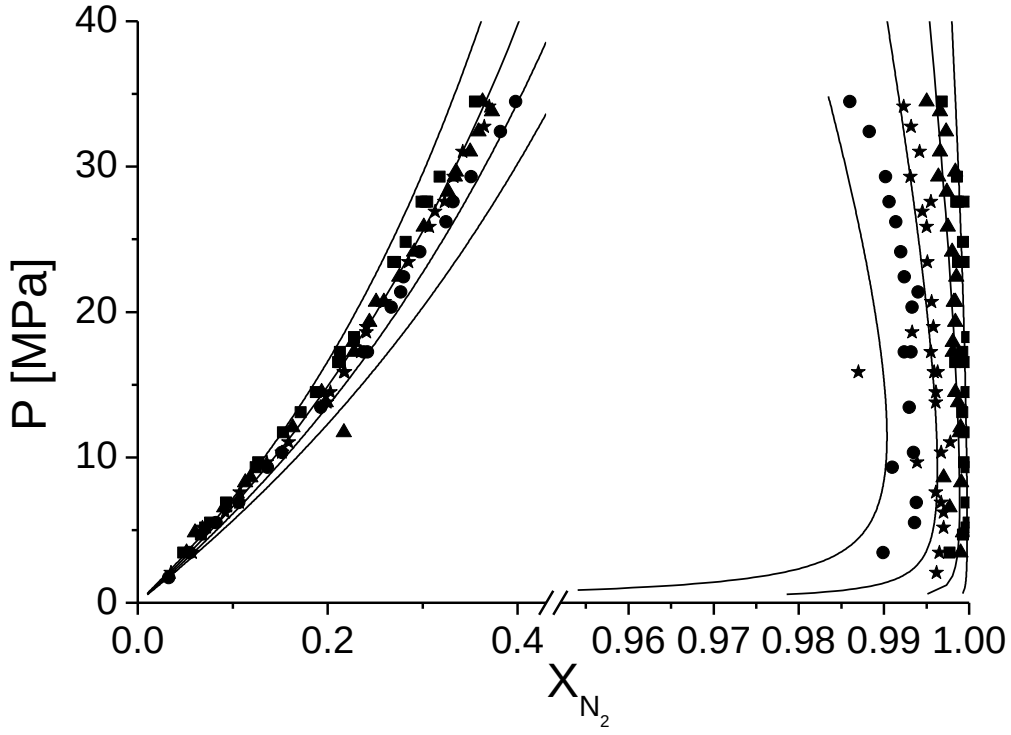

Figure 25: VLE for the system nitrogen + n-decane. Data from the literature [78] at 310.93 K (squares), 344.23K (triangles), 377.59K (stars) and 410.93K (circles). Solid lines show the calculations with PC-SAFT with $k_{ij} = 0.1$.

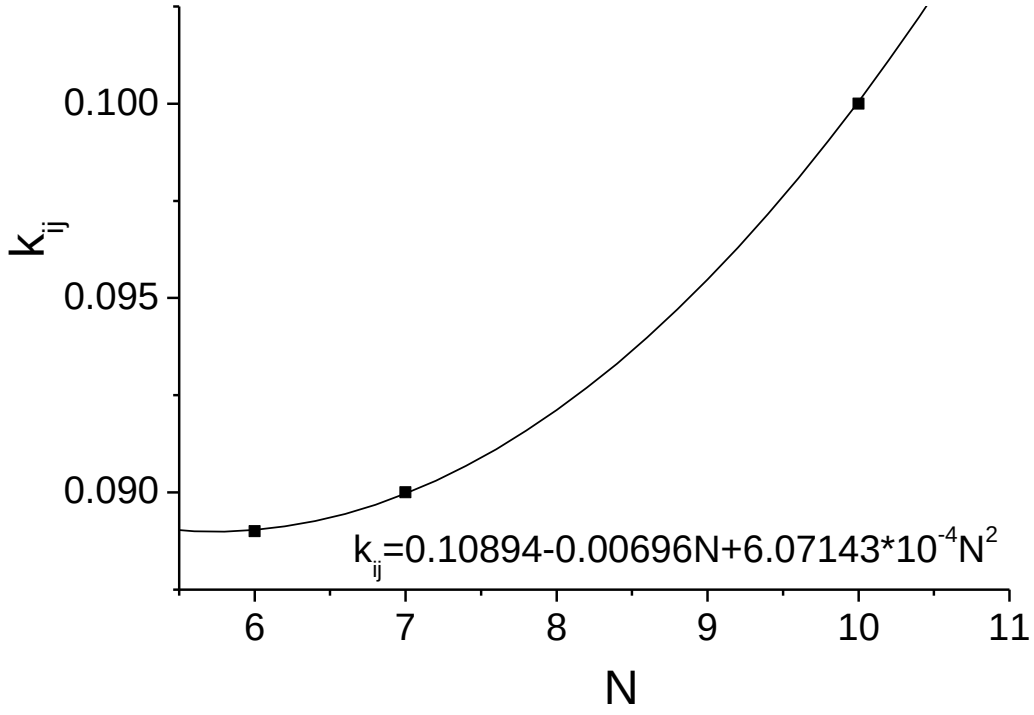

Figure 26: Dependency of the binary interaction parameter to the number of carbons in a chain for nitrogen + n-alkane mixtures.

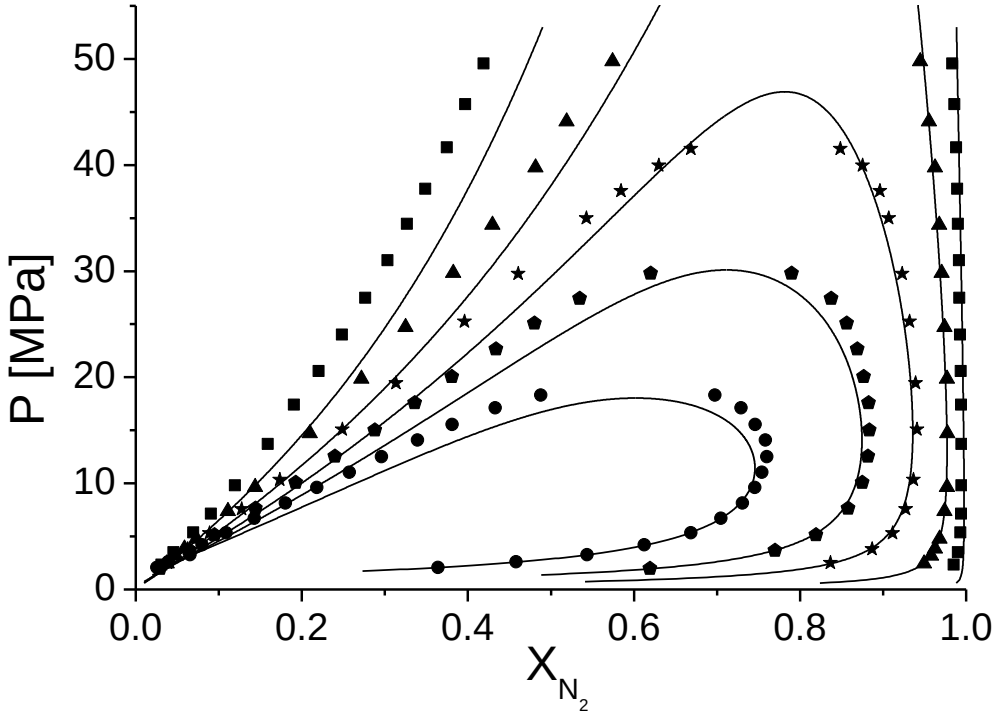

Figure 27: Full prediction of the VLE for the system nitrogen + n-nonane. Data from the literature [57] at 344.3 K (squares), 423.5K (triangles), 473.4K (stars), 508.1K (pentagons) and 543.4 (circles). Solid lines show the predictions with PC-SAFT with a $k_{ij} = 0.0955$.

The DGT can also be applied for nitrogen mixtures, as seen in Figure 28. The experimental data [79] measured the dependency of the interfacial tensions over a broad pressure range for mixtures of nitrogen + hexane, octane and decane. It is interesting to see the ability of the DGT + PC-SAFT to describe accurately the systems nitrogen + hexane and nitrogen + decane. In the case of the mixture with octane, the agreement is also good, but larger deviations arise. It is difficult to find a reason for these deviations in the theoretical calculations. But observing the points, it might be possible that a higher pressures the experimental data presents some problems for this mixture. Measurement of interfacial tension for these mixtures is not easy. Any impurity can drastically modify the measured value. This might be the case in the mixture of nitrogen + n-octane. It is otherwise not to explain the way the curve always comes closer to the values of the hexane mixture, while the decane one remains with a more or less equal distance over the whole pressure range.

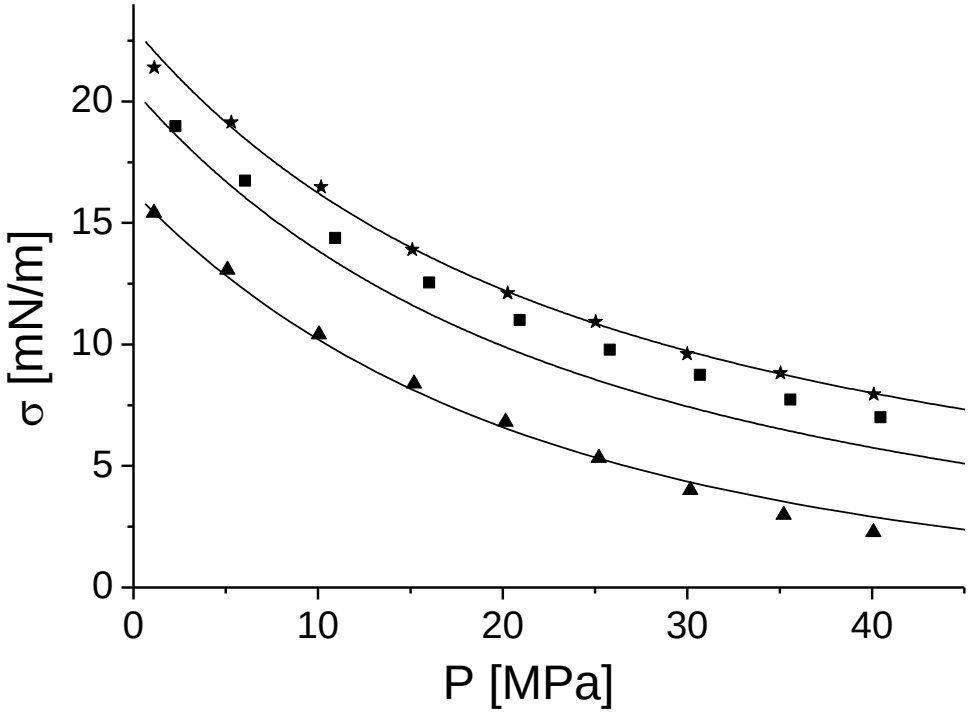

Figure 28: Calculated and experimental surface tensions for several nitrogen + n-alkane mixtures at 313.15K. Experimental data [79]: nitrogen + n-hexane (triangles), nitrogen + n-octane (squares), nitrogen + n-decane (stars). Solid lines represent the DGT + PC-SAFT calculations.

Another experimental dataset was used for validation of the calculations of nitrogen mixtures, namely the system nitrogen + n-heptane at different temperatures, as seen in Figure 29. In this case, the calculations were carried out for a mixture at different

temperatures and a variable pressure range. In all cases, the DGT is able to qualitatively describe the behaviour of the interfacial tension; furthermore, in the higher temperatures there is a very good agreement between the calculated and the data from the experiments [80].

In the framework of the DGT, the so called partial density profiles were calculated in order to be able to integrate the given expression for the interfacial tension of the mixture. An example of these profiles can be seen in Figure 30 for the mixture of nitrogen and n-heptane, at a given temperature and composition of the liquid phase. While the hydrocarbon, being the less volatile component, presents a continuous and monotonic density profile at the interface, the much more volatile nitrogen exhibits the presence of a peak between both bulk phase partial densities. This peak, called relative enrichment, is of great importance and has to be taken into account due to the possibility of mass transfer hindrance for this component between both phases, since there is a “potential” difference that needs to be overcome for a molecule to migrate from one phase to the other.

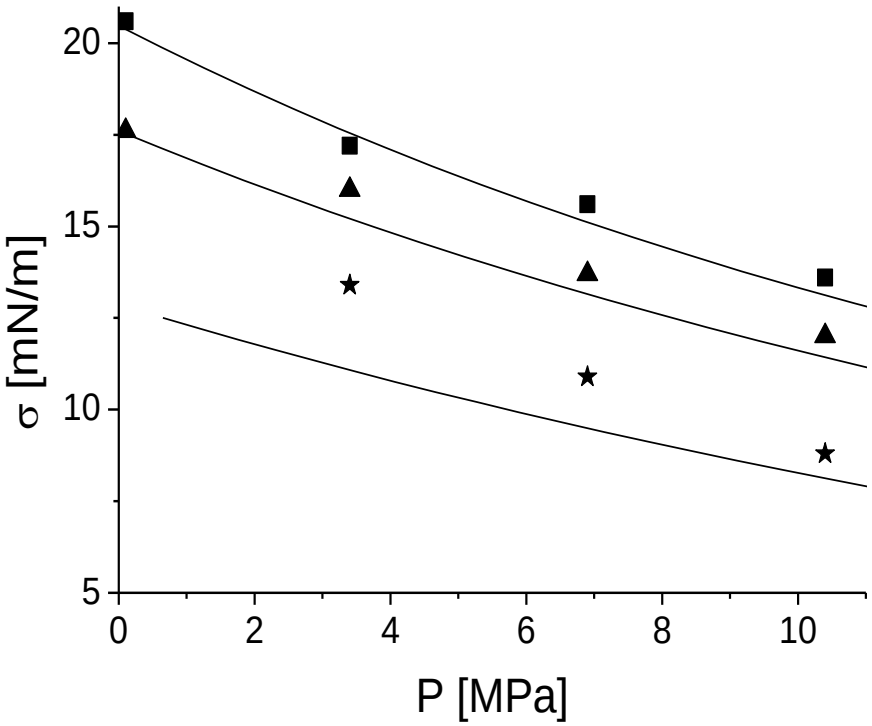

Figure 29: Calculated and experimental [80] surface tensions for the system nitrogen + n-heptane at 295K (squares), 323K (triangles) and 373K (stars). Solid lines represent the calculated values with help of the combination of the DGT + PC-SAFT.

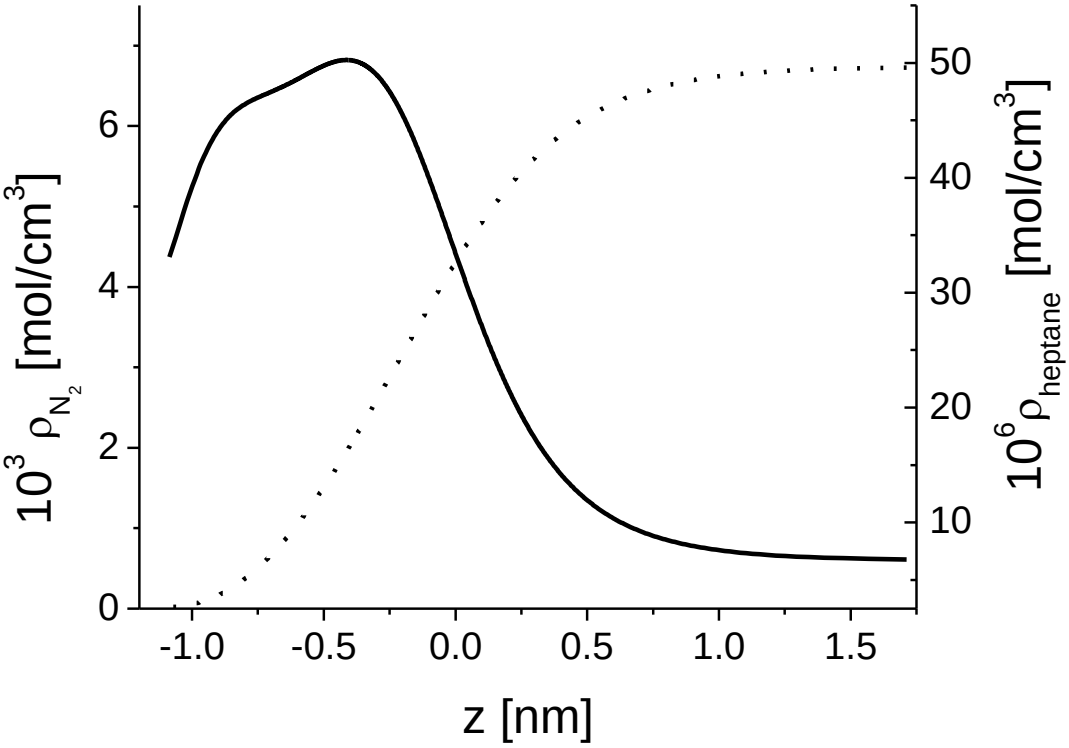

Figure 30: Partial density profiles across the vapour-liquid interface for the mixture nitrogen + n-heptane at $X^L_{N_2} = 0.001$ and 295 K. Solid line: partial density profile for nitrogen. Dashed line: partial density profile for n-heptane.

Mixtures of a polar and a non-polar component

In order to study the possibility to predict the surface tension of mixtures containing one non-polar and one component having a polar or quadrupole moment the system CO_2 + n- alkane with different chain lengths of the n-alkanes and the system CO_2 + cyclohexane were chosen. There is data measured by Hsu et al. [81] for the systems containing n-alkanes. The phase equilibria of the system CO_2 + butane was already calculated by Gross [36]. In this paper [36] a temperature-independent binary interaction parameter $k_{ij} = 0.036$ was found. Using this binary interaction parameter phase equilibria, shown in Figure 31 and Figure 32, were calculated. Both coexisting volumes at equilibrium condition could be predicted with a high accuracy (Figure 31), even in the critical region. Beside the volumes also the phase composition can be modelled with a high accuracy (Figure 32). The improvement of the performance of different EOS can also be recognized by analyzing the k_{ij}-value. Using a cubic EOS (Peng-Robinson), k_{ij} has to be 0.124. With SAFT-EOS or PC-SAFT one has a value of $k_{ij} = 0.12$ [82]. With PCP-SAFT-EOS this value decreases ($k_{ij} = 0.036$).

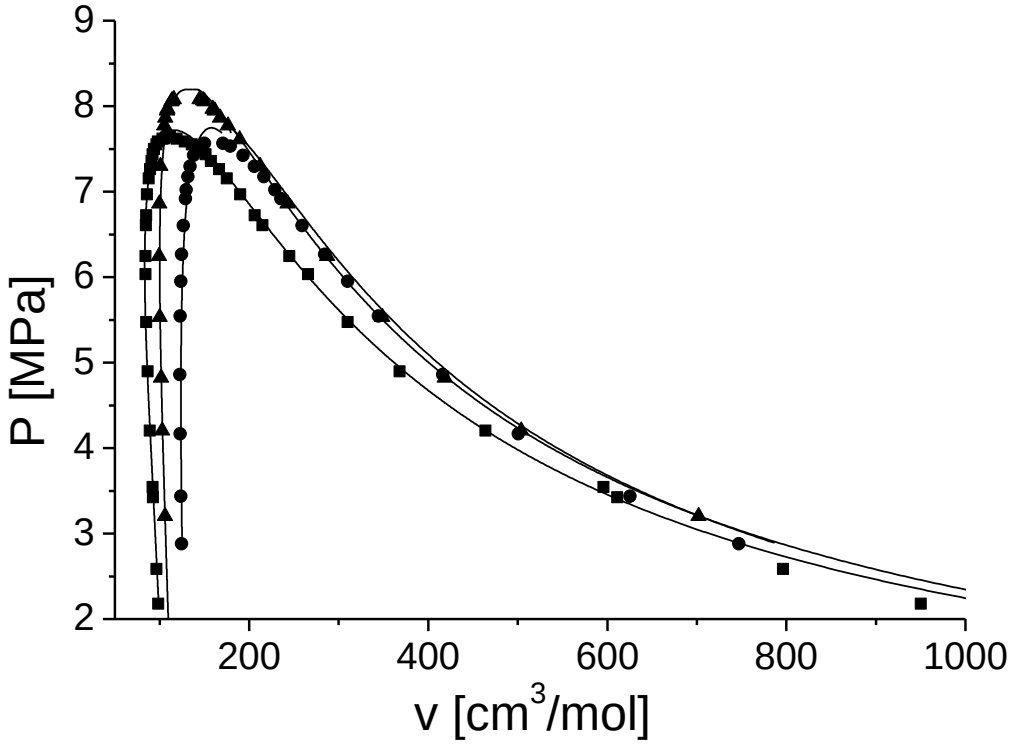

Figure 31: Experimental [81] and predicted phase equilibrium volumes using PCP-SAFT with $k_{ij} = 0.036$ [36] of the system CO_2 and n-butane at 319.3K (squares), 344.3K (triangles) and 377.6K (circles).

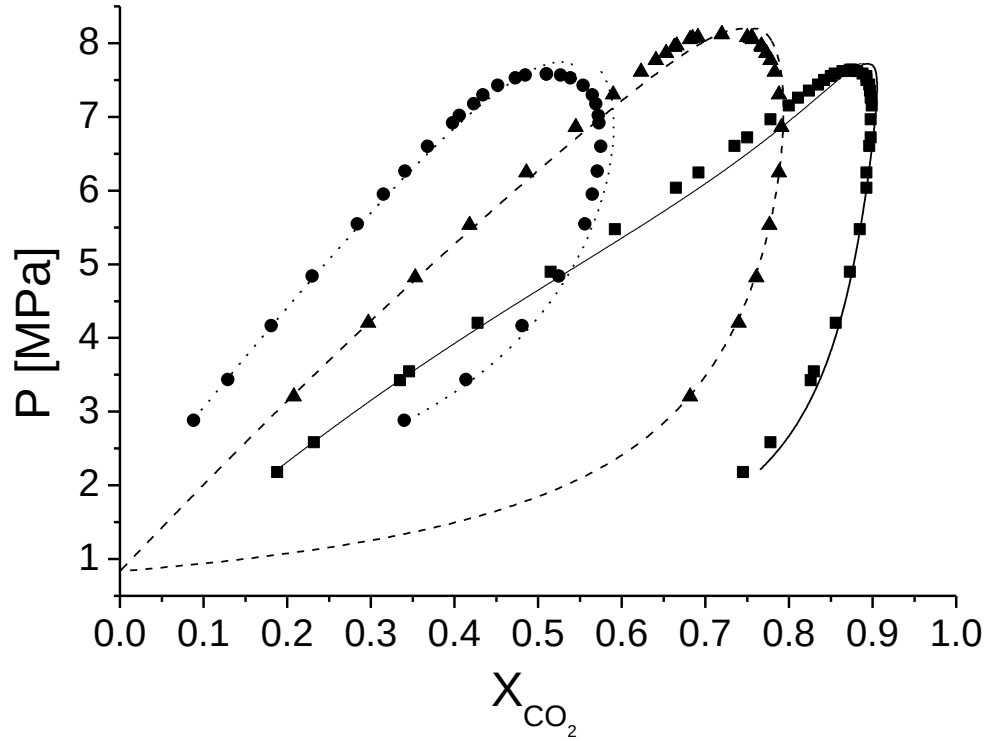

Figure 32: Experimental [81] (squares T=319.3K, triangles T=344.3K and circles T=377.6K) and calculated (solid line T=319.3K, broken line T=344.3K and dotted line T=377.6K) VLE for CO_2 and n-butane using PCP-SAFT-EOS with $k_{ij} = 0.036$ [36].

After phase equilibria calculations the surface tension can be predicted. In Figure 33 the predicted surface tensions are compared with experimental data taken from the literature [81]. At 344.3K and 377.6K the predicted surface tensions are within the experimental error. Similar calculations were carried out by Cornelisse [83] using the Peng-Robinson EOS; however, for the influence parameters of both components, κ_A and κ_B , and for the binary interaction parameter, k_{ij} , a linear temperature dependency was assumed. Taking the quadrupole moment of CO_2 into account via the PCP-SAFT-EOS leads to an improvement of the prediction results and the temperature dependency of the adjustable parameters can be neglected.

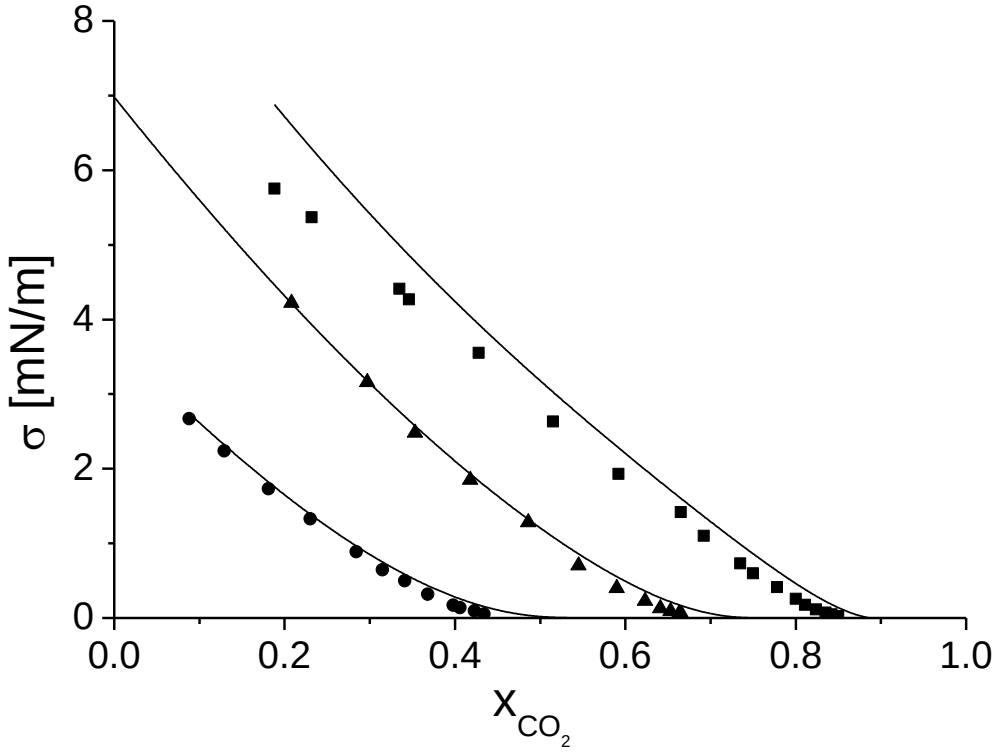

Figure 33: Experimental [81] and predicted surface tension of the system CO_2 and n-butane at different temperatures (squares T=319.3 K, triangles T=344.3 K, circles T=377.6 K) using PCP-SAFT with $k_{ij} = 0.036$ [36].

The density gradient theory allows also the calculation of the surface profiles (Figure 34). These profiles for CO_2 run through a maximum and hence CO_2 will be enriched in the surface and can lead to a barrier for mass transport through the interface, especially at low CO_2 mole fractions in the liquid mixture. The profiles for butane have the usually tanh-shape without a maximum.

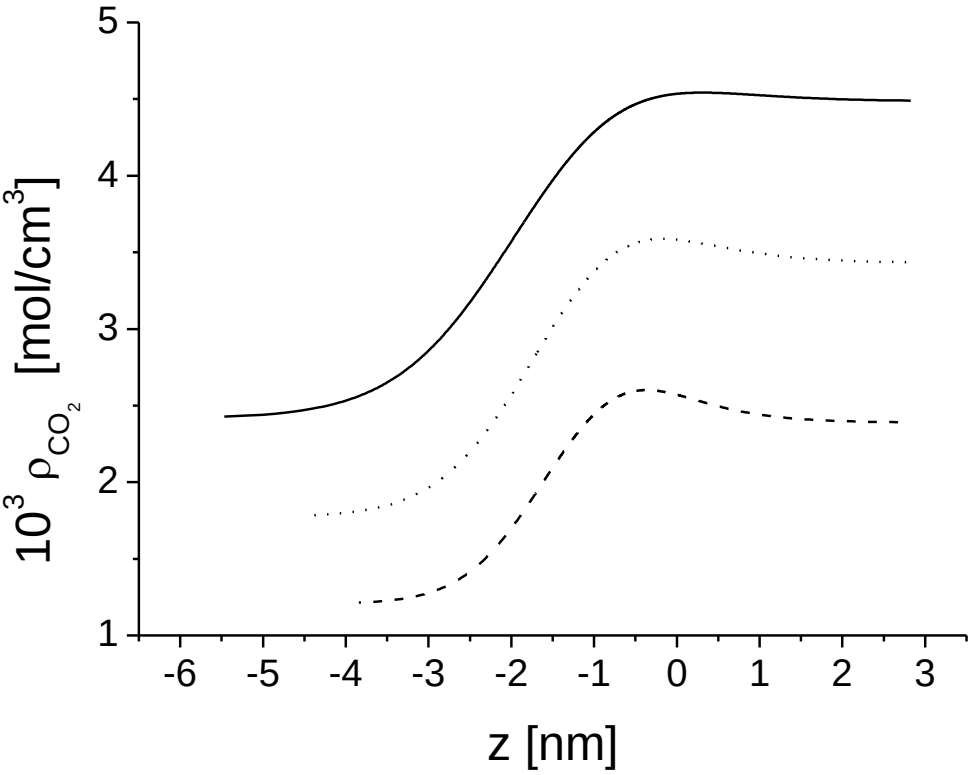

Figure 34: Surface density profiles of CO_2 at different CO_2 levels in the liquid phase (solid line 45 mole percentage of CO_2 in the liquid phase, broken line 35 percentage of CO_2 in the liquid phase and dotted line 25 percentage of CO_2 in the liquid phase and at 344.3K for the system CO_2 + butane.

Increasing the chain length of the n-alkane present in the mixture leads to larger derivation form the ideal mixing behaviour. In order to investigate this effect, calculations for the system CO_2 + heptane were carried out. Phase equilibrium calculations are demonstrated in Figure 35. The experimental data can be described in a high quality using $k_{ij} = 0.039$. Similar to the system CO_2 + butane the reduction of this values shows clearly the performance of the improved EOS (PR-EOS: $k_{ij} = 0.107$, SAFT-EOS or PC-SAFT-EOS: $k_{ij} = 0.129$ and PCP-SAFT-EOS: $k_{ij} = 0.036$ [36]).

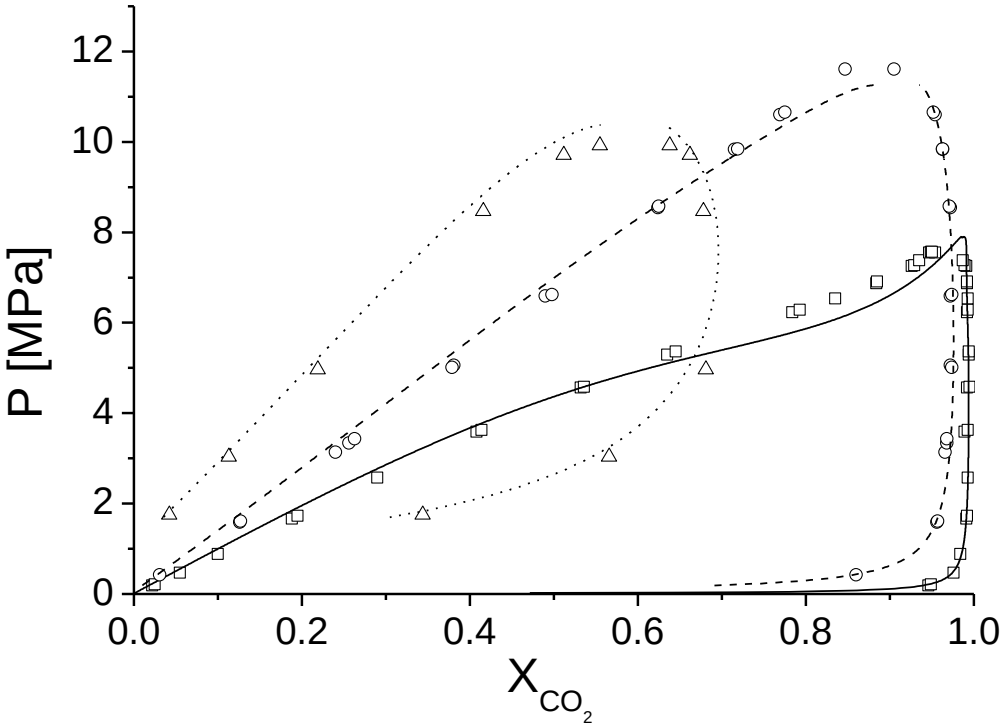

Figure 35: Experimental (squares: T=310.65 K [84], circles: T=352.59 K [84] and triangles: T=477.21 K [85]) and calculated (PCP-SAFT-EOS with $k_{ij} = 0.039$; solid line: T=310.65 K, broken line: T=352.59 K and dotted line: T=477.21 K) vapour pressures for the system CO_2 + heptane at different temperatures.

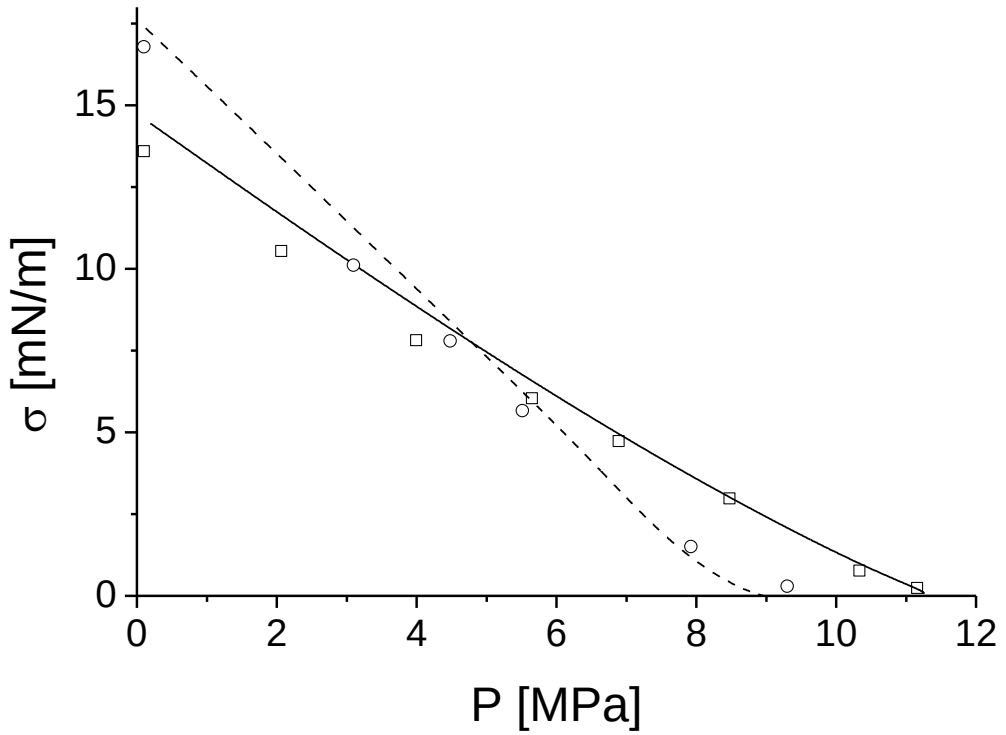

Figure 36: Experimental [80] (squares: T=353.15K and circles: T=323.15K) and predicted (solid line: T=353.15K and broken line: T=353.15K; PCP-SAFT-EOS with $k_{ij} = 0.039$) surface tension for the system CO_2 + heptane at two temperatures.

In Figure 36 the experimental data [80] are compared with the predicted surface tension for the system CO_2 + heptane. Again, it can be concluded, that the theoretical framework works very well in prediction of surface tension for this system over a broad temperature and pressure range.

A further increase of the chain length of the n-alkane in the mixture leads to a stronger derivation from the ideal mixing behaviour. For this reason the next system, which will be studied, is CO_2 + decane. With the help of phase equilibria data taken from the literature [86, 87] the binary interaction parameter k_{ij} is adjusted. The result can be seen in Figure 37, where the experimental data are compared with the modeling results. It can be concluded, that the selected EOS is able to describe the experimental findings in a good quality.

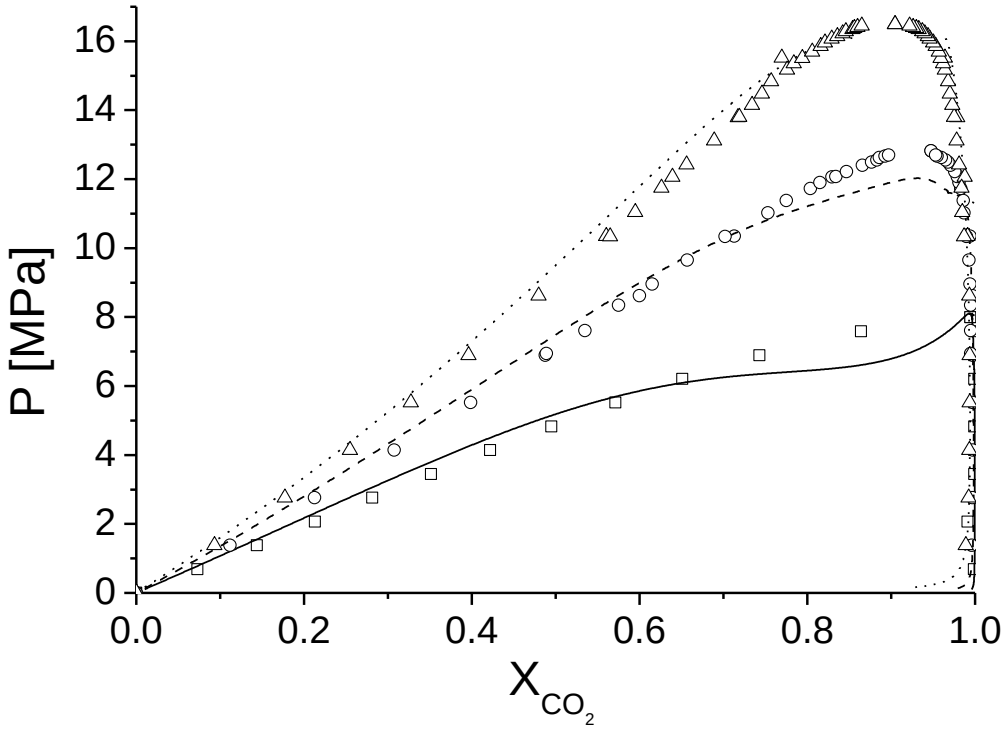

Figure 37: Experimental (squares: T=310.9 K [86], circles: T=344.3 K [87], triangles: T=377.6 K [87]) and modeled (solid line: T=310.9 K, broken line: T=344.3 K, dotted line: T=377.6 K, PCP-SAFT-EOS with $k_{ij} = 0.042$) vapor pressure for the system CO_2 + decane at different temperatures.

Nagarajan and Robinson [87] measure also the surface tension for this system at two temperatures. In Figure 38 the experimental and the predicted surface tensions are

plotted as function of liquid composition. Except the critical region, the DGT can predict the surface tension in a satisfactory quality.

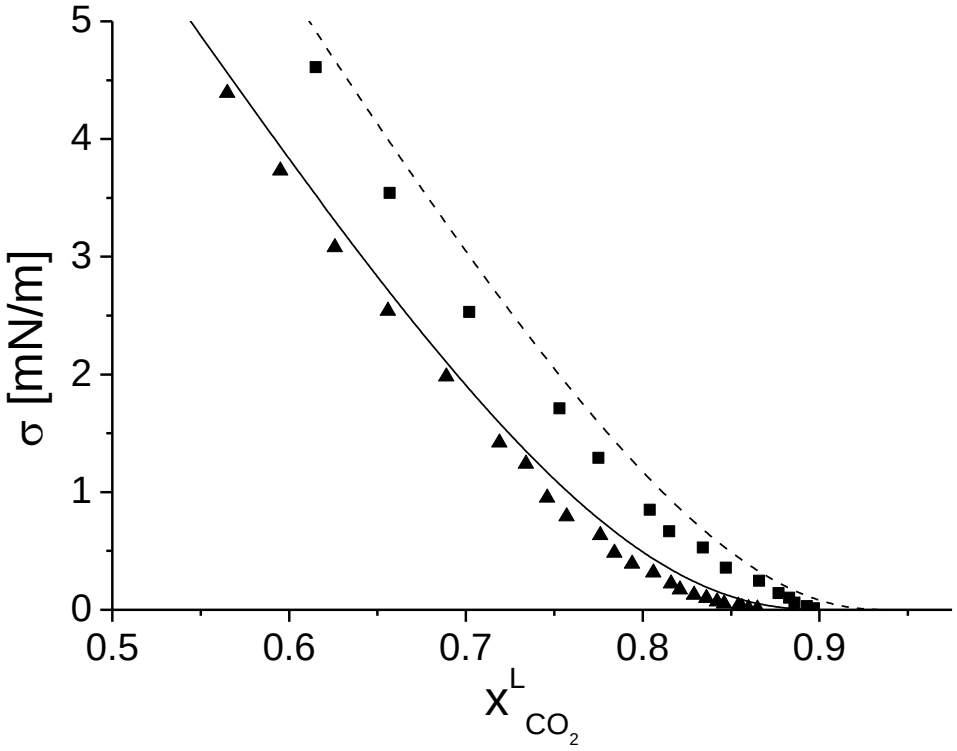

Figure 38: Experimental [87] (triangles: T=344.3 K, squares: T=377.6 K) and predicted (solid line: T=344.3 K, broken line: T=377.6K) surface tension using PCP-SAFT-EOS with $k_{ij} = 0.042$ for the system CO_2 + decane.

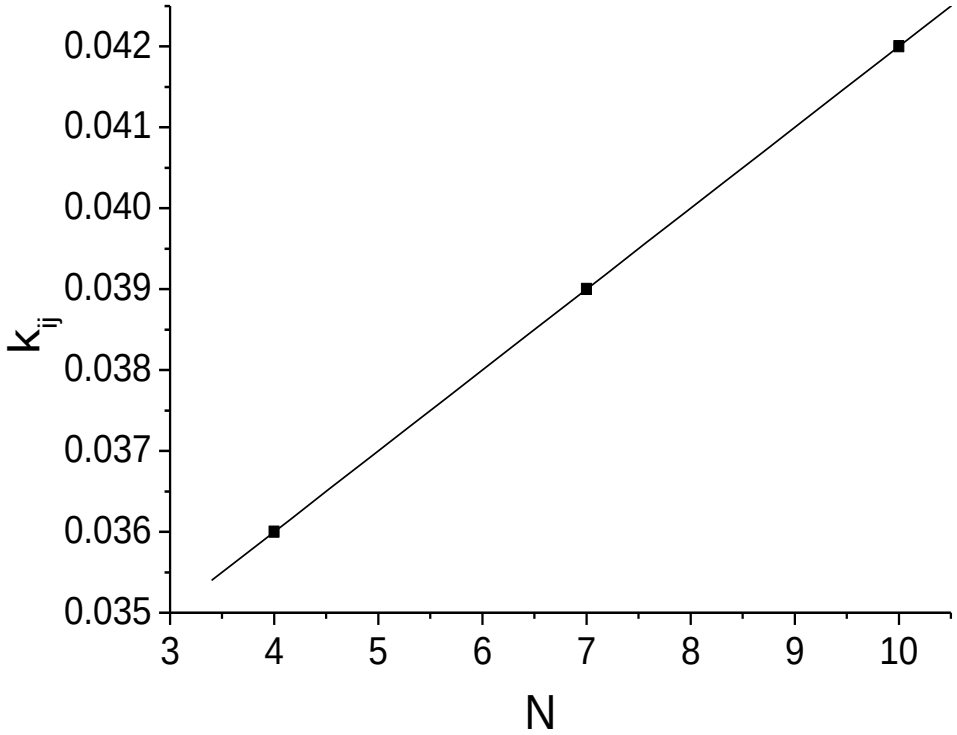

Figure 39: Binary interaction parameter, k_{ij}, in Eq. 111 as function of the chain length, N, of the n-alkane for mixtures made from CO_2 + n-alkane.

The binary interaction parameter k_{ij} for the systems CO_2 + n-alkane, differing in the number of carbon atoms of the n-alkane N, depends linearly from the number of carbon atoms. This relation can be seen in Figure 39. The fitted straight line is given by:

$$k_{ij} = 0.032 + 10^{-3} N \tag{111}$$

This relation (Eq. 111) allows the prediction of k_{ij} for other mixtures made of CO_2 and n-alkane, for instance CO_2 + tetradecane, if no or not enough experimental information available. The results from this pure prediction can be seen in Figure 40

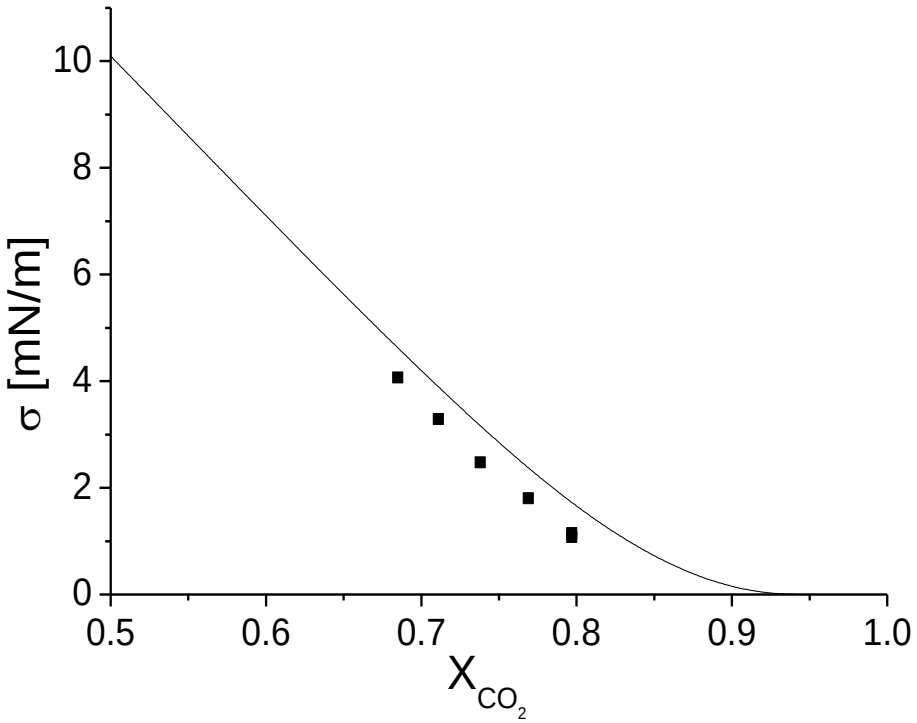

Figure 40: Prediction of the interfacial tension of the system CO_2 + tetradecane with use of Eqs. 101 and 111 and comparison with experimental data [88].

Finally, the theoretical framework should be applied for a mixture, where the n-alkane is replaced by cyclohexane, measured by Nagarajan and Robertson [89]. The k_{ij}-value is fitted to the VLE at T=344.3K (Figure 41). The fitting procedure results in $k_{ij} = 0.07$.

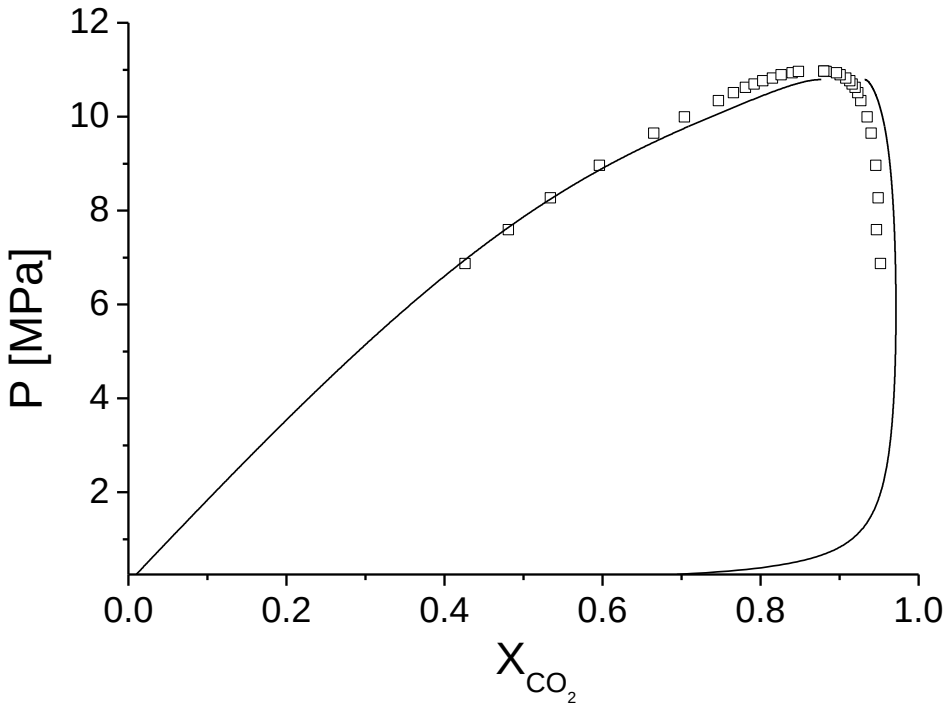

Figure 41: Experimental (squares [89]) and calculated VLE (solid line) for carbon dioxide + cyclohexane using PCP-SAFT-EOS with $k_{ij} = 0.07$ at T=344.3K.

Using the DGT the surface tension of this mixture can be predicted, as seen in Figure 42. Again it can be seen, that the theory does an excellent job regarding the prediction of the surface tension.

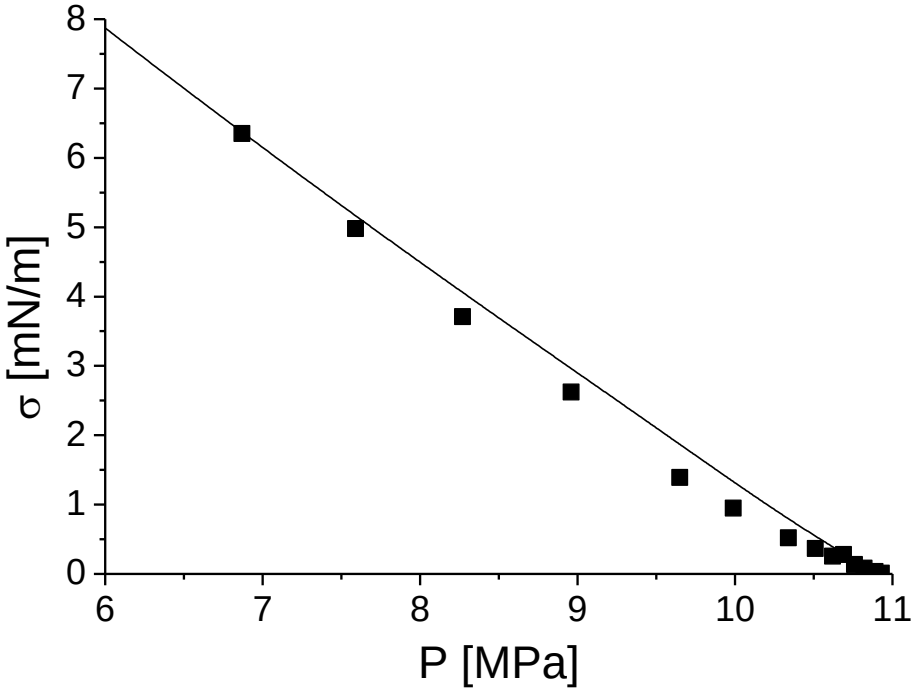

Figure 42: Experimental (squares [89]) and predicted (line PCP-SAFT with $k_{ij} = 0.07$) surface tension for the system CO_2 + cyclohexane at T=344.3 K.

Water Mixtures

The new framework for PCP-SAFT EOS can also be used for mixtures of water and CO_2. Figure 43 shows the VLE of this system at 333.2K. With help of experimental data from the literature [90] it is possible to define a value for the binary interaction parameter, k_{ij}. The same procedure can be applied for a new temperature, namely 313.2K, also seen in Figure 43. A new binary interaction parameter is then use to fit the experimental data [91, 92, 93]. This leads to the hypothesis that the binary interaction parameter for this mixture is temperature dependent. Successive steps can then be done in order to continue on seeing the predictive capability of this assumption. In order to prove this a linear temperature dependency of the form:

$$k_{ij} = \frac{4.95 \cdot T}{10000K} - 0.34693 \tag{112}$$

is assumed. As first step an interpolation is made, namely for T=323.2K. Results of these calculations are depicted in Figure 44. The predicted VLE data has in this case an excellent agreement with the data from the literature, not only on the liquid side but also on the gas side of the equilibrium. Similar data has been presented by Lafitte et al. [58] with use of another SAFT-type equation of state with comparative results on the gas side of the VLE. The liquid side, however, seems to be better described with PCP-SAFT. It is to note that in the mentioned paper a single binary interaction parameter was taken into account for the whole temperature range, while this work considers a linear temperature dependency of it. This might explain the difference on the results.

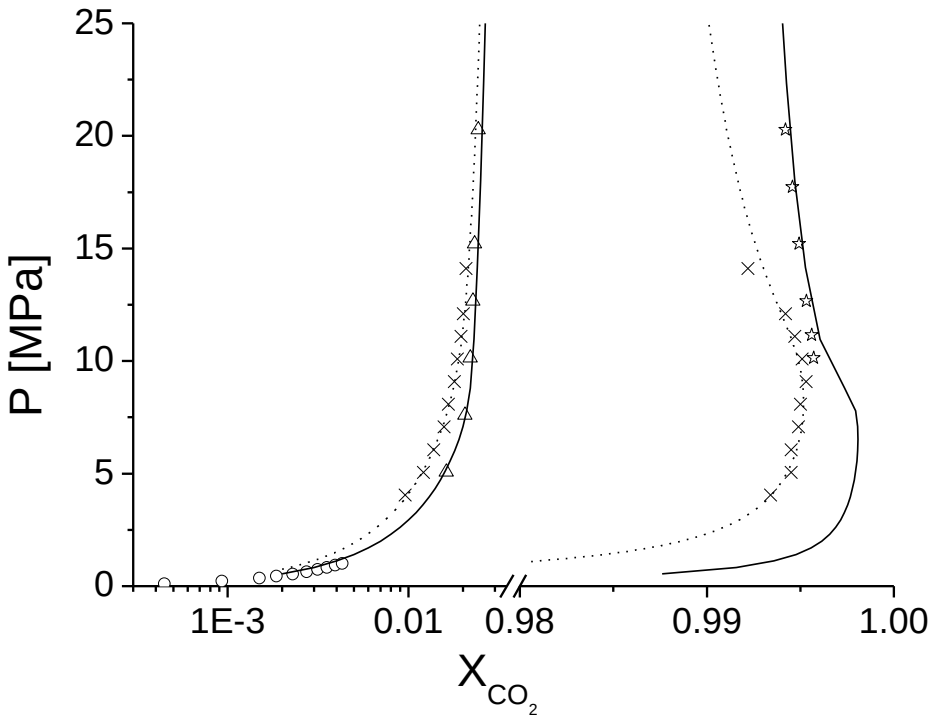

Figure 43: VLE of the mixture CO_2 + water at T=333.2 (crosses: experimental points [90] dotted line: PCP-SAFT with $k_{ij} = -0.182$) and at T=313.2 (experimental points: circles [91] stars [92] and triangles [93]; solid line: PCP SAFT with $k_{ij} = -0.192$).

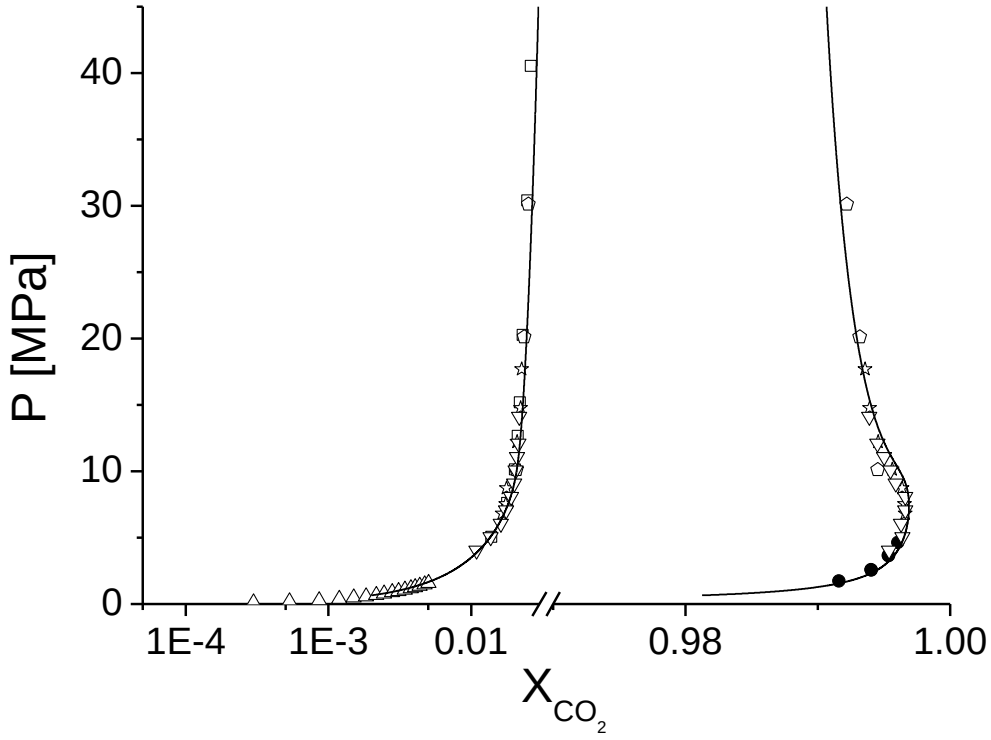

Figure 44: VLE of the mixture CO_2 + water at T=323.2K (experimental points: squares [93], circles [94], stars [95], pentagons [96], triangles [91] and inverted triangles [90]; solid line: PCP-SAFT with $k_{ij} = -0.187$).

The next step to test the accuracy of predictions with our new assumptions is the extrapolation of k_{ij} to lower or higher temperature in the VLE region. A small extrapolation, namely to T=308.2, can be seen in Figure 45. Agreement between calculated results and available data from the literature [92, 97] can be observed. Figure 46 shows a further extrapolation to much higher temperatures ($T = 473K$). The VLE calculations with help of the correlated binary interaction parameter deliver good results all over the liquid equilibrium line; however, the gas side of the VLE begins to fail at higher pressures. Despite of this the accuracy on the gas side of the VLE up to reasonably high pressures confirms the good choice of the type of correlation for the temperature dependency of the binary interaction parameter, k_{ij} .

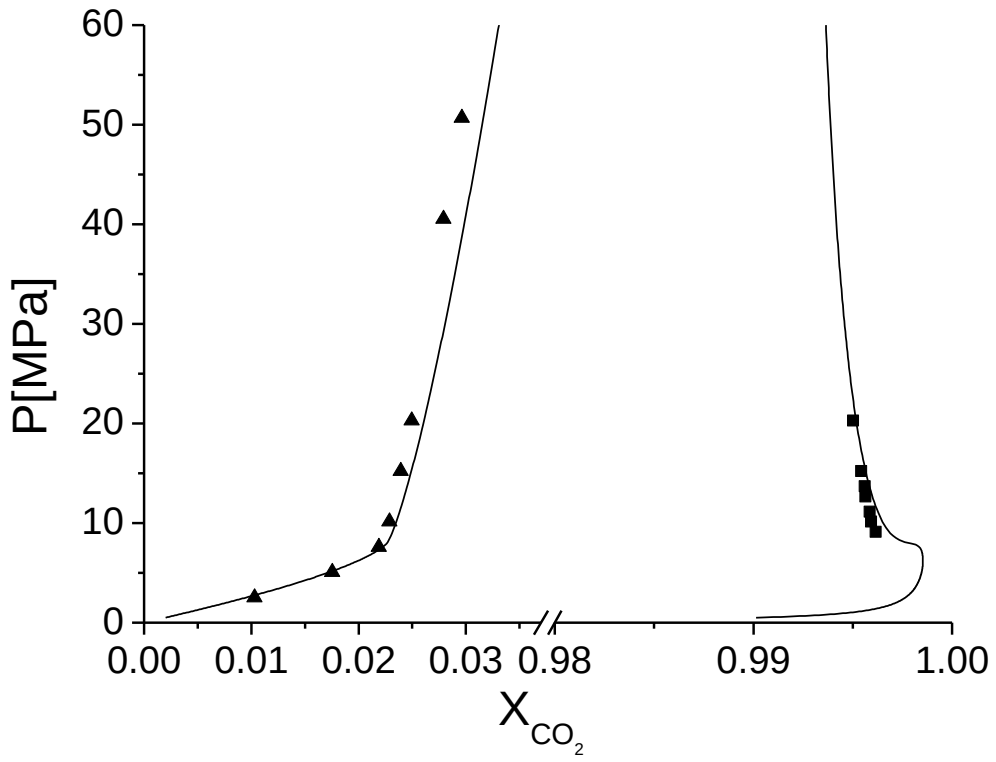

Figure 45: VLE of the mixture CO_2 + water at T=308K (experimental points: squares [92], triangles [97]; solid line: PCP-SAFT with $k_{ij} = -0.1945$).

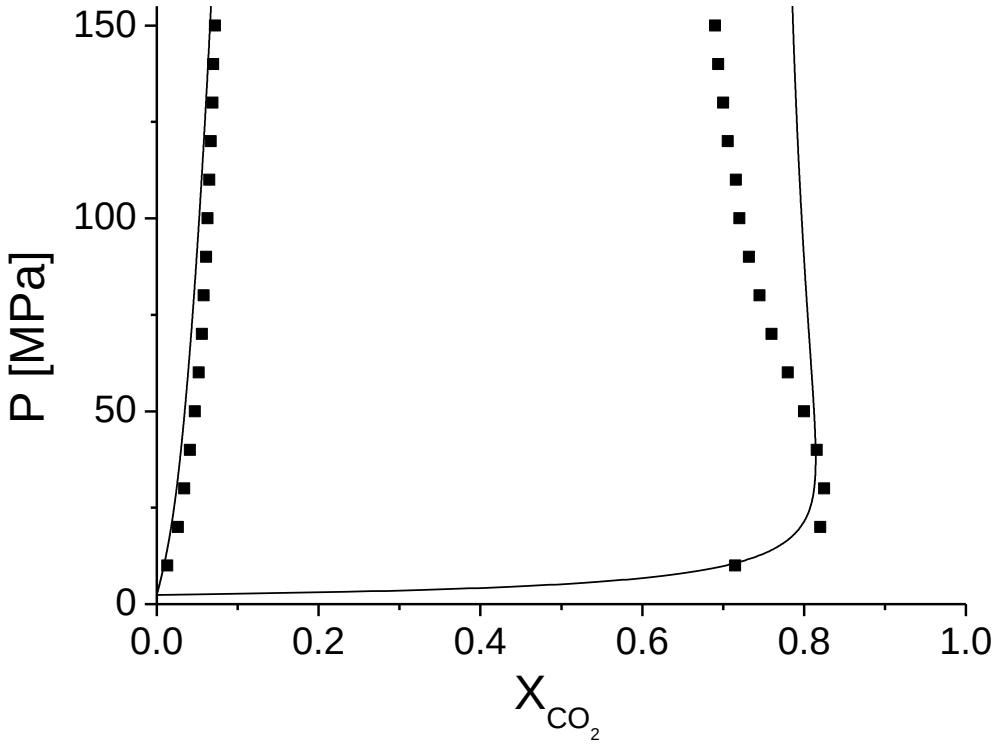

Figure 46: VLE of the mixture CO_2 + water at T=473K (experimental points: squares [98]; solid line: PCP-SAFT with $k_{ij} = -0.112$).

A very important test to see the predictive behaviour of the theoretical framework is to move to temperatures below the critical temperature of CO_2. Below this temperature the thermodynamic equilibrium between water and CO_2 can be divided in three: at the beginning, a regular VLE. At a given pressure, a point appears where a third fluid phase (VLLE), a liquid, arises. At pressures higher from this point the vapour phase vanishes and two liquid phases will be in equilibrium (LLE). It is then the challenge to be able to describe not only the VLE in this temperature region but also the LLE with help of the temperature dependency given by Eq. (112). Figure 47 shows an example of this, for $T = 298.2\,K$. The use of PCP-SAFT with the temperature dependent value of k_{ij} is able to describe all regions quantitatively. Furthermore, the framework is also able to accurately predict the three-phase points (VLLE) along almost the whole temperature region where this phenomenon arises, as seen in Figure 48. Only at the lower temperatures it is not possible to find any calculated three-phase point. This might happen due to the fact that at temperatures below $283\,K$ (about $1\,K$ below the last calculated three-phase point) one of the liquid

phases disappears and a hydrate phase occupies the place for the third coexisting phase. These hydrates cannot be described under the classical framework of the only use of an equation of state.

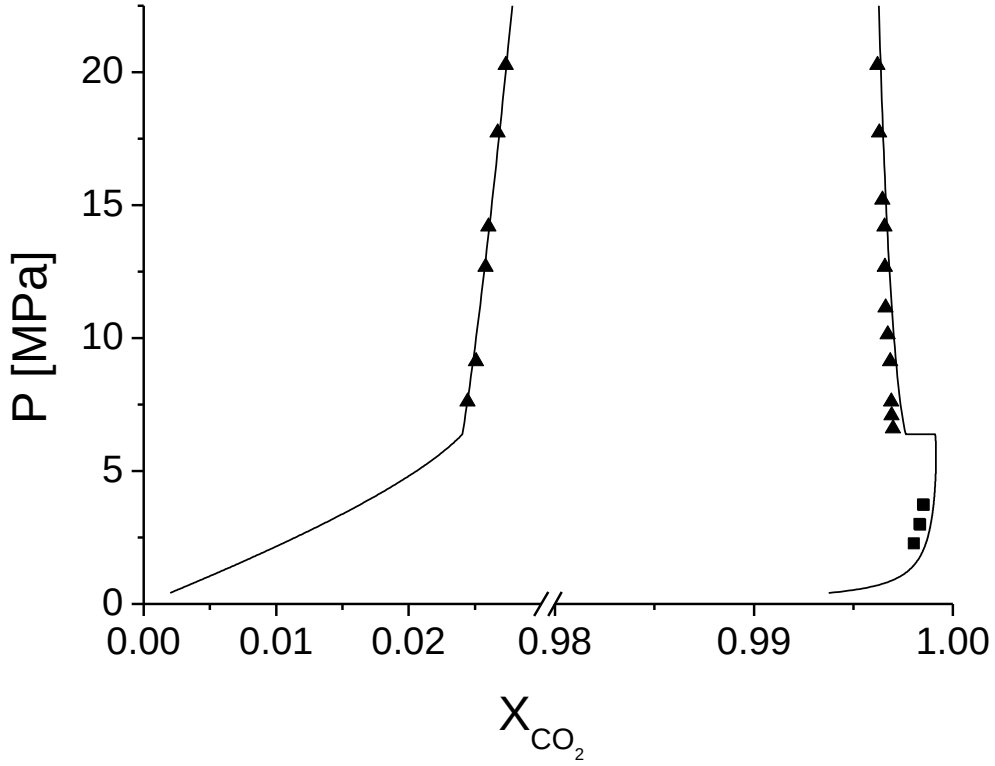

Figure 47: VLE of the mixture CO_2 + water at T=298.2K (experimental points: squares [94], triangles [92]; solid line: PCP-SAFT with $k_{ij} = -0.112$).

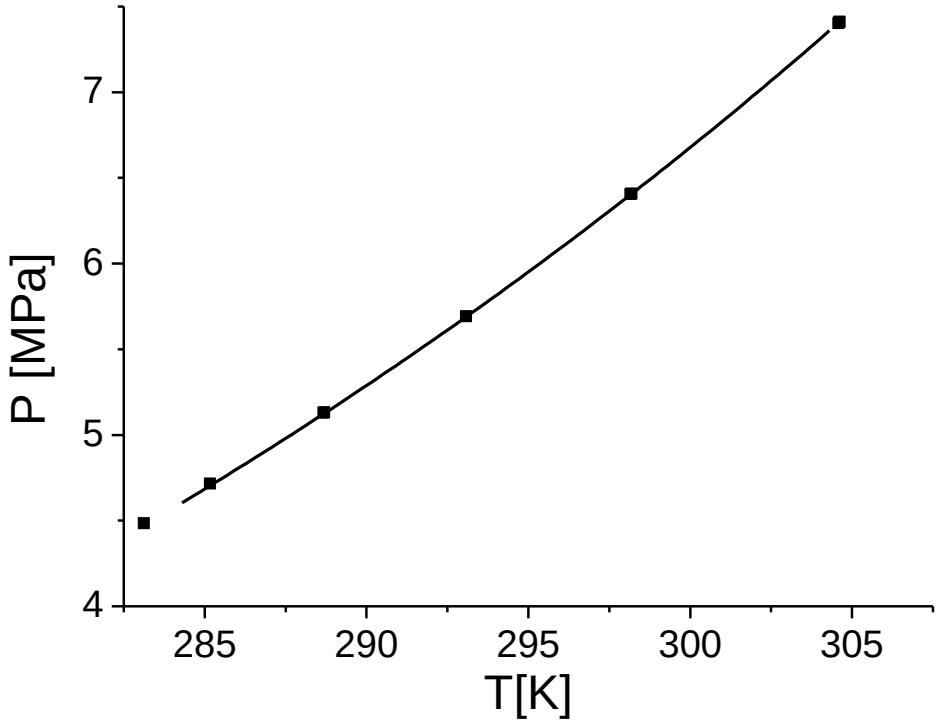

Figure 48: VLLE of the mixture CO_2 + water (experimental points: squares [99]; solid line: PCP-SAFT).

The former analysis supports the assumption of a linear temperature dependency of the binary interaction parameter k_{ij}. Tang and Gross [68] also tried to describe the phase behaviour of the mixture using PCP-SAFT with the 2B association scheme already given in the original PC-SAFT version [34]. They used experimental data over a broad range of temperatures to see the dependency of the binary interaction parameter with respect to the temperature. This resulted in an equation of second order. The use of the 4C scheme in this work causes a very important change in this behaviour, reducing one order of the temperature dependency and delivering results with a good quantitative agreement with those from the literature. The theoretical results are clearly an improvement in the accuracy of phase equilibrium calculations in comparison the temperature-independent binary interaction parameters [68], especially, if the LLE occurs.

Once the phase equilibrium for the system has been described it is possible to go further to the analysis of the interfacial properties of the system CO_2 + water. With help of the density gradient theory it is possible to use the influence parameters of the pure components in order to make a pure prediction of the interfacial tension of the mixture using $\beta = 1$, as seen in Figure 49 for $T = 333.2K$. Unfortunately, the results from this pure prediction are able to describe qualitatively the behaviour of the interfacial tension over a pressure range at the given temperature, yet present a very poor quantitative agreement with the data from Hebach et al. [100]. This problem can be solved with help of the introduction of a binary parameter β in the mixing rule for the influence parameters.

The new calculations are also illustrated on Figure 49. A big improvement is made with the use of this new β parameter, as seen also in the Figure. With help of this new parameter it is possible to do predictions of the interfacial tension of the mixture at other temperatures, as seen in Figure 50 for two temperatures above the critical temperature of CO_2. Same as in the case of $T = 333.2K$, the combination of DGT with PCP-SAFT EOS is able to describe the behaviour of the interfacial tensions. Greater deviations can be seen on the low pressure region; with increase of the pressure, the predictions of the theoretical framework get closer to the ones given by

the literature. This is also the case for temperatures at which a VLLE appears, as seen in Figure 51 for $T = 298.2K$. The typical jump from the interfacial tension, related with the change of VLE to LLE can be observed.

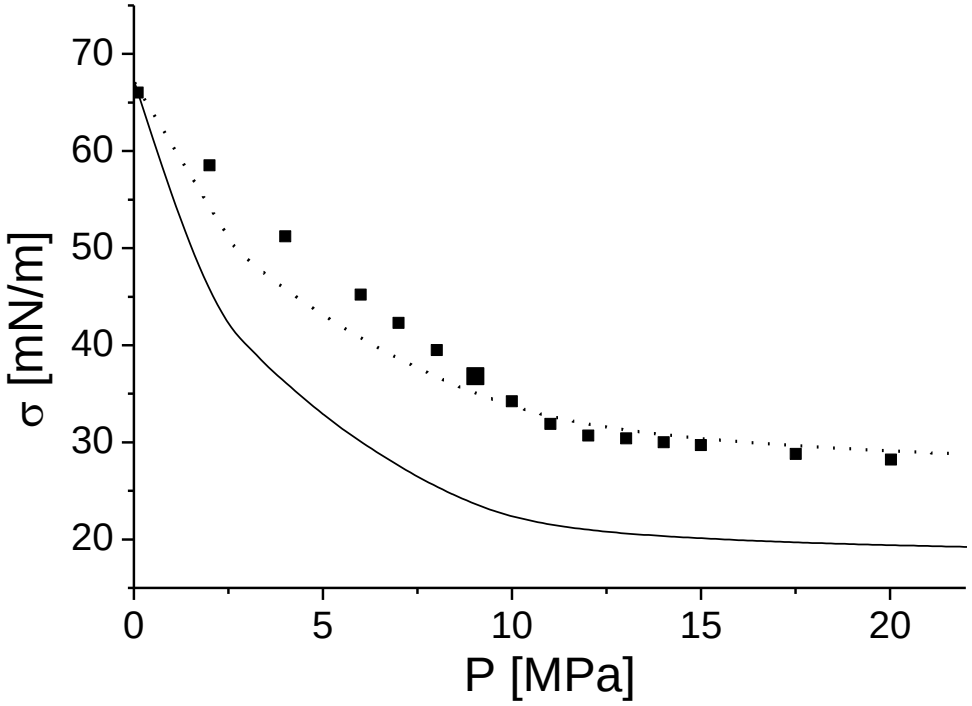

Figure 49: Prediction (solid line) and calculation (dotted line) with help of one experimental [100] point ($\beta = 0.25$) of the interfacial tension of the mixture CO_2 + water at T=333.2.

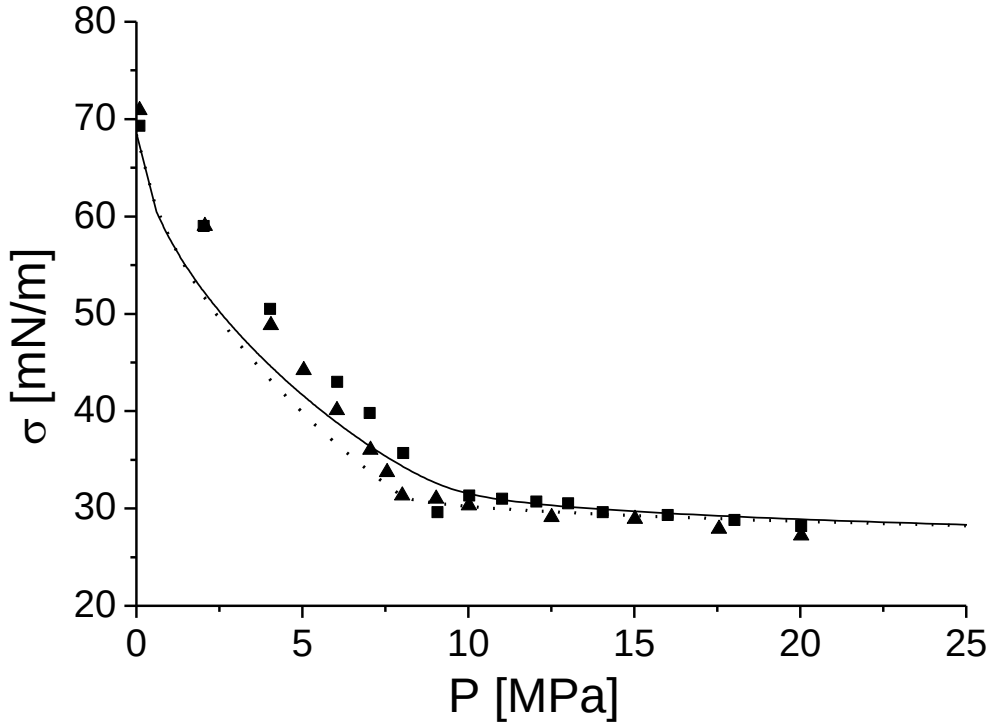

Figure 50: Prediction of the interfacial tension of the mixture CO_2 + water at T=318.5K (PCP-SAFT: solid line; experimental data: squares [100]) and at T=308.2K (PCP-SAFT: dotted line; experimental data: triangles [100]) with $\beta = 0.25$.

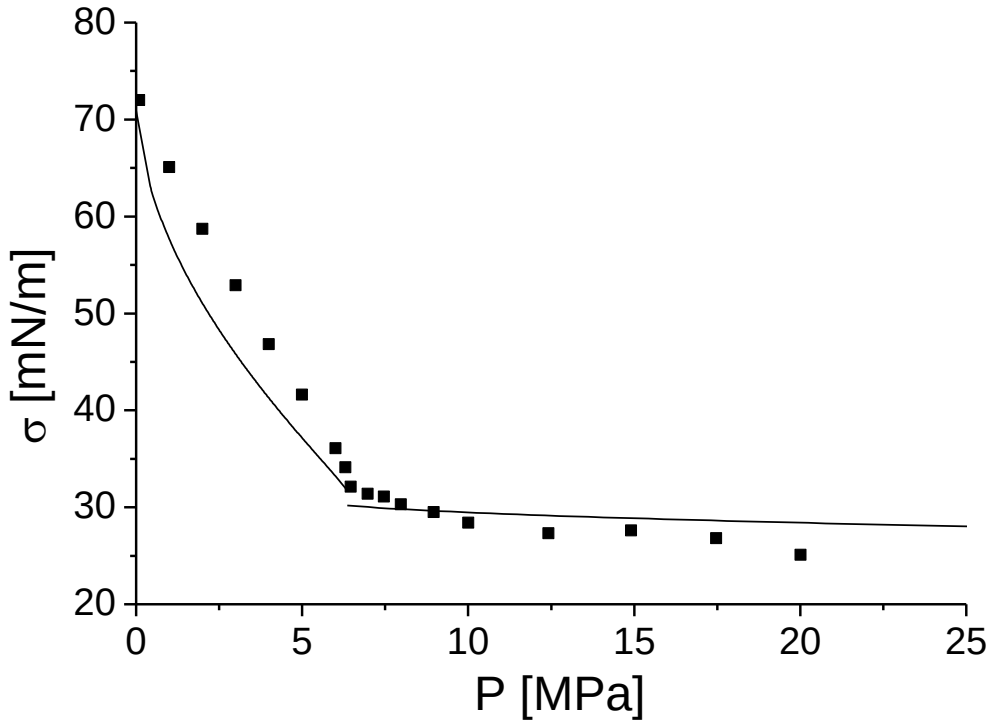

Figure 51: Prediction of the interfacial tension of the mixture CO_2 + water at T=298.2K (PCP-SAFT: solid line; experimental data: squares [100]) with $\beta = 0.25$.

In order so solve the integral for the interfacial tension, the set of equations 89 and 90 must be solved numerically in order to find the partial density profiles across the interface. An example of these density profiles can be seen in Figure 52 for $T = 308.2K$. A very sharp peak in the partial density profile of CO_2 across the interface is observed. This peak is related to the relative enrichment of the much more volatile component in the interface. This peak is very sharp at low pressures (diluted solutions of CO_2 in water). As the pressure of the system increases, the peak diminishes until it disappears, as shown in Figure 52. A better schematic presentation of this can be seen with use of the relative adsorption curves of CO_2 (A) in water (B), as explained already in the theoretical background. Figure 53 shows this relative adsorption at different temperatures. The results differ from those given by Lafitte et al. [32]. While the relative adsorption in our case seems to decrease with increasing pressure at a constant temperature, theirs increases while moving to higher pressures. This is a surprising outcome. As already seen in the density profiles from Figure 52, the sharpness of the peak of the partial density of CO_2 decreases with increasing pressure. This peak is directly related to the relative enrichment of the component on the interface and thus to the relative adsorption. It is therefore to

expect that the relative adsorption will decrease with vanishing of the peak, as seen in Figure 53. It is also possible to note that at temperatures below the critical temperature of pure CO_2 a discontinuity occurs in the relative adsorption. This discontinuity is in this case related to the change of the second phase from vapour to liquid. After this abrupt jump caused by this transition, the relative enrichment of CO_2 in water is practically negligible.

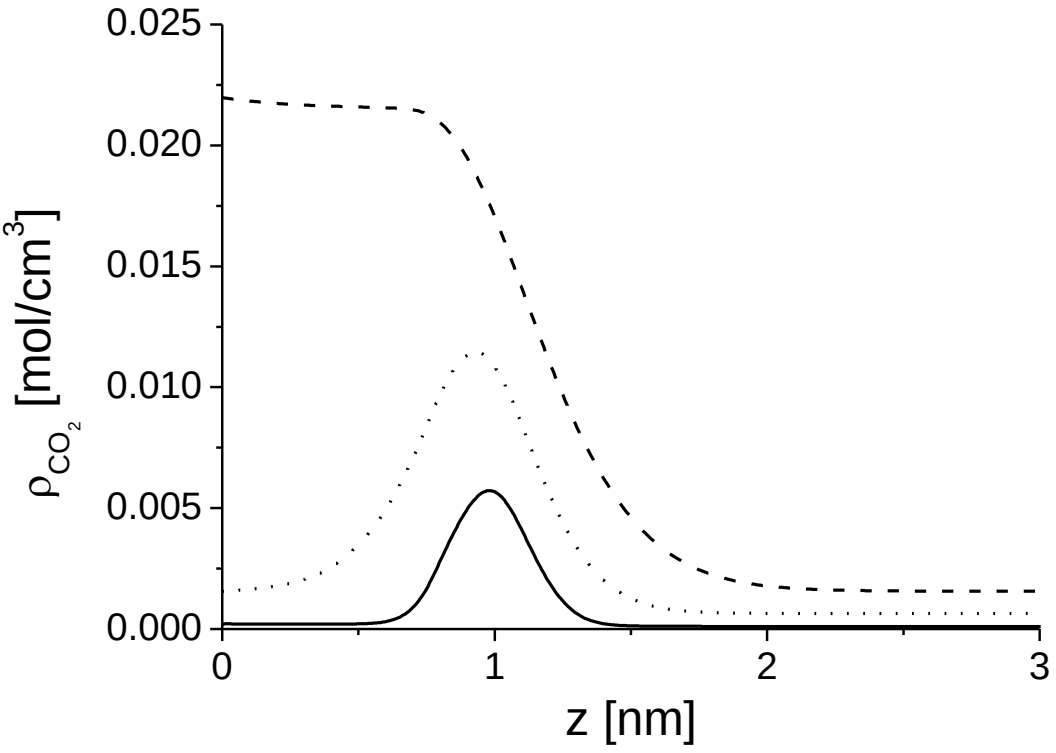

Figure 52: Partial density profiles for CO_2 at T=308.2 and different CO_2 concentrations in the liquid phase (solid line $x^L_{CO_2} = 0.002$ (P=0.51 MPa), dotted line $x^L_{CO_2} = 0.0119$ (P=3.28 MPa), broken line $x^L_{CO_2} = 0.0294$ (P=38.96 MPa)).

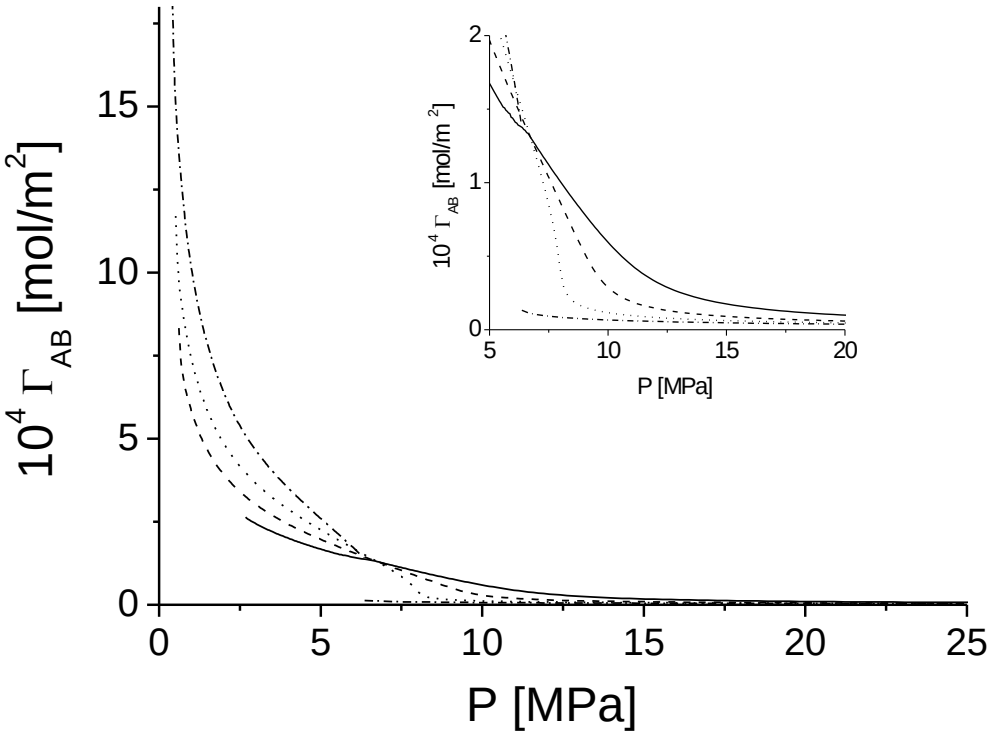

Figure 53: Relative adsorption curves of CO_2 (A) in water (B) at different temperatures (solid line: T=333.2; broken line: T=318.5; dotted line: T=308.2; dotted-dashed line: T=298.2). The insert enlarged the relative adsorption at high pressures.

An analysis of the phase equilibrium of the mixture methane + water for a SAFT-type EOS was made by Vega et al. [101]. In the work, the solubility of water in gaseous methane was described with help of a k_{ij} value of 0.32; however, no information is given about the description of the aqueous phase. A preliminary analysis with PC-SAFT and the given parameters also proved to be able to describe the methane-rich phase with a k_{ij} value of 0.2. A further analysis showed on the opposite the inability to use this value of the binary interaction parameter on the liquid phase, in order to describe the experimental data. Haslam et al. [74] already discussed about the possibility of considering two different binary interaction parameters for different phases. The idea arises due to the fact that a mixture like methane + water shows two very different phases: the liquid phase, with a high concentration of water, will show strong association phenomena; on the other side, the gas phase will be highly methane-rich and will be predominantly non-polar. The problem that arises with his assumption is the application of the DGT for a mixture. Since the DGT makes an analysis of the system through the interface, at some point the value of k_{ij} from the liquid phase cannot be used for the calculations approaching the gas phase. The

proposed solution is the use of a concentration-dependant value of k_{ij} , which would avoid the problems in the interface. The binary interaction parameter can be described as

$$k_{ij} = \left(0.2 - a(T)\right)\mathrm{X}_{CH_4} + a(T) \tag{113}$$

As a first approach, the value of $a(T)$ was fit to VLE data over a range of temperature. With help of these temperatures it was possible to correlate the dependency of $a(T)$ to temperature, on the way:

$$a(T) = 0.04881 - 1.33218\ (0.99365^{T/K}) \tag{114}$$

A description of the values of $a(T)$ with respect to the temperature can be seen in Figure 54. The depiction of the VLE data used to fit the binary interaction parameter can be seen from Figure 55 to Figure 58

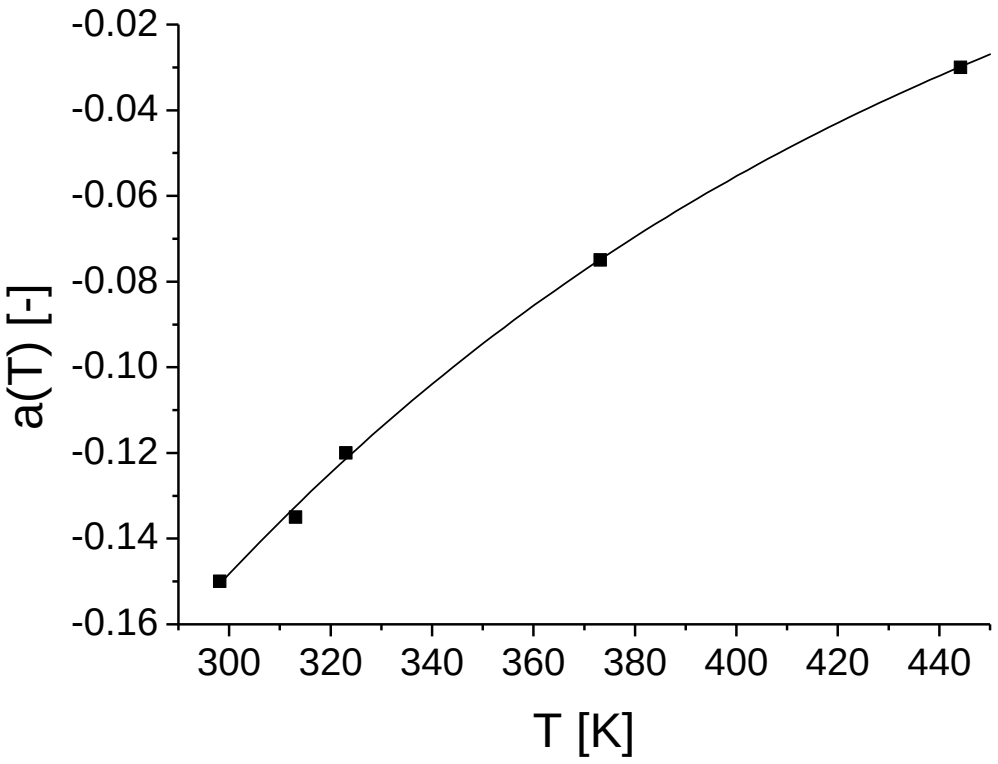

Figure 54: Correlation for the value of $a(T)$ with respect to temperature for the system water + methane.

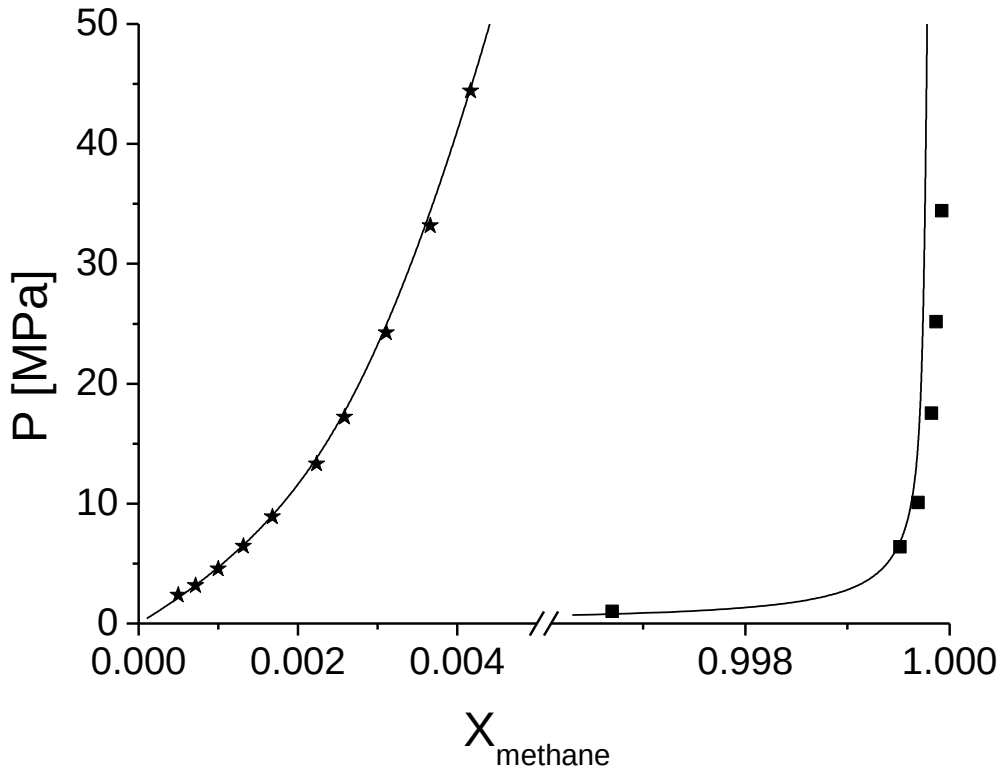

Figure 55: VLE methane + water at 298.15 K (experimental points: stars [102] and squares [103]; solid line: PC-SAFT with $k_{ij} = 0.351 X_{CH_4} - 0.151$).

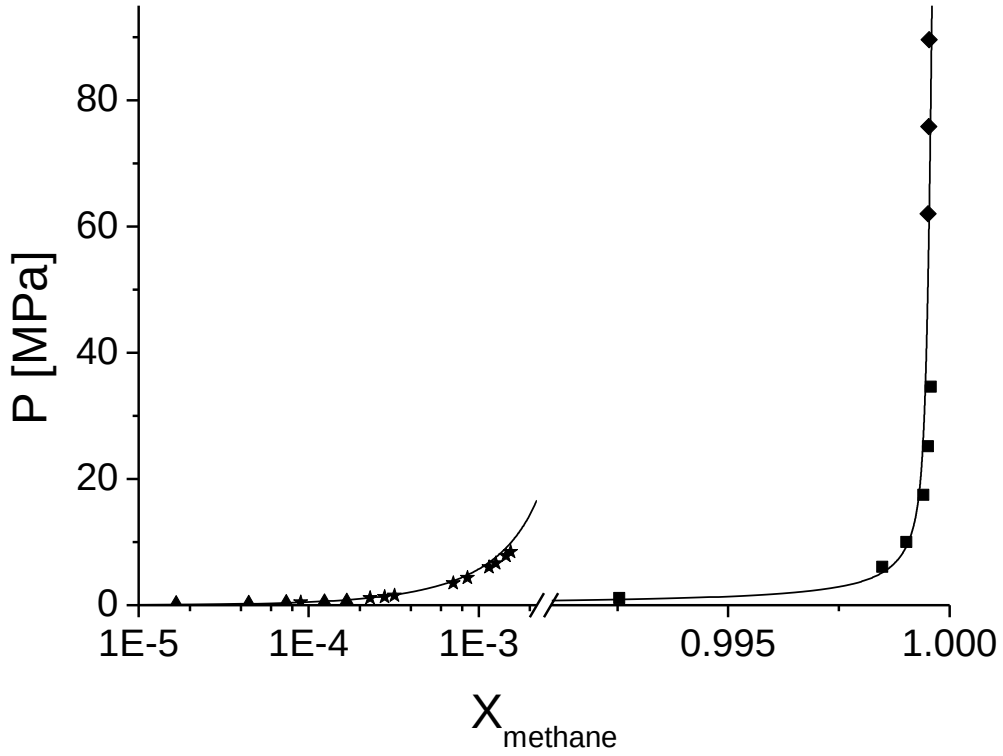

Figure 56: VLE methane + water at 313.2 K (experimental points: squares [103], stars [104], diamonds [105] and triangles [106]; solid line: PC-SAFT with $k_{ij} = 0.3324 X_{CH_4} - 0.1324$).

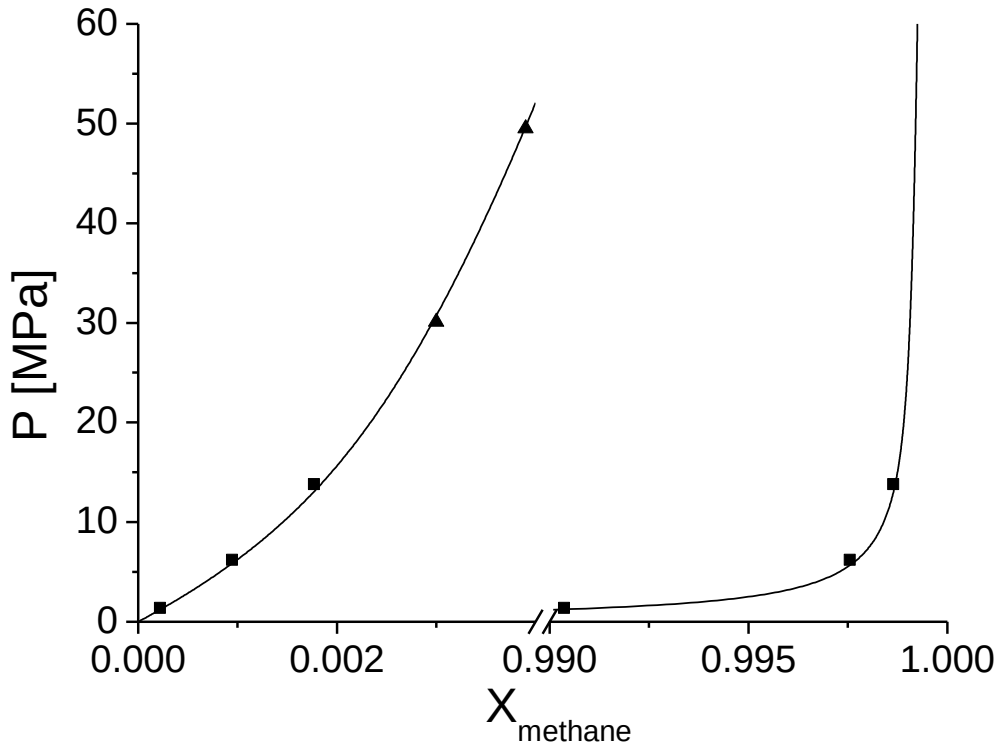

Figure 57: VLE methane + water at 323 K (experimental points: triangles [107] and squares [108]; solid line: PC-SAFT with $k_{ij} = 0.3214 X_{CH_4} - 0.1214$).

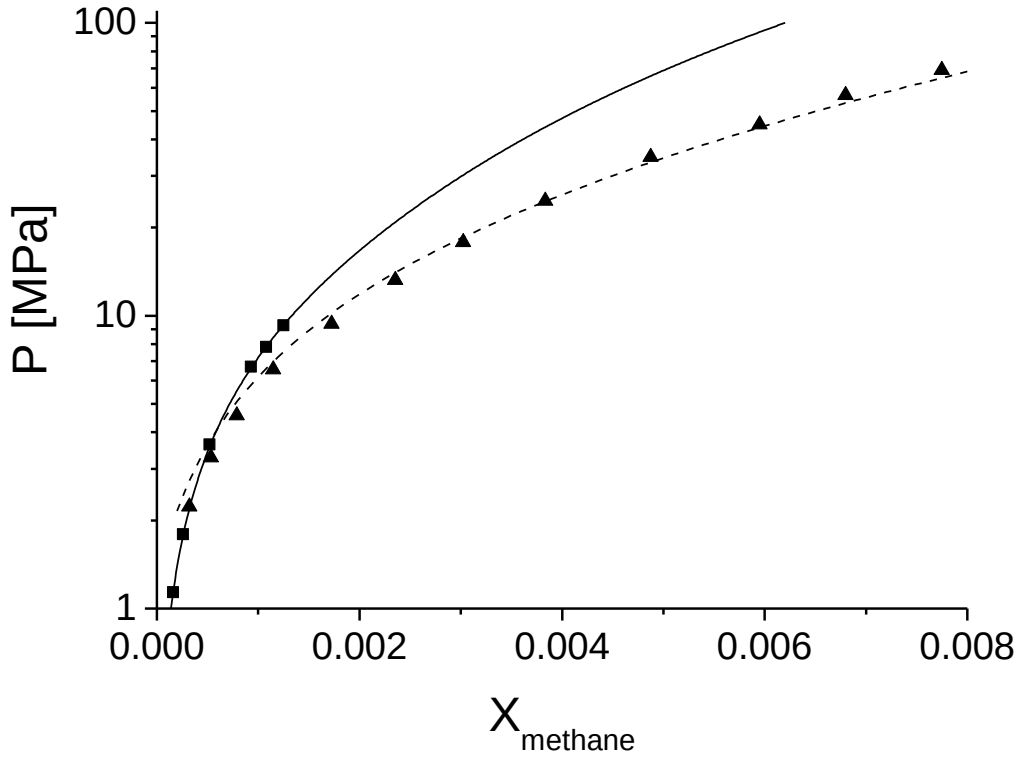

Figure 58: Solubility of methane in water at 373.15 K (experimental points: squares [103]; solid line: PC-SAFT with $k_{ij} = 0.275 X_{CH_4} - 0.075$) and 444.2 K (experimental points: triangles [102]; dashed line: PC-SAFT with $k_{ij} = 0.23 X_{CH_4} - 0.03$).

With help of Eq. 113 it is possible to make predictions on the VLE behaviour and solubilities of the hydrocarbon in the aqueous phase for the mixture water + methane. A description of experimental data from the literature is given from Figure 59 to Figure 61. The used parameters and correlation for the binary interaction parameter are able in this case to reproduce the solubilities of methane in water and the water content in the gas phase. The description of the gas phase is similar to the one given by Vega et al. [101] using a SAFT-type EOS, but in this work it is also possible to see a good agreement of the liquid phase with the used framework. The other work using a SAFT-type EOS, written by Miqueu et al. [109] doesn't show the agreement of the theoretical framework with experimental VLE data, or the necessary binary interaction parameters to be used.

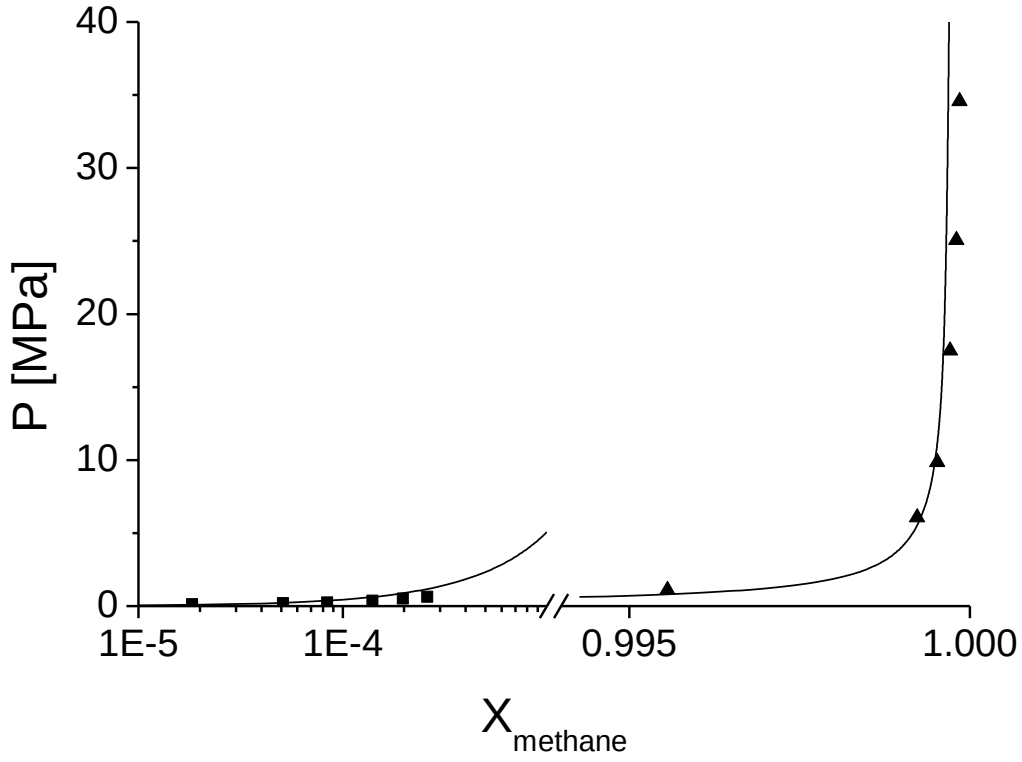

Figure 59: VLE methane + water at 303 K (experimental points: triangles [103] and squares [106]; solid line: PC-SAFT with $k_{ij} = 0.3445 X_{CH_4} - 0.1445$).

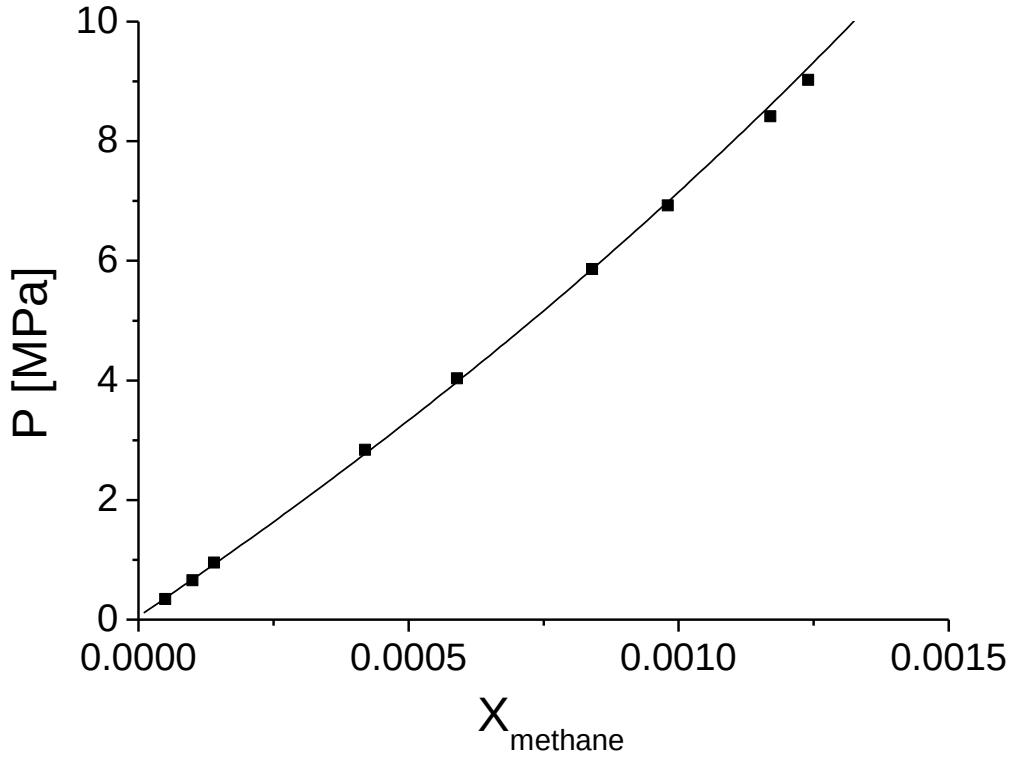

Figure 60: Solubility of methane in water at 353 K (experimental points: squares [104]; solid line: PC-SAFT with $k_{ij} = 0.2918 X_{CH_4} - 0.0918$).

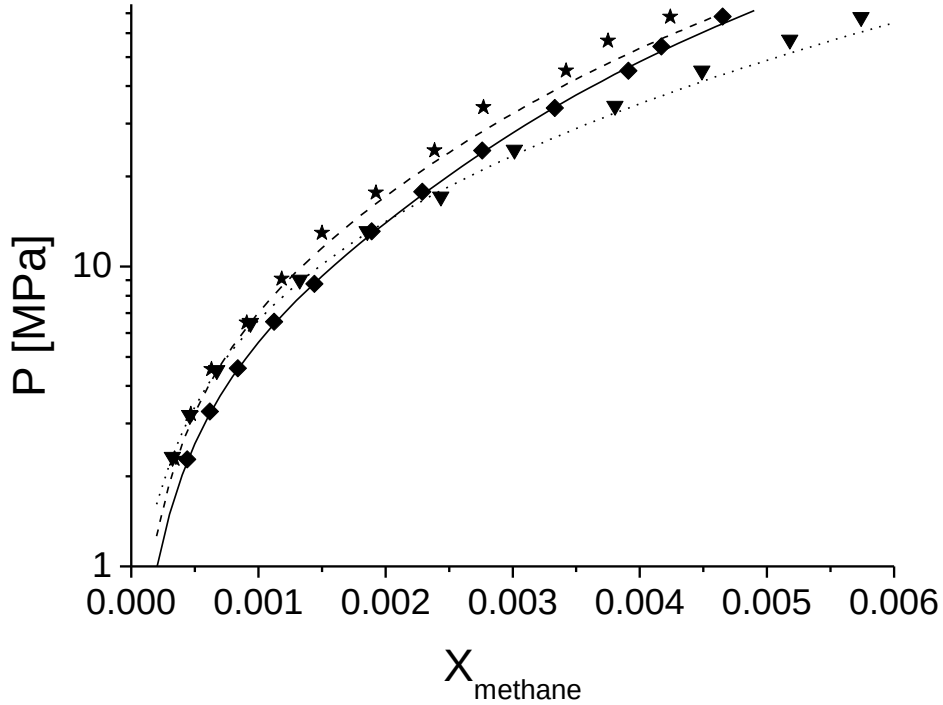

Figure 61: Solubility of methane in water at 310.93 K (experimental points: diamonds [102]; solid line: PC-SAFT with $k_{ij} = 0.335 X_{CH_4} - 0.135$) 344.26 K (experimental points: stars [102]; dashed line: PC-SAFT with $k_{ij} = 0.2998 X_{CH_4} - 0.0998$) and 410.93 K (experimental points: inverted triangles [102]; dotted line: PC-SAFT with $k_{ij} = 0.2484 X_{CH_4} - 0.0484$).

The second part of the theoretical framework of the combination of the DGT and PC-SAFT is, once the vapour-liquid equilibrium has been calculated, the calculation of the interfacial tension at a given temperature. Figure 62 shows these calculations. Water has very strong interactions that cannot be easily modelled, so as already observed in the case of mixtures of water + CO_2 the use of the modified geometrical rule for the influence parameter of the mixture is needed for this mixture. The parameter was set to fit the data at T = 313.15 K. A value of $\beta = 0.55$ was needed to do this. This parameter is lower than the one given for the same mixture by Miqueu et al. [109] in a similar work; however, the main goal of this work is to be able to describe both phase equilibrium and interfacial properties. In the mentioned work, as stated before, no information is given about this. With help of the modified mixing rule for the influence parameter of the mixture further calculations were made for two temperatures, as seen in Figure 63. There is good agreement with the experimental data, especially at lower pressures. At higher pressures an EOS usually presents difficulties to be able to describe the phenomena arising. It is therefore expected that the agreement might decrease with increasing pressure of the system. All calculations are comparable with the ones given not only by Miqueu et al. [109] but also from Schmidt et al. [110]. About the first work it has already been discussed. Regarding the second paper, a modification of the DGT is used in combination with the Soave-Redlich-Kwong EOS, constraining the behaviour of the density profiles across the interface. Results show similar agreement on the calculated surface tensions; however, a temperature dependent influence parameter is needed to reproduce the experimental data, probably due to the already mentioned reason and also due to the difficulties arising from modelling such a system with a cubic equation of state.

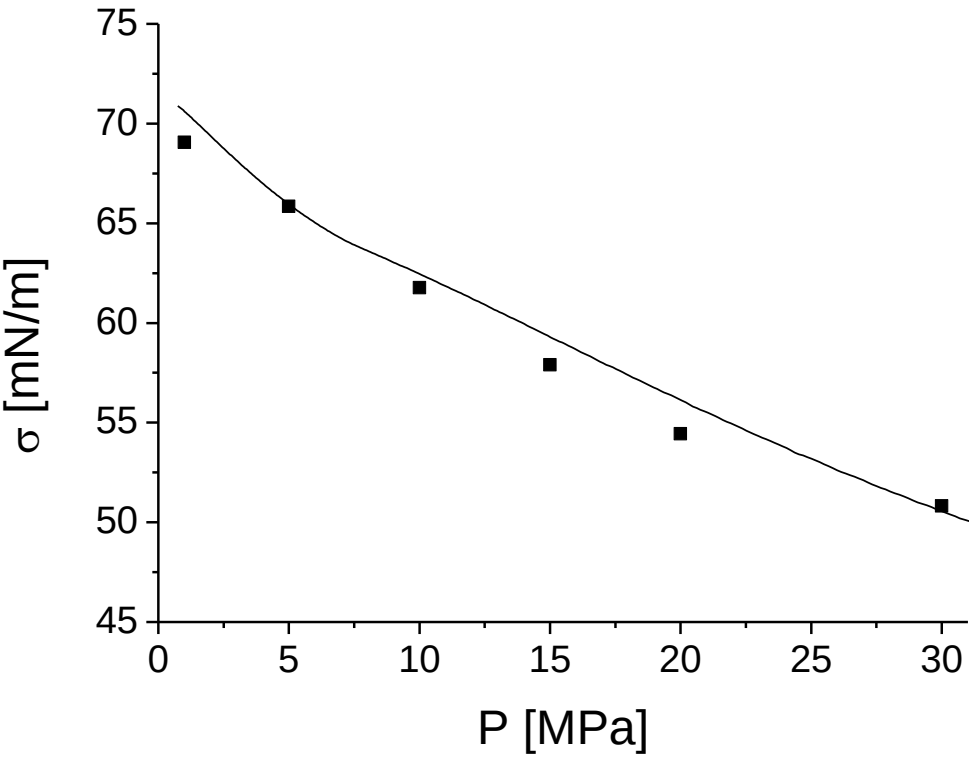

Figure 62: Interfacial Tension of methane + water at 313.15 K (experimental points: squares [111]; solid line: DGT + PC-SAFT with $k_{ij} = 0.3324 X_{CH_4} - 0.1324$ and $\beta = 0.55$).

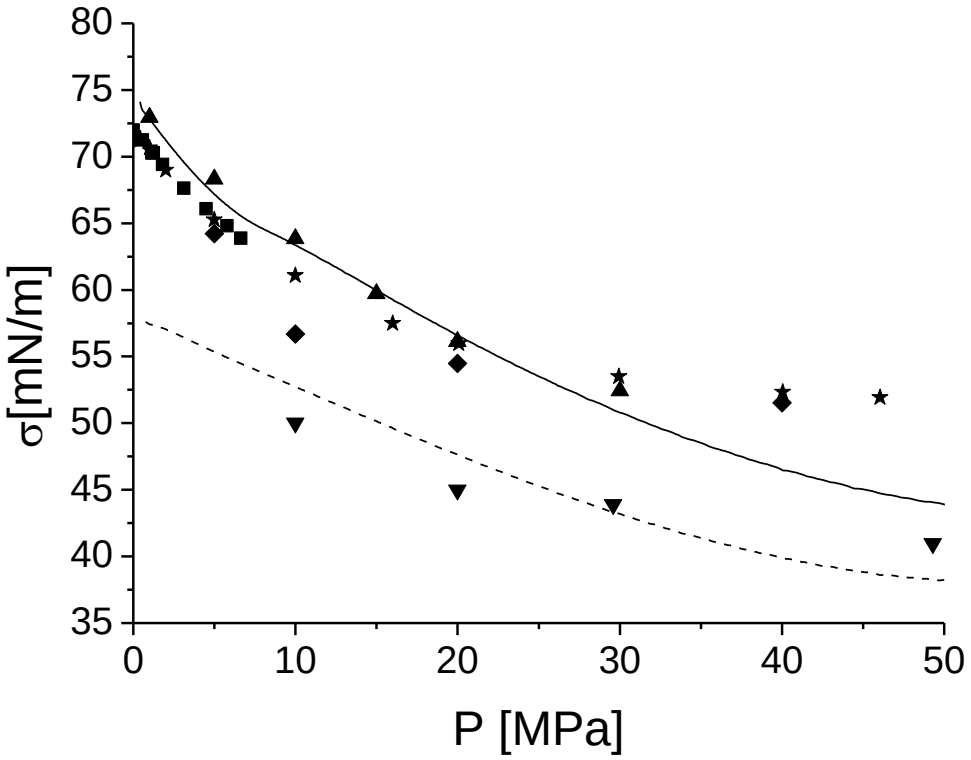

Figure 63: Interfacial Tension of methane + water at 298.15 K (experimental points: triangles [111], squares [112], diamonds [113] and stars [114]; solid line: DGT + PC-SAFT with $k_{ij} = 0.351 X_{CH_4} - 0.151$ and $\beta = 0.55$) and 373.15 K (experimental points: inverted triangles [115]; dashed line: DGT + PC-SAFT with $k_{ij} = 0.2702 X_{CH_4} - 0.0702$ and $\beta = 0.55$).

The density gradient theory relies on the calculation of partial density profiles across the interface in order to calculate the interfacial tension of a given mixture. An example of these density profiles can be seen in Figure 64 at 313.15 K and different pressures. It is to note the peak for the partial density of methane. This peak gives a hint for relative enrichment of the gas at the interface. The relative height of this peaks seems to decrease with increasing pressure, hence, the enrichment on the interface is expected to vanish at very high pressures, as already observed in the case of water + CO_2 mixtures.

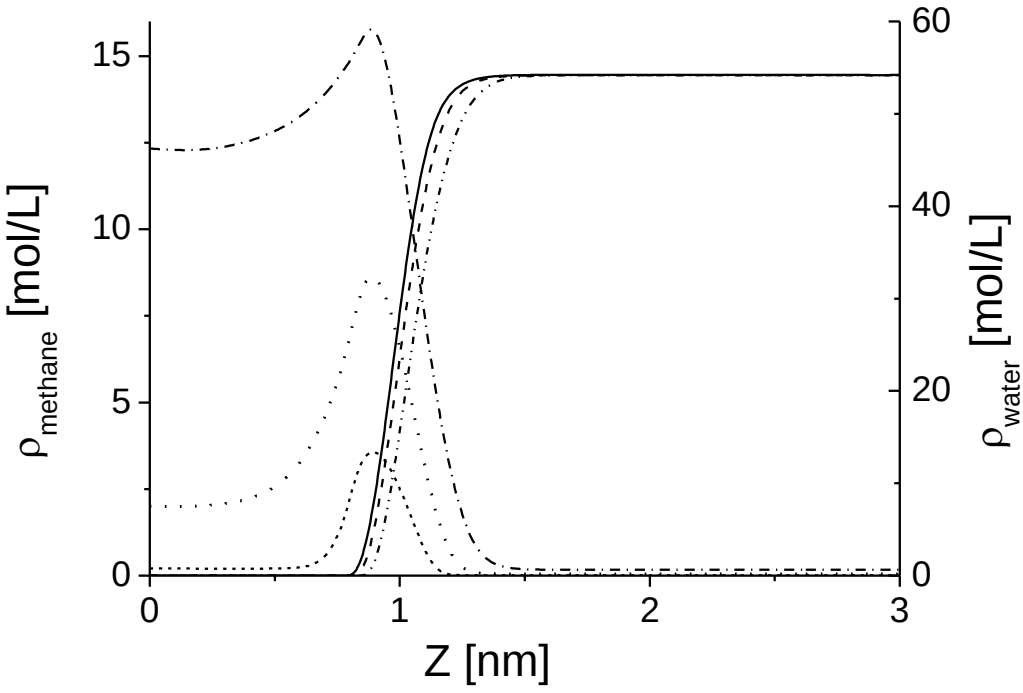

Figure 64: Partial density profiles for methane (short dashed line for P=0.55 MPa; dotted line for P=4.86 MPa and dashed dotted line for P=30 MPa) and water (solid line for P=0.55 MPa; dashed line for P=4.86 MPa and dashed double dotted line for P=30 MPa) across the interface for T= 313.15 K.

As the molecular weight of a hydrocarbon rises, the incompatibilities with water also increase, making the VLE migrate into systems of two liquid phases, one which is predominantly aqueous, and an organic one, close to being the pure hydrocarbon. In order to see the abilities of the PC-SAFT EOS under the 4C association scheme, calculations for the system water + heptane were carried out. With help of the acquired experience from the system water + methane, a similar approach for the

binary interaction parameter was proposed (Eq. 113), with a new temperature dependency for $a(T)$ of the form

$$a(T) = \frac{5.7T/K - 2377}{10000} \tag{115}$$

The calculations of the LLE of the system water + heptane can be seen in Figure 65. The mutual solubilities of the mixture vary in several orders of magnitude; however, the proposed scheme is able to describe the behaviour of both phases over a wide temperature range. Furthermore, the densities of both phases can also be accurately described, as seen in Figure 66.

Figure 67 shows the extrapolation of the model to a higher pressure, namely 7 bar. The available data from the literature [120] only shows the solubility of heptane in the aqueous phase. The calculations with PC-SAFT are able to describe the behaviour of the mixture in a good manner; at higher temperatures, this accuracy seems to decrease.

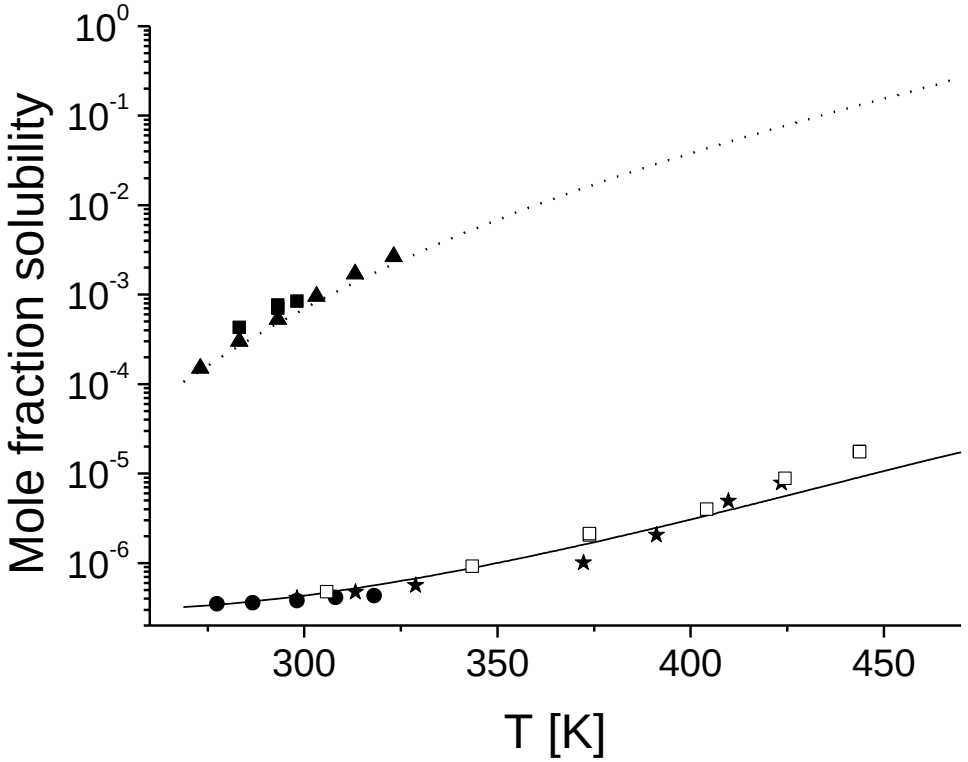

Figure 65: Mutual solubility of water + heptane at 1 bar. Comparison of the solubility of water in n-heptane (squares [116], and triangles [117]) with the model calculations (dotted line) and of the solubility of n-heptane in water (Experimental data: circles [118], stars [119] and open squares [120]; PC-SAFT: solid line).

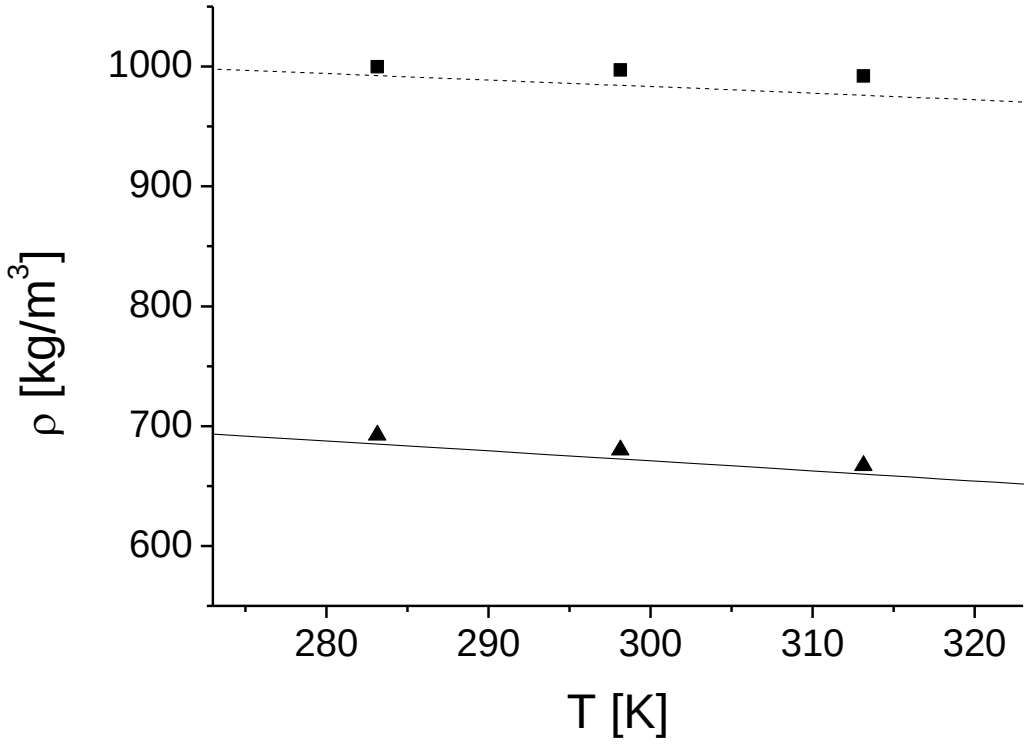

Figure 66: Comparison between experimental [121] and calculated densities of the liquid phases of the system water + heptane at 1 bar. Squares and dotted line: aqueous phase; triangles and solid line: organic phase.

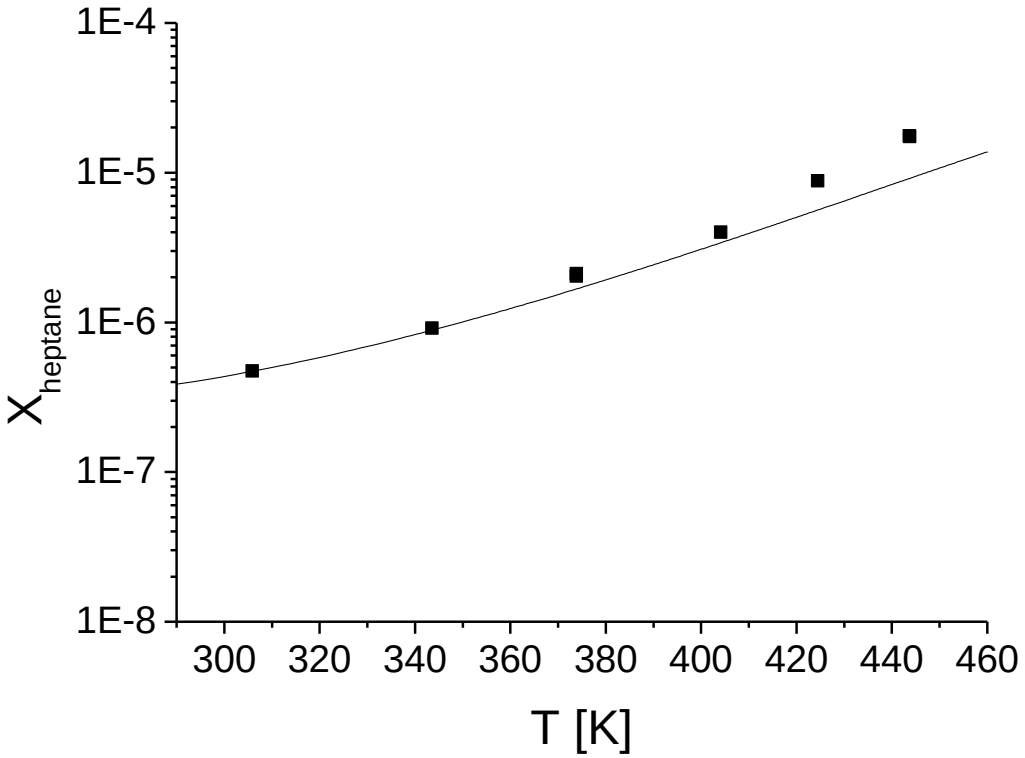

Figure 67: Solubility of n-heptane in water at 7 bar. Comparison between experimental data (squares [120]) and calculations with PC-SAFT (solid line).

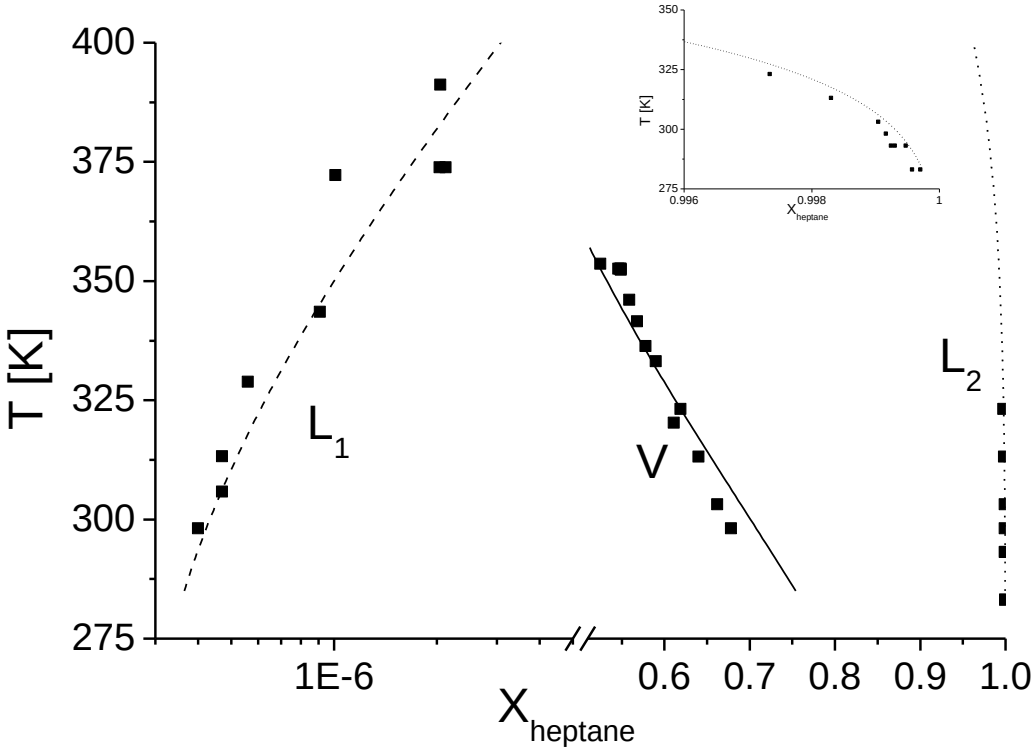

Figure 68: Comparison between experimental [116, 117, 118, 119, 120, 122, 123] and calculated data for the VLLE of the system water + heptane. Dashed line: aqueous liquid phase; solid line: vapour phase; dotted line: organic liquid phase. Inlet: zoom of the organic liquid phase.

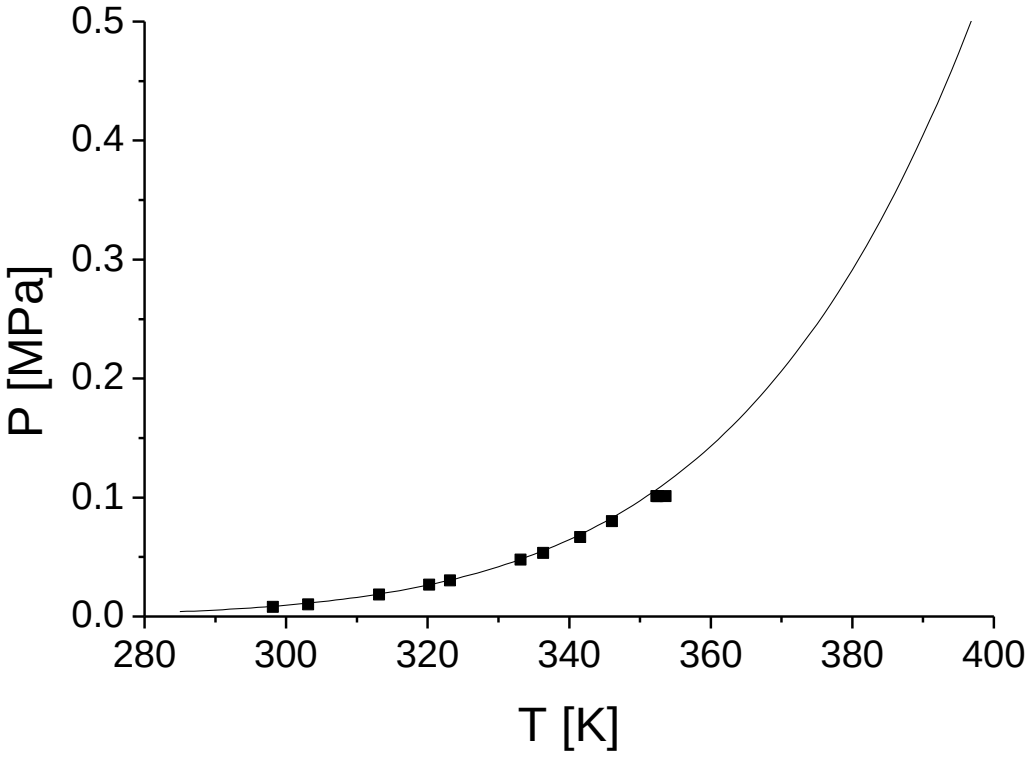

Figure 69: P-T Diagram for the VLLE water + heptane. Comparison between experimental data [122, 123] and calculations with PC-SAFT.

The water + heptane, same as the water + CO_2 system, exhibits a VLLE at several temperatures. Figure 68 and Figure 69 show a comparison between experimental data [116 - 123] and the calculated VLLE values with help of PC-SAFT. The PC-SAFT EOS is able to describe accurately not only the compositions of the three different phases, but also the P-T behaviour at which this phenomenon arises.

The available data for the interfacial tension of the system water + heptane is very scarce. Figure 70 depicts a comparison between calculated values for the LLE of this mixture at 1 bar and experimental data [121, 124, 125]. Equally as in the system methane + water, the sole geometric mean rule for the influence parameters is not enough, and thus a value of $\beta = 0.33$ was fitted to one experimental point. The fitted value seems to be able to give a good performance in predicting the interfacial tension of the mixture at different temperatures. Only one value, which also strongly deviates from the experimental data of other authors, does not seem to be in agreement with the calculations of the framework DGT + PC-SAFT.

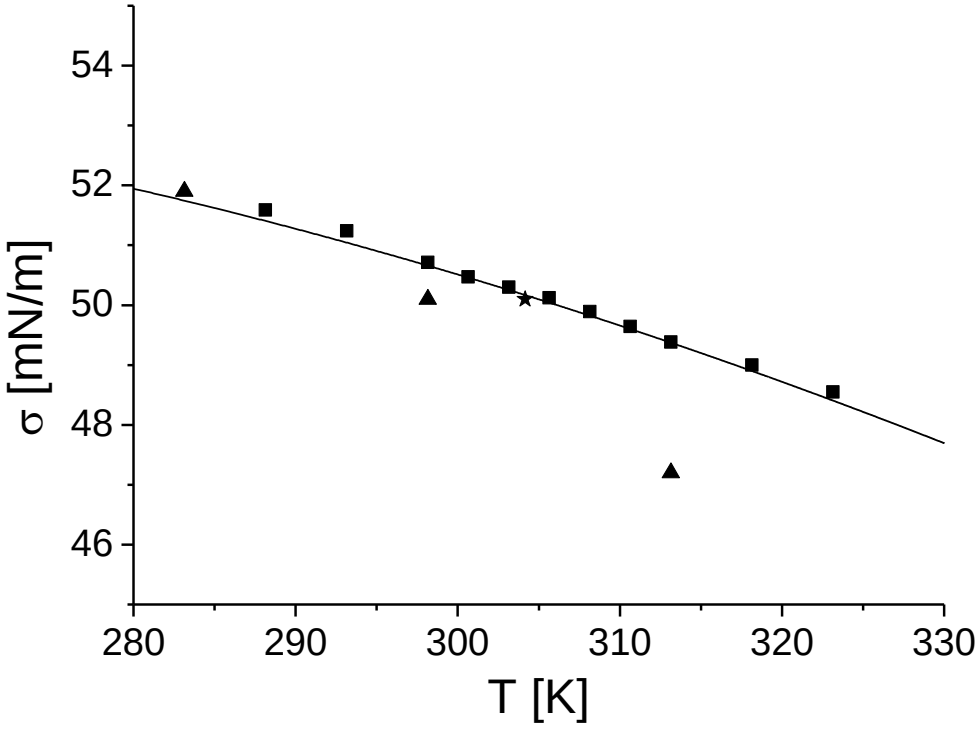

Figure 70: Interfacial tension of the system water + heptane at 1 bar. Comparison between experimental data (triangles [121], squares [124] and stars [125] and) and calculations of the DGT + PC-SAFT (solid line) with $\beta = 0.33$.

5.2. Ternary Mixtures

A last approach to validate the ability of the model is the extension of the calculations to ternary systems. This represents a big step in the validation of the modelling; all parameters have been defined in the binary subsystems, and therefore the calculations made are a pure prediction. This can be a risk in the case that calculations do not match the experimental data, since there are no further possibilities to correct the calculations in any way. For the extension to ternary mixtures, the system heptane + CO_2 + methane was chosen. This system is of high interest in the oil industry, and represents a case study between oil (represented by heptane), natural gas (represented by methane) and an injection fluid that can be pumped for so called enhanced oil recovery (represented by CO_2). Figure 71 shows a comparison between the predicted and the experimental data [126] for this system at 343.2K and different pressures. All binary interaction parameters for the subsystems have been defined during the work. The PCP-SAFT EOS is able to describe with very good accuracy the VLE of this mixture at different conditions

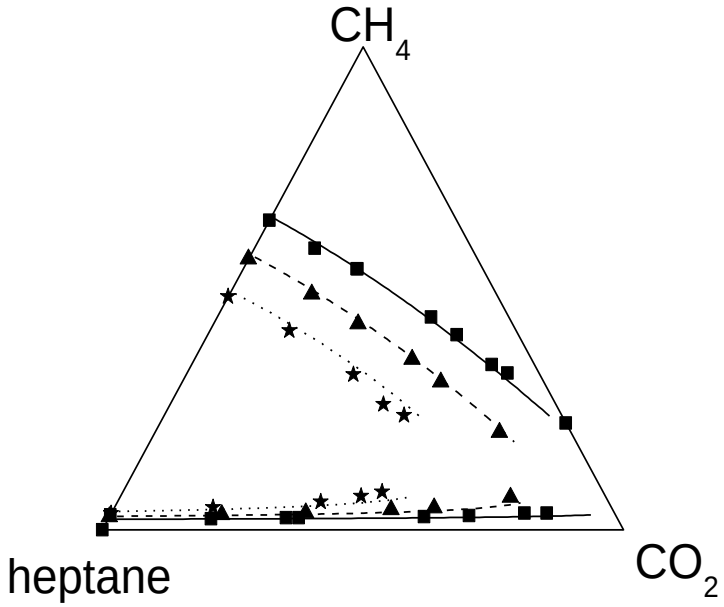

Figure 71: Comparison for the VLE of the system heptane (1) + carbon dioxide (2) + methane (3) at 343.2 K and 10 MPa (squares), 13 MPa (triangles) and 16 MPa (stars). Experimental Data taken from the literature [126]; the PC-SAFT binary interaction parameters are $k_{12} = 0.039; k_{23} = 0.033; k_{13} = 0.03$.

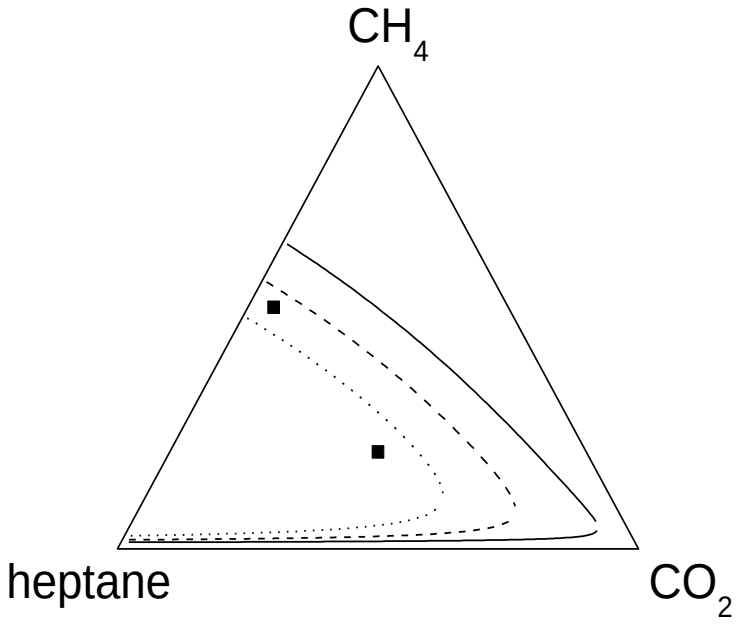

Figure 72: Calculated VLE of the system heptane (1) + carbon dioxide (2) + methane (3) at 323.2 K and 10 MPa (solid line), 13 MPa (dashed line) and 16 MPa (dotted line). Squares represent the initial feed concentrations for the experiment (TU-HH); the PC-SAFT binary interaction parameters are $k_{12} = 0.039; k_{23} = 0.033; k_{13} = 0.03$.

In order to prove the prediction of interfacial tensions of the mixture, several experiments were carried out by the Technical University Hamburg-Harburg [127]. Two mixtures of the three components were tempered to 323.2 K and densities and surface tensions of the mixtures were measured. Figure 72 shows the initial feed compositions in Gibbs' triangle.

A comparison of the measured and the calculated densities can be seen in Figure 73. The calculations are able to describe not only qualitatively but also with high accuracy the densities of the mixtures at different pressures, with deviations lower than 2%. Also the interfacial tensions, as seen in Figure 74 show deviations inside the experimental error. These results prove the efficacy of the DGT + PCP-SAFT theoretical framework for pure predictions with high accuracy in the ternary system. Furthermore, in the special case of the mixture, the DGT side has been extrapolated from the pure compound up to the ternary mixture. In the case of the VLE, some binary interaction parameters have been fitted to experimental data [57, 84], whereas others have also been calculated with help of correlations from this work. Figure 75 shows a schematic picture of the partial density profiles of the components across

the interface. As already noticed along the work, the more volatile components have a strong tendency to accumulate in the interface. This is also the case of the two gases present in the mixture.

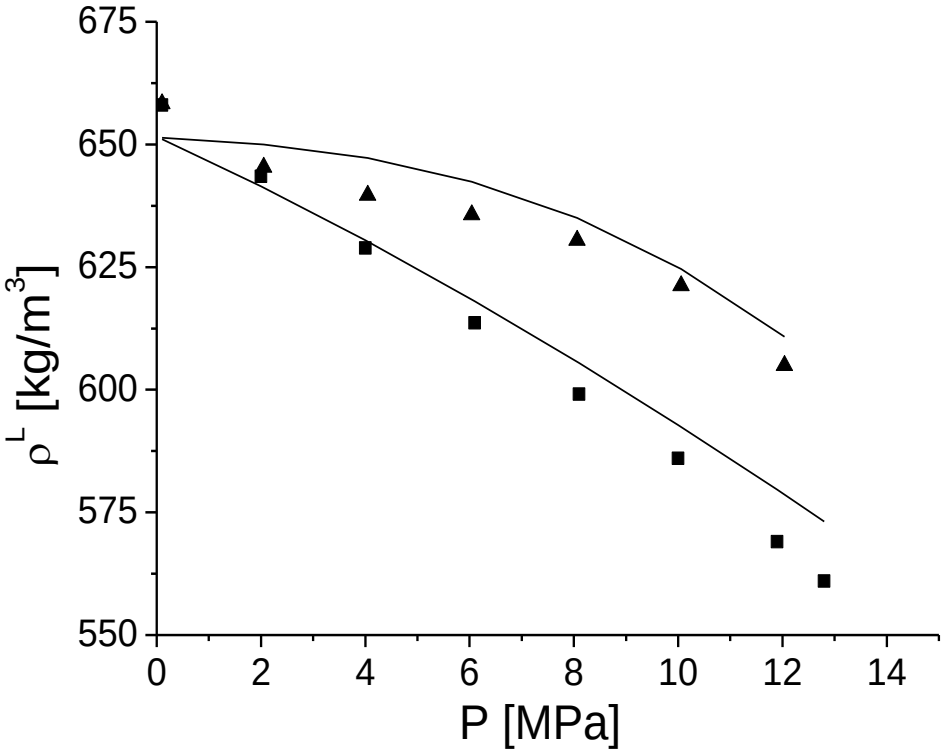

Figure 73: Comparison between experimental [127] and predicted densities of the system heptane (1) + carbon dioxide (2) + methane (3) at 323.2 K with two different feed compositions: $x_1^F = 0.5; x_2^F = 0.5$ (squares) and $x_1^F = 0.2; x_2^F = 0.4$ (triangles).

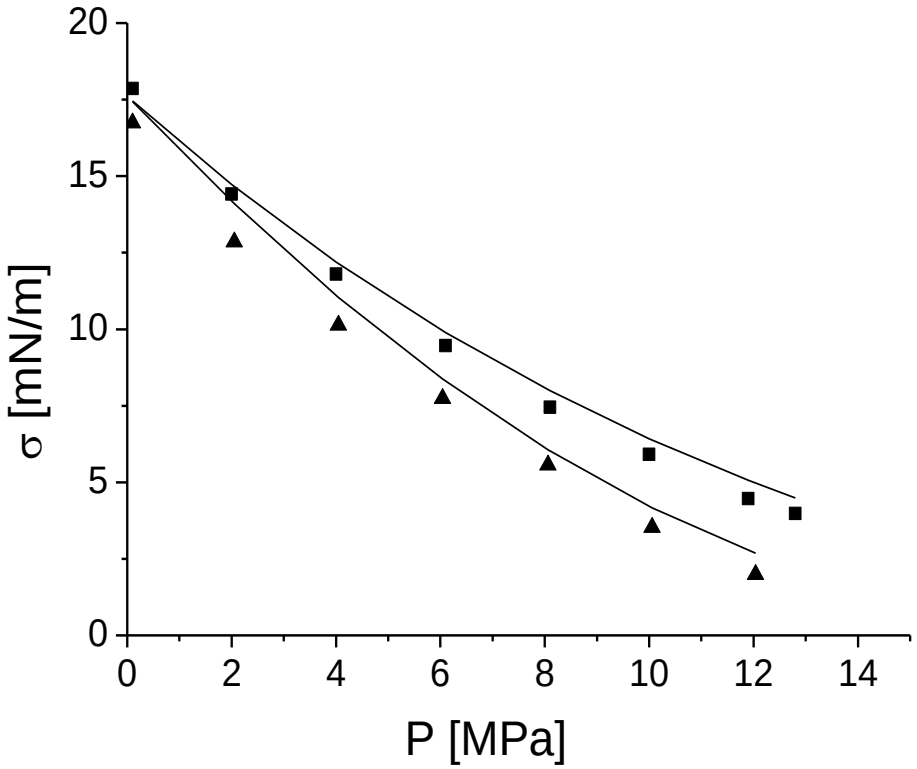

Figure 74: Comparison between the experimental [127] and the predicted VLE-interfacial tensions for the system heptane (1) + carbon dioxide (2) + methane (3) at 323.2 K with two different feed compositions: $x_1^F = 0.5; x_2^F = 0.5$ (squares) and $x_1^F = 0.2; x_2^F = 0.4$ (triangles).

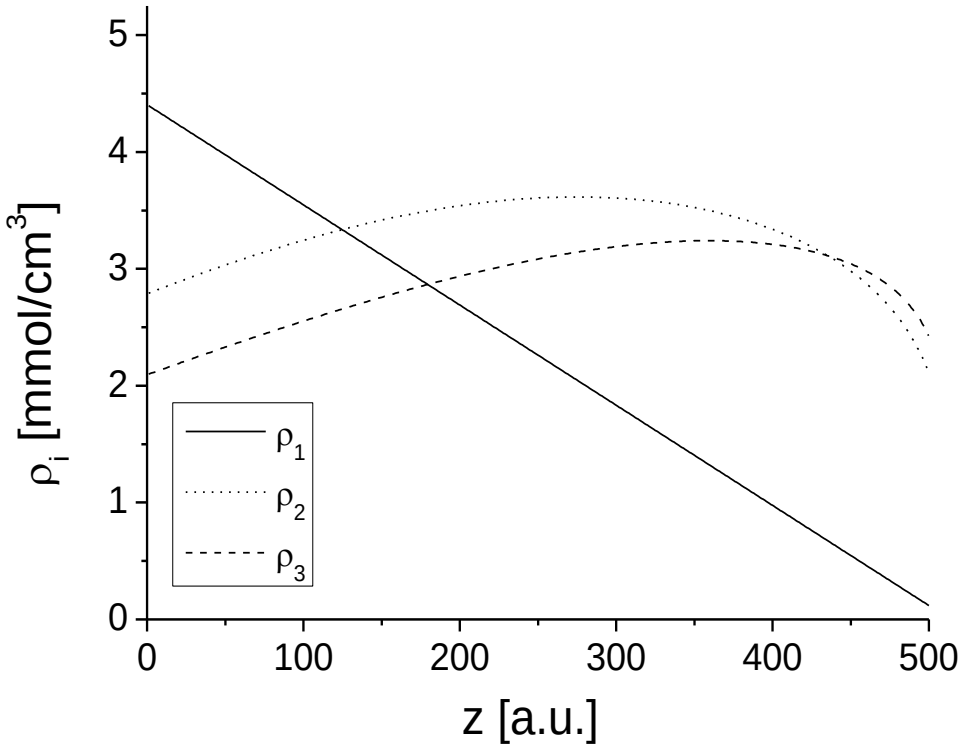

Figure 75: Density profiles across the VLE-interface for the system heptane (1) + carbon dioxide (2) + methane (3) at 343.2 K an 10 MPa, with $x_2^L = 0.3$.

6. CONCLUSIONS AND OUTLOOK

Within this work, the density gradient theory DGT has been combined with the PC(P)-SAFT Equation of state in order to calculate or predict interfacial tensions of fluids in equilibrium. The applied theoretical framework is able to describe the interfacial and phase equilibrium behaviour of pure substances accurately. In order to achieve this, the equation of state has had more or less contributions, theoretically based, that take into account the difference phenomena that can arise in a fluid. This is an advantage of the thermodynamic perturbation theory. Not only several parameters from the literature have been retested, but also new parameters for new substances have been fitted, having a good agreement with experimental data. In the case of the description of the interfacial tension, the DGT combined with PCP-SAFT gives a good description of the pure substances over large ranges of temperature. Furthermore, correlations have been found in the case of the n-alkanes that can allow a prediction of the interfacial tension of substance of this chemical type.

In the case of mixtures, a various group of mixtures has been evaluated. In the case of non-polar mixtures, both phase equilibrium and interfacial properties can be accurately described with the proposed methodology, and some correlations have been found in order to predict the binary interaction parameter of the phase equilibrium. This opens a door to a fully predictive methodology for phase equilibrium and interfacial phenomena of mixtures, based only in the pure-component properties.

In the case of mixtures with polar molecules, the DGT is also able to predict the interfacial properties of mixtures with carbon dioxide over a broad range of mixtures. In the case of water, some correlations have also been found to define the phase equilibrium and interfacial tension of its mixtures. In the case of the mixture of water + carbon dioxide a temperature dependent binary interaction parameter was able to describe phase equilibrium over a wide range of temperature; furthermore, it was possible to describe the different kinds of phase equilibrium present in this mixture. In

the case of the interfacial tension, a modified geometric mixing rule had to be used in order to calculate the interfacial tensions with a quantitative agreement.

Water mixtures with hydrocarbons are important in the oil industry, but also reveal a high difficulty in its modelling. This has been confirmed with the results from this work. The high asymmetry of the present substances makes it difficult to model accurately both phases at the same time. In order to overcome this problem, a concentration dependent binary interaction parameter has been defined. Results prove the validity of this assumption, making it possible to describe the aqueous and organic phase at the same time. In the case of the interfacial tension, a modified geometric rule was also proven to be the way to describe the different interfacial tensions arising in systems of water + hydrocarbons.

One highlight of this work is the presentation of data describing both phase equilibrium and interfacial tensions of ternary mixtures. This is a very important step in the validation of the methodology, since at the calculations of the ternary system a pure prediction is being made, since it is no longer possible to insert parameters of any kind that would correct possible errors; however, this is not necessary, as shown in the results. The framework is able to describe both phase equilibrium and interfacial tensions of a ternary mixture with great accuracy, proving the methodology to be in the right direction.

Several options are open for the continuation of this work. First, the parameters for water were fit assuming a contribution only base on association. Due to the strong dipolar moment of water, it should be considered if the introduction of the dipolar term in PCP-SAFT is necessary and would improve the results when extrapolated to mixtures. In the case of hydrogen sulphide, several parameter sets are available in the literature, and a new one has been presented here. The new parameter follows the considerations of the nature of the molecule in order to define the possible contributions in the PCP-SAFT framework. It would be good to go on with this analysis by testing the performance of this parameter set together with other substances in a mixture.

The ternary calculation shows good perspectives for the combination of the DGT +PCP-SAFT. It is therefore also recommendable to try calculations on other systems, increasingly complex, ending up with water mixtures, which seem to be difficult to model in an accurate way.

7. REFERENCES

1 Porter, A.W. Trans. Faraday Soc. 16 (1921), 336-345.

2 Redlich, O.; Kister, A.T.; Turnquist, C.E. Chem. Eng. Prog. Symp. Ser. 48 (1952), 49-61.

3 Wilson, G.M. J. Am. Chem. Soc. 86 (1964), 127-130.

4 Renon, H.; Prausnitz, J.M. AIChE J. 14 (1968), 135 – 144.

5 Abrams, D.; Prausnitz, J.M. AIChE J. 21 (1975), 116-127.

6 Fredenslund, A.; Jones, R.L.; Prausnitz, J.M. AIChE J. 21 (1975), 1086-1099.

7 Hansen, K.H.; Schiller, M.; Fredenslund, A.; Gmehling, J.; Rasmussen, P. Ind. Eng. Chem. Res. 30 (1991), 2352-2355.

8 Weidlich, U.; Gmehling, J. Ind. Eng. Chem. Res. 26 (1987), 1372-1381.

9 Van der Waals, J. D. PhD Thesis, Leiden University, 1873.

10 Redlich, O.; Kwong, J.N.S. Chem. Rev. 44 (1949), 233-244.

11 Soave, G. Chem. Eng. Sci. 27 (1972), 1197-1203.

12 Peng, D,; Robinson, D.B. Ind. Eng. Chem. Fundam. 15 (1976), 59-64.

13 Kontogeorgis, G.M.; Michelsen, M.L.; Folas, G.K.; Derawi, S.; von Solms, N.; Stenby, E.H. Ind. Eng. Chem. Res. 45 (2006), 4855-4868.

14 Patel, N.C.; Teja, A.S. Chem. Eng. Sci. 37 (1982), 463-473.

15 Ahlers, J.; Gmehling, J. Fluid Phase Equilibria 191 (2001), 177-188.

16 Guggenheim, E. A. Molecular Physics 9 (1965), 199–200.

17 Carnahan, N.F.; Starling, K.E. J. Chem. Phys. 51 (1969), 635-636.

18 Boublik, T. Ber. Bunsenges. Phys. Chem. 85 (1981), 1038–1041.

19 Beret, S.; Prausnitz, J. M. AIChE Journal 21 (1975), 1123–1132.

20 Prigogine, I. (1957). The Molecular Theory of Solutions, North –Holland Publishing Company, Amsterdam, 1957.

21 Kim, C. H.; Vimalchand, P.; Donohue, M. D.; Sandler, S. I. AIChE J 32 (1986), 1726 - 1733.

22 Wertheim, M.S. J. Stat. Phys. 42 (1986), 459-476.

23 Wertheim, M.S. J. Chem. Phys. 87 (1987), 7323-7331.

24 Chapman, W.G.; Jackson, G.; Gubbins, K.E. Mol. Phys. 65 (1988), 1057-1079.
25 Jackson, G.; Chapman, W.G.; Gubbins, K.E. Mol. Phys. 65 (1988), 1-31.
26 Chapman, W.G.; Gubbins, K.E.; Jackson, G.; Radosz, M. Ind. Eng. Chem. Res. 29 (1990), 1709-1721.
27 Huang, S.H.; Radosz, M. Ind. Eng. Chem. Res. 29 (1990), 2284-2294.
28 Alder, B.J.; Young, D.A.; Mark, M.A. J. Chem. Phys. 56 (1972), 3013-3030.
29 Chen, S.S.; Kreglewski, A. Ber. Bunsenges. Phys. Chem. 81 (1977), 1048-1052.
30 Galindo, A.; Davies, L.A.; Gil-Villegas, A.; Jackson, G. Mol. Phys. 92 (1998), 241-252.
31 Blas, F.J.; Vega, L.F. J. Chem. Phys. 109 (1998), 7405-7413.
32 Lafitte, T.; Bessieres, D.; Pineiro, M.M.; Daridon, J.L. J. Chem. Phys. 124 (2006), 16-31.
33 Gross, J.; Sadowski, G. Ind. Eng. Chem. Res. 40 (2001), 1244–1260.
34 Gross, J.; Sadowski, G. Ind. Eng. Chem. Res. 41 (2002), 5510–5515.
35 Barker, J.A.; Henderson, D. J. Chem. Phys. 47 (1967), 635-636.
36 Gross, J. AIChE Journal 51 (2005), 2556–2568.
37 Gross, J.; Vrabec, J. AIChE Journal 52 (2006), 1194–1204.
38 Wilhelmy, L. Ann. Phys. Chem. 4 (1863), 177-217.
39 Lecomte du Nouy, P. J. Gen. Physiol. 1 (1919), 521-524.
40 Rusanov, A.I.; Prokhorov, V.A. Interfacial Tensiometry, Elsevier, Amsterdam, 1996.
41 Van der Waals, J. D. Z. Phys. Chem. 13 (1894), 657-672.
42 Cahn, J.W.; Hilliard, J.E. J. Chem. Phys. 28 (1958), 258-267.
43 Poser, C.I.; Sanchez, I.C. Macromolecules 14 (1981), 361-370.
44 Nino-Amezquita, O.G.; van Putten, D.; Enders, S. Fluid Phase Equilibria 332 (2012), 40-47.
45 Telo da Gama, M.M.; Evans, R. Mol. Phys. 48 (1983), 229-250.
46 Wadewitz, T.; Winkelmann, J. Ber. Bunsenges. Phys. Chem. 100 (1996), 1825-1832.
47 Wohlfarth, Ch.; Wohlfarth, B. in M.D. Lechner (Ed.) Numerical Data and Functional Relationships in Science and Technology, Vol. 16 Surface Tension of Pure Liquids and Binary Liquid Mixtures, in Landoldt-Börnstein, New Series Group IV Physical Chemistry, Springer Verlag Berlin, Heidelberg, 1997.

48 Busch, A.; Grau, G.G.; Kast, W.; Klemnec, A.; Kohl, W.; Kux, C.; Meyerhoff, G.; Neckel, A.; Ruhtz, E.; Schäfer, K.; Valentiner, S. in Schäfer, K. and Lax, E. (Eds.), Eigenschaften der Materie in ihren Aggregatzuständen 2. Teil, Gleichgewichte Dampf- Kondensat und osmotische Phänomene, in Landoldt Börnstein IV. 6, Springer, Berlin, Göttingen, Heidelberg, 1960.

49 Vargaftik, N.B. Tables on Thermophysical Properties of Liquids and Gases, Hemisphere Publishing Corporation, John Wiley & Sons Inc., New York, USA. 1975.

50 Wadewitz, T. PhD Thesis, University Halle, 1997.

51 Jasper, J.; Kring, E. J. Phys. Chem. 59 (1955), 1019-1021.

52 Enders, S.; Kahl, H.; Winkelmann, J. J. Chem. Eng. Data 52 (2007), 1072-1079.

53 Li, H. ; Chen, W. Phys. Chem. Liq. 43 (2005), 343.

54 Kahl, H.; Wadewitz, T.; Winkelmann, J. J. Chem. Eng. Data 48 (2003), 1500-1507.

55 Laine, B. IV.Congr. Int. Chauff. Ind. Paris No.129 (1952).

56 Verschaffelt, J.E. Commun. Phys. Lab. Univ. Leiden 28 (1894), 1896.

57 Soerensen, J.M.; Arlt, W. Vapour-Liquid Equilibrium Data Collection, DECHEMA Frankfurt/Main, 1979.

58 Lafitte, T.; Mendiboure, B.; Piñeiro, M. M.; Bessières, D.; Miqueu, C. J. Phys. Chem. B 114 (2010), 11110–11116.

59 Luck, W.A.P.; Angew, Chem. Int. Ed. Eng. 19 (1980), 28-41.

60 Gloor, G.J.; Jackson, G.; Blas, F.M.; del Ro, E.M.; Miguel, E.. J. Phys. Chem. C 111 (2007), 15513-15522.

61 Medard, L. Gas Encyclopaedia, Elsevier Science Ltd., Amsterdam, 1976.

62 Liessmann, G.; Schmidt, W.; Reiffarth, S. Recommended Thermophysical Data: Data Compilation of the Saechsische Olefinwerke Boehlen Germany.

63 Raznjevic, K. Thermodynamische Tabellen, VDI-Verlag, 1977.

64 Stowe, V. J. Am. Chem. Soc 51 (1929), 410-415.

65 Seyer, W.F.; Peck, W.S. J. Am. Chem. Soc. 52 (1930), 14-23.

66 Nasrifar, K.; Tafazzol, A. Ind. Eng. Chem. Res. 49 (2010), 7620-7630.

67 Aparicio-Martínez, S.; Hall, K. R. Ind. Eng. Chem. Res. 46 (2007), 291–296.

68 Tang, X.; Gross, J. Fluid Phase Equilib. 293 (2010), 11-21.

69 Linstrom, P.J.; Mallard, W.G. (Eds) NIST Chemistry Web Book, NIST Standard Reference Database Number 69.
70 Guggenheim, E.A. J. Chem. Phys. 13 (1945), 253 – 262.
71 Roth, W.A.; Scheel, K. Landolt Börnstein Physikalisch – Chemische Tabellen, Springer, Heidelberg, 1927.
72 Danzer, A. Bachelor Thesis, TU-Berlin, 2013.
73 Nino-Amezquita, O.G.; Enders, S.; Jaeger, P.T.; Eggers, R. Ind. Eng. Chem. Res. 49 (2010), 592-601.
74 Haslam, A. J.; Galindo, A.; Jackson, G. Fluid Phase Equilibria 266 (2008), 105–128.
75 Hudson, G.H.; McCoubrey, J.C. Trans. Faraday Soc. 56 (1960), 761-766.
76 London, F. Trans. Faraday Soc. 33 (1937), 8-26.
77 Poston, R.S.; McKetta, J.J. J. Chem. Eng. Data 11 (1966), 364-367.
78 Azarnoosh, A; McKetta, J.J. J. Chem. Eng. Data 8 (1963), 494-496.
79 Tang, J.; Satherley, J.; Schiffrin, D.J. Chin. J. Chem. Eng. 1 (1993), 223-231.
80 Niño Amézquita, O.G.; Enders, S.; Jaeger, P.T.; Eggers, R. The Journal of Supercritical Fluids, 55 (2010), 724-734.
81 Hsu, J.J.C.; Nagarajan, N.; Robinson, R.L. J. Chem. Eng. Data 30 (1985), 485-491.
82 Gross, J. PhD Thesis, TU-Berlin, 2001.
83 Cornelisse, P. PhD Thesis, Technical University Delft, 1997.
84 Robinson, D.B.; Kalra, J. GPA Research Report, RR-18, (1976), 1-19.
85 Kalra, J.; Kubota, H.; Robinson, D.; Ng, H. J. Chem. Eng. Data 23 (1978), 317-321.
86 Reamer, H.H.; Sage, B.H. J. Chem. Eng. Data 8 (1963), 508-513.
87 Nagarajan, N.; Robinson, R.L. J. Chem. Eng. Data 31 (1986), 168-171.
88 Gasem K.A.M.; Dickson, K.B.; Dulcamara, P.B.; Nagarajan, N.; Robinson, J.R. J. Chem. Eng. Data 34 (1989), 191-195.
89 Nagarajan, N.; Robertson, R.L. J. Chem. Eng. Data 32 (1987), 369-371.
90 Bamberger, A.; Sieder, G.; Maurer, G. J. Supercrit. Fluids 17 (2000), 97-110.
91 Fischer, K.; Petri, M.; Noll, O.; Gmehling, J; Unpublished Data, 1995, DETHERM.
92 King, M.B.; Mubarak, A.; Kim, J.D.; Bott, T.R. J Supercrit. Fluids 5 (1992), 296-302.

93 Weibe, R.; Gaddy, V.L. J. am. Chem. Soc. 62 (1940), 815-817.

94 Coan, C.R.; King, A.D. J. Chem. Am. Soc. 93 (1971), 1857-1862.

95 Briones, J.A.; Mullins, J.C.; Thies, M.C.; Kim, B.U. Fluid Phase Equilibria 36 (1987), 235-246.

96 Dohrn, R.; Buenz, A.P.; Devlieghere, F.; Thelen, D. Fluid Phase Equilibria 83 (1993), 149-158.

97 Spycher, N.; Pruess, K.; Ennis-King, J. Geochim. Cosmochim. Acta 67 (2003), 3015-3031.

98 Takenouchi, S.; Kennedy, G.C. Am. J. Sci. 262 (1964), 1055-1074.

99 Wendland, M.; Hasse, H.; Maurer, G.; J. Chem. Eng. Data 44 (1999), 901-906.

100 Hebach, A.; Oberhof, A.; Dahmen, N.; Kögel, A.; Ederer, H. Dinjus, E. J. Chem. Eng. Data 47 (2002), 1540-1546.

101 Vega, L. F.; Llovell, F.; Blas, F. J. J. Phys. Chem. B 113 (2009), 7621–7630.

102 Culberson, O. L.; McKetta, J. J. Jr.Trans. AIME 192 (1951), 223-226.

103 Chapoy, A.; Coquelet, C.; Richon, D. Fluid Phase Equilibria 214 (2003) 101–117.

104 Kiepe, J.; Horstmann, S.; Fischer, K.; Gmehling, J. Ind. Eng. Chem. Res. 42 (2003), 5392–5398.

105 Yarrison, M.; Cox, K. R.; Chapman, W. G. Ind. Eng. Chem. Res. 45 (2006), 6770–6777.

106 Siqueira Campos, C. E. P.; Penello, J. R.; Pellegrini Pessoa, F. L.; Cohen Uller, A. M. J. Chem. Eng. Data 55 (2010), 2576–2580.

107 Qin, J.; Rosenbauer, R. J.; Duan, Z. J. Chem. Eng. Data 53 (2008), 1246–1249.

108 Gillespie, P. C.; Wilson, G. M. GPA Research Report 1982, RR-48, 1-73.

109 Miqueu, C.; Míguez, J. M.; Piñeiro, M. M.; Lafitte, T.; Mendiboure, B. J. Phys. Chem. B 115 (2011), 9618–9625.

110 Schmidt, K. A. G.; Folas, G. K.; Kvamme, B. Fluid Phase Equilibria 261 (2007), 230–237.

111 Ren, Q.-Y.; Chen, G.-J.; Yan, W.; Guo, T.-M. J. Chem. Eng. Data 45 (2000), 610–612.

112 Jho, C.; Nealon, D.; Shogbola, S.; King Jr., A. . J. Colloid Interface Sci. 65 (1978), 141–154.

113 Wiegand, G.; Franck, E. U. Ber. Bunsenges. Phys. Chem. 98 (1994), 809–817.

114 Sachs, W.; Meyn, V. Colloids Surf. A 94 (1995), 291–301.

115 Jennings Jr., H.; Newman, G. Soc. Pet. Eng. J. 6 (1971),171.

116 Black, C.; Joris, G.G.; Taylor, H.S. J. Chem. Phys. 16 (1948), 537-548.

117 Englin, B.A.; Plate, A.F.; Tugolukov, V.M.; Pryanishnikova, M.A. Khim. Tekhnol. Topliv Masel 10 (1965), 42.

118 Nelson, H.D.; de Ligny, C.L. Recl. Trav. Chim. Pays Bas 87 (1968), 528-544.

119 Price, L.C. Am. Assoc. Pet. Geol. Bull. 60 (1976), 213-244.

120 Marche, C.; Ferronato, C.; Jose, J. J. Chem. Eng. Data 48 (2003), 967-971.

121 Backes, H.M. Fortschr. Ber. VDI Z. Reihe 3, 97 (1984), 0506-3108.

122 Rezanova, E.N.; Toikka, A.M.; Markuzin, N.P. Vestn. Leningr. Univ. Ser. 4 Fiz. Khim. 3 (1991), 53-56.

123 Kudryavtseva, L.S.; Toome, M.Y.; Eizen, O.G. Eesti NSV Tead. Akad. Toim. Keem. Geol. 25 (1976), 16-21.

124 Zeppieri, S.; Rodriguez, J.; Lopez de Ramos, A.L. J. Chem. Eng. Data 46 (2001), 1086-1088.

125 Sokolovski, A.; Zielonka, B.; Piasecki, A.; Wilk, K.A.; Burczyk, B. J. Phys. Chem. B 103, 26 (1999), 5512-5516.

126 Nagahama, K.; Suzuki, S.; Oba, S.; Hirata, M. Sekiyu Gakkai Shi 28 (1985), 63-69.

127 Jaeger, P.T.; Eggers, R. J. Supercrit. Fluids 66 (2012), 80-85.

APPENDIX 1: SUMMARY OF FITTED PC(P)-SAFT PURE COMPONENT PARAMETER FOR DIFFERENT SUBSTANCES

Substance	**Model**	**m**	σ **[Å]**	ε / k_B **[K]**	ε^{AB} / k_B **[K]**	κ^{AB}
water	PC-SAFT 4C	1.0656	3.0007	366.51	1800	0.01
sulphur trioxide	PC-SAFT	3.6315	3.4991	204.9	-	-
sulphur dioxide	PCP-SAFT	2.9101	2.6361	195.5	-	-
hydrogen sulphide	PCP-SAFT	1.6615	3.055	224.5	-	-

APPENDIX 2: SUMMARY OF PC(P)-SAFT CORRELATIONS FOR THE BINARY INTERACTION PARAMETER FOR DIFFERENT MIXTURES

Substance 1	Substance 2	Correlation	Comments
n-alkane	n-alkane	$k_{ij} = \left(1 - \frac{2^7 \sigma_{jj}^3 \sigma_{ii}^3}{\left(\sigma_{ii} + \sigma_{jj}\right)^6} \frac{\sqrt{I_i I_j}}{(I_i + I_j)}\right)$	Based on the Haslam et al.[74] extension of the Hudson and McCoubrey Theory.
nitrogen	n-alkane	$k_{ij} = 0.10894 - 0.00696N + 6.07143*10^{-4} N^2$	N= number of carbons in the n-alkane chain
carbon dioxide	n-alkane	$k_{ij} = 0.032 + 10^{-3} N$	N= number of carbons in the n-alkane chain
carbon dioxide	water	$k_{ij} = \frac{4.95 \cdot T}{10000K} - 0.34693$	T = Temperature
methane	water	$k_{ij} = \left(0.2 - a(T)\right) \mathrm{X}_{CH_4} + a(T)$	$a(T)$=0.04881-1.33218(0.99365$^{T/K}$)
n-heptane	water	$k_{ij} = \left(0.2 - a(T)\right) \mathrm{X}_{CH_4} + a(T)$	$a(T) = \frac{5.7T/K - 2377}{10000}$

APPENDIX 3: SUMMARY OF DGT INFLUENCE PARAMETERS FOR DIFFERENT SUBSTANCES

Substance	Model	10^{-20} κ [Jm^5/mol^2]
methane	PC-SAFT	1.973
propane	PC-SAFT	10.00
butane	PC-SAFT	17.81
pentane	PC-SAFT	25.91
hexane	PC-SAFT	36.298
heptane	PC-SAFT	50.92
n-alkane N= # carbon	PC-SAFT	$1.17164 - 0.09767N + 1.0178N^2$
toluene	PC-SAFT	31.89
cyclohexane	PC-SAFT	34.07
nitrogen	PC-SAFT	1.048
water	PC-SAFT 2B	1.3785
water	PC-SAFT 4C	0.84
sulphur trioxide	PC-SAFT	5.675
sulphur dioxide	PC-SAFT	3.4720
sulphur dioxide	PCP-SAFT	4.3725
hydrogen sulphide	PCP-SAFT	3.428

APPENDIX 4: ABSTRACT – ENGLISH VERSION

The interfacial tension of mixtures plays an important role in industrial processes when various fluid phases are involved, like in distillation columns and enhanced oil and gas recovery. Knowledge on the interfacial tension is needed for process design especially regarding transport properties. Systematic experimental work covering the commonly required large range of conditions is quite costly. For this reason a theoretical method in order to predict the interfacial tension using only bulk properties of the mixture and the surface tensions of pure components is very helpful. One possibility for a theoretical approach is the density gradient theory in combination with a suitable equation of state (EOS). This work focuses on the development of a methodology combining the density gradient theory together with the perturbed-chain statistical associating fluid theory equation of state (PC-SAFT EOS). The use of an equation of state allows the use of the framework on pure substances with a further extension to mixtures. Pure components of highly differing characteristics were used in the density gradient theory framework, with excellent results when compared to literature data. Some new parameter sets for the EOS are also presented according to physical assumptions. The extension of the proposed framework to binary mixtures delivers good predictions in a broad field of mixtures; however, when applied to water-containing mixtures, a few extra assumptions have to be made both on phase equilibrium and DGT. The approach leads to a description of both mutual solubility and interfacial tension in water mixtures, including water + hydrocarbon systems. A pure prediction of a ternary system, based only on the findings from the binary subsystems, poses a big challenge for validation of the framework. First results for a ternary system are presented and show promising perspectives for the use of the methodology for multicomponent mixtures, based purely on the pure and binary system outcomes.

APPENDIX 5: ABSTRACT – DEUTSCHE FASSUNG

Die Grenzflächenspannung von Mischungen spielt eine entscheidende Rolle in verschiedenen Bereichen der Verfahrenstechnik, wenn verschiedene fluide Phasen aufeinandertreffen, beispielsweise in Rektifikationskolonnen oder in der Erdöl- bzw. Erdgasförderung. Eine genaue Kenntnis der Grenzflächenspannung in solchen Systemen ist entscheidend für ein geeignetes Prozessdesign, besonders für die optimale Gestaltung des Stofftransports. Messungen der Grenzflächenspannung als Funktion der Zusammensetzung, der Temperatur und des Druckes sind in der Regel sowohl kosten- als auch zeitaufwändig. Aus diesem Grund wäre eine Berechnungsmethode wünschenswert, die die Grenzflächenspannung einer Mischung aus beliebig vielen Komponenten aus den bulk-Eigenschaften der binären Randsysteme und den Reinstoffeigenschaften vorhersagen kann. Eine geeignete Methode ist die Dichtegradiententheorie in Kombination mit einer thermischen Zustandsgleichung.

Diese Arbeit beschäftigt sich mit der Kombination der Dichtegradiententheorie mit der störungstheoretischen Zustandsgleichung (perturbed-chain statistical associating fluid theory, PC-SAFT). Diese Vorgehensweise erlaubt, ausgehend von der Beschreibung reiner Stoffe, die Extrapolation auf Mischungen. Die thermodynamischen Eigenschaften von Reinstoffe mit unterschiedlichen Polaritäten konnten in sehr guter Übereinstimmung mit experimentellen Daten aus der Literatur berechnet werden. Die Erweiterung der Methode für binäre Mischungen liefert auch ebenso gute Ergebnisse für eine Vielzahl von Mischungen. Nur in Mischungen, die aus Wasser und einer unpolaren Komponente bestehen, müssen weitere Annahmen getroffen werden. Somit war auch die Beschreibung von Mischungen aus Wasser und Kohlenwasserstoffen möglich. Basierend auf den Daten für die reinen Stoffe und die binären Randsysteme gelang die vollständige Vorhersage des Phasenverhaltens und der Grenzflächeneigenschaften von einfachen, ternären Mischungen. Somit konnte das Potential für die Anwendung dieser Methode auf Vielstoffsysteme, wie beispielsweise Erdöl oder Erdgas demonstriert werden.